Ludwig-Maximilians-Universität München
Fakultät für Biologie

Looming-Evoked Escape Behavior and its Visual Pathway in the Larval Zebrafish

Dissertation zur Erlangung des akademischen Grades
des Doktors der Naturwissenschaften
DR. RER. NAT.

Vorgelegt von
Incinur Temizer
aus Istanbul (Türkei)

München, November 2015

Erstgutachter: Prof. Dr. Herwig Baier

Zweitgutachter: Prof. Dr. Andreas Herz

Datum der Abgabe: 12.11.2015

Datum der mündlichen Prüfung: 18.03.2016

To my mother, Reyhan Temizer, for all her beauty and wisdom.

Acknowledgements

First, I would like to thank Herwig Baier for giving me the chance to pursue my PhD in the exciting field of zebrafish neuroscience and for supervising my thesis.

This work would not have been possible without the strong support and valuable feedback from Thomas Misgeld, Ruben Portugues and Fabrizio Gabbiani. I am extremely thankful to them. I would also like to thank Michael Orger for his presence and contribution to my first thesis advisory meeting. I am thankful to my thesis examination committee for their patience to evaluate my thesis. I especially owe my deepest gratitude to Andreas Herz for his sharp analysis of this work. I very much enjoyed the scientific discussions we had during the revisions. I wish I had known him earlier so that I could benefit from his scientific enthusiasm and expertise a little more.

I was lucky enough to become a part of the Boehringer Ingelheim Fonds (BIF) family. The BIF has supported me not only financially but also nurtured me in many different aspects of life. In retrospective, I frankly believe that being a BIF fellow was one of the best things that happened to me during my PhD. I have been very much inspired and motivated by my fellows' drive, intellect, authenticity and humility. Thank you.

I am thankful to all the past and present members of the Baier Lab for helping me to evolve to become a neuroscientist. We shared many happy and fun moments as well as the misery of non-working-experiments together. I am glad to have met each of them and thankful to all their contributions, the fruitful discussions we had and their support during my PhD. Special thanks to Joe Donovan, my friend and closest collaborator, for his great help and support, his endless passion for science, technology, Python and food, silly late-lab conversations, discussions and contemplations, clumsy tobacco pipe smoking trials, chess playing challenges (next time I will win), guitar playing sessions and many more. Big thanks to Johannes Larsch and Amelia Douglass for proof reading my thesis and for their valuable comments. I wish to thank Katrin Vogt and Simone Wendlinger for the help with German translations in my thesis. I also want to thank all the Tanimoto Lab and the

Portugues Lab members, for their presence, friendship and the colors they brought into the department. Thanks to the friendship of Julia, Pia and Arne. Last but not least I want to say thank you to our department secretary Annegret Cerny for doing such a good job.

Munich has generously offered me encounters with people who touched my life in unexpected ways: Ben, Magali and Marion, thank you very much. Hakan, Habibe, Sercan and Tuğçe, thank you for making me feel at home, for your precious friendship, intelligence and the great sense of humor. Sağolun gençler! Ivana, thank you for your practical wisdom and the joy you spread.

I am immensely thankful to my former teachers Avadis Hacinliyan, İpek Karaaslan, Ercüment Akat, Nihat Berker, Franco Weth, who had an impact on the course of my life and where I ended up now. I am grateful to you for being there, teaching, inspiring and supporting many more young people to move forward.

Gülçin, Ruken, Zehra, Oya, Merve, Sezin, Gaye, thanks for the good vibes and enduring me for such a long time. I would also like to thank to Aslı Erdoğan, Sabahattin Ali, Haruki Murakami, Kurt Vonnegut and Oğuz Atay for their books, imagination and understanding of human nature, which helped me keep going in difficult times.

Finally, I am grateful to my parents and my entire family for the love and education that I have received from them. During my studies abroad, I could not have enough time for my sister, Bahar. I owe deeply to her for her forgiveness and acceptance of me. There are people that I do not know how to thank properly. Thus, I quietly leave their names here: Mathieu, Colette, Wolfgang, Gabi, Thesy, Karl, Tine and CP.

Thank you serendipity.

Martinsried, May 2016

Incinur Temizer

Publications and contributions

The results presented in this PhD thesis were published in Current Biology in July 2015:

Incinur Temizer, Joseph C. Donovan, Herwig Baier, Julia L. Semmelhack. A Visual Pathway for Looming-Evoked Escape in Larval Zebrafish. *Current Biology*, Volume 25, Issue 14, 20 July 2015, Pages 1823 - 1834, DOI: http://dx.doi.org/10.1016/j.cub.2015.06.002.

Author contributions:

I.T., H.B. and J.L.S. conceived the study. **I.T.** designed and performed all the experiments in this thesis unless stated otherwise, conducted data analysis and wrote the manuscript. J.C.D wrote Python scripts for calcium imaging data, performed pixelwise imaging analysis, helped with statistics and figure graphics. H.B., J.L.S. and J.C.D. were involved in editing the manuscript.

Kurzfassung

Um einem herannahenden Angreifer auszuweichen oder zu entfliehen, ist eine schnelle visuelle Wahrnehmung von Vorteil, da dadurch ein schnelles präzises Fluchtmanöver eingeleitet werden kann. Bei verschiedenen Tierarten wurden bereits Nervenzellen entdeckt, welche auf die Wahrnehmung solcher visuellen Reize spezialisiert sind, es ist jedoch nicht bekannt welche spezifischen visuellen Informationen die schnellen Fluchtmanöver auslösen. Darüber hinaus ist größtenteils auch nicht bekannt, welche neuronalen Mechanismen der Erkennung herannahender Objekte zugrunde liegen.

Um die neuronale Grundlage des visuell hervorgerufenen Fluchtverhaltens von Zebrafischlarven zu untersuchen, habe ich eine Reihe psychophysischer Experimente und Zwei-Photonen-Mikroskop Aufnahmen durchgeführt, die mit gezielten Laserablationen von Nervenzellen kombiniert wurden. Dafür habe ich zuerst einen neuen Verhaltensaufbau etabliert, mit dem ich das Antwortverhalten von teilweise immobilisierten Zebrafischlarven auf herannahende Objekte untersucht habe. Durch die Fixierung des Larvenkopfes werden die Kontrolle des verabreichten visuellen Stimulus und die Verfolgung der Schwanzflossenbewegung vereinfacht. Ich fand heraus, welche spezifischen Parameter des visuellen Stimulus für das Auslösen eines schnellen Fluchtmanövers notwendig sind. Zum Beispiel leiten Fischlarven ein Fluchtmanöver ein, sobald der herannahende Stimulus im Sichtfeld eine Größe von ca. 20° überschreitet.

Um die für dieses Verhalten relevanten rezeptiven Felder im Gehirn zu identifizieren, habe ich Ca^{2+}-Signale in den Axon-Endungen von retinalen Ganglienzellen (RGZ) während der visuellen Stimulation aufgenommen. Damit konnte ich drei Gehirnregionen bestimmen, in denen RGZ-Axonen auf den gezeigten visuellen Stimulus antworten. Mit Hilfe einer detaillierten Auswertung der aufgenommenen neuronalen Aktivität fand ich heraus, dass ein Teil der Antworten, die selektiv für verhaltensrelevante Stimuli sind, im Tektum zu erkennen sind. Mittels gezielter Laserablationen von Nervenzellen im Tektum konnte ich weiterhin zeigen, dass ein intaktes Tektum eine wichtige Rolle bei der Flucht vor herannahenden Objekten spielt.

Der wissenschaftliche Beitrag dieser Arbeit liegt in der Etablierung und Charakterisierung eines bei Zebrafischlarven bisher nicht untersuchten, visuell erzeugten Fluchtverhaltens vor herannahenden Objekten. Meine Arbeit ermöglicht einen grundlegenden Einblick in die komplexe Verarbeitung von visuellen Signalen im Gehirn, welche unmittelbar eine Flucht vor herannahenden Bedrohungen auslösen. Zusammengenommen mit bereits veröffentlichten Ergebnissen anderer Autoren deuten die von mir gewonnenen Erkenntnisse des Weiteren darauf hin, dass ähnliche neuronale Mechanismen in verschiedenen Tierstämmen für die Erkennung herannahender Bedrohungen verantwortlich sind.

Abstract

Avoiding the strike of an approaching predator requires rapid visual detection of its looming image, followed by a directed escape maneuver. While looming-sensitive neurons have been discovered in various animal species, the relative importance of different stimulus features that are extracted by the visual system is still unclear. Furthermore, the neural mechanisms that compute object approach are largely unknown.

To investigate the neural basis for visually-evoked escape in zebrafish larvae, I devised a series of psychophysical and imaging experiments, combined with targeted laser ablations of specific brain regions. I first established a new behavioral paradigm to examine the behavioral response to looming stimuli in head-restrained zebrafish larvae. A head-restrained preparation facilitates stimulus control and tracking of tail kinematics. I found specific features of the looming stimulus that are critical to elicit rapid escape maneuvers. Furthermore, I demonstrated that larvae initiate escapes when the angular size of the looming stimulus surpasses about 20°. To identify the retinorecipient areas responding to behaviorally relevant stimuli, I imaged Ca^{2+} signals in retinal ganglion cell (RGC) axon terminals during stimulus presentation. I identified three visual brain areas in which RGC axons responded to looming stimuli. Pixelwise analysis of the neuronal activity allowed me to detect a subset of these inputs within the tectum that selectively responded to behaviorally relevant stimuli. Through targeted laser ablations in the tectal neuropil, I showed that an intact tectum plays an important role in looming-triggered escapes.

Taken together, this work demonstrates and characterizes a previously unknown visually mediated escape behavior in zebrafish larvae exposed to objects approaching on a collision course. Furthermore, my findings reveal a threshold angular size for looming detection which is comparable to the ones seen in phylogenetically distant organisms, such as locusts. This result suggests that zebrafish larvae may use similar neuronal mechanisms to compute approach of a threatening stimulus and initiate escape as across animal phyla. Finally, this study also provides fundamental insights into how the brain makes complex evaluations of visual inputs to direct escape behavior in the face of impending threats.

Contents

List of Figures

List of Abbreviations

AF	Arborization field
CNS	Central nervous system
dpf	Days post fertilization
DS	Direction selective
DNA	Deoxyribonucleic acid
DLR	Dorsal light reflex
DiI	1,1'-Dioctadecyl-3,3,3',3'-Tetramethylindocarbocyanine Perchlorate
ET	Enhancer trap
EGFP	Enhanced green fluorescent protein
fps	Frames per second
GECI	Genetically encoded calcium indicator
GFP	Green fluorescent protein
GEE	Generalized estimating equations
GT	Gene trap
GCL	Ganglion cell layer
hpf	Hours post fertilization
IR	Infrared
IPL	Inner plexiform layer
INL	Inner nuclear layer
LGMD	Lobula giant movement detector
M-cell	Mauthner cell
nMLF	Nucleus of the medial longitudinal fasciculus
OKR	Optokinetic response

OMR	Optomotor response
ONL	Outer nuclear layer
OPL	Outer plexiform layer
RGC	Retinal ganglion cell
SC	Superior colliculus
SIN	Superficial interneuron
SO	Stratum opticum
SFGS	Stratum fibrosum et griseum superficiale
SGC	Stratum griseum centrale
SAC	Stratum album centrale
SPV	Stratum periventriculare
TL	Tüpfel long-fin
TeO	Optic tectum
UV	Ultraviolet

1 Introduction

1.1 The zebrafish as a model organism for systems neuroscience

One of the main goals of systems neuroscience is to understand how higher brain functions arise from individual neurons and their connections. From a simple perspective, genes underlie development and organization of specific neuronal cell types. Then, the neuronal activity in these specific cell types and networks orchestrates a particular behavior. To dissect the neuronal circuits in their relation to behavior, we need to gain quantitative insights into their structure and function. Importantly, we should establish causal relationships between the arising neuronal activity patterns and behavioral actions.

In the context of vision, our brain constantly transforms visual signals into meaningful inner representations of the outside scene. Light triggers a cascade of electro- and biochemical reactions after entering our eyes and falling onto our retina. The retina, with its specific cell types and circuits, is the first computational unit of visual processing (Azeredo da Silveira and Roska, 2011). Retinal ganglion cells (RGCs), output neurons of the retina, convey the initially processed information to higher visual areas in the brain for further, detailed processing. Ultimately, functionally specialized neurons respond to different features of the visual scene such as direction, orientation or speed of motion; size, texture and shape of an object in the visual field. By doing so, these selective neurons can signal the presence of a potential prey or predator in the visual field and trigger downstream neurons to direct an appropriate behavior. What are the cellular mechanisms underlying circuit level computations of the visual system? How do neuronal networks extract essential visual features? How can we tie these neuronal phenomena to perception and behavior?

Recent advances in genetic tools, high-resolution imaging methods for visualizing neurons within a circuit and manipulating neuronal activity during behavior enable us to dissect the circuits and their function. When we consider a model animal for circuit neuroscience in the light of these advances, we should take into account the size of the brain and the number of neurons it contains. The brain of a well-suited model organism should be small in number of neurons, yet sufficiently complex to generate various behaviors.

Known as an Indian freshwater teleost and originally introduced to laboratory research by Georg Streisinger (Streisinger et al., 1981), the zebrafish (*Danio rerio*) emerged as a promising vertebrate model organism initially for developmental biology and later on for neurophysiology and ethology. With a wealth of genetic and molecular techniques, imaging know-how and cellular manipulation methods available, the zebrafish quickly became an established, popular vertebrate model.

The zebrafish offers many advantages in laboratory research:

- Compared to the human brain with its 10^{11} neurons, the larval zebrafish contains approximately 100,000 neurons (Naumann et al., 2010) with the whole brain size about 300 µm thick, 400 µm wide and 800 µm long, eliminating high-level complexity while conforming to the basic vertebrate brain organization.
- During the early developmental stages the zebrafish larvae are transparent, allowing for sophisticated imaging and light-induced manipulation in an intact, behaving animal (Ahrens et al., 2013; Kubo et al., 2014).
- Numerous available transgenic lines and mutants ensure information from genetically defined population of neurons (Scott and Baier, 2009; Gahtan and Baier, 2004).
- Zebrafish has a rich behavioral repertoire, which provides insights into neural pathways and circuits (Kalueff et al., 2013).

All these facts make the small zebrafish larvae an ideal model animal to investigate neural substrates of visually mediated behaviors and distill knowledge by manipulating these relevant neural circuits.

1.2 The visual system of zebrafish

The zebrafish central nervous system consists of two major parts: the spinal cord and the brain; including forebrain, midbrain and hindbrain (Figure 1.1). While the spinal cord functions primarily in motor control, the brain is involved in sensory integration, processing and decision making. Specifically, the forebrain has the most complex structure in terms of connectivity and is involved in memory, basic emotions and olfactory processing. The hindbrain, with its reticulospinal neurons, is located between the midbrain and the spinal cord and controls locomotion. The optic tectum, constituting the dorsal part of the midbrain, is innervated by RGC axons presynaptically. Crucially, the optic tectum forms topographically ordered connectivity with retinal afferents to create a two dimentional map of the visual field. Thus, the midbrain processes visual information and directs the output to the hindbrain in order to control visually-mediated behaviors.

The zebrafish visual system is ideal for studying vertebrate vision since it possesses a canonical vertebrate retina. Moreover, it develops rapidly (Fleisch and Neuhauss, 2006), providing a broad repertoire of visually-guided behaviors at the age of only 5 days-post-fertilization (dpf). Thus, the visual system of translucent zebrafish larvae offers a valuable tool to dissect the circuits of visual feature processing at the cellular level.

1.2.1 Retina

The retina forms the neural layer of the eye and its specific, intricate structural organization is well conserved across all vertebrates. In zebrafish, a fully layered retina develops by 60 hours-post-fertilization (hpf) (Schmitt and Dowling, 1999) and consists of five neuronal cell types (photoreceptors, bipolar cells, horizontal cells, amacrine cells and retinal ganglion cells) and one type of glial cell (Mueller glial cells). In addition, the retina's laminar organization has an inverted structure, meaning that light has to pass through the entire neural retina to finally reach the photoreceptors, just before the pigment epithelium (see Figures 1.2 and 1.5) which absorbs the scattered light. Mueller glia cells span the

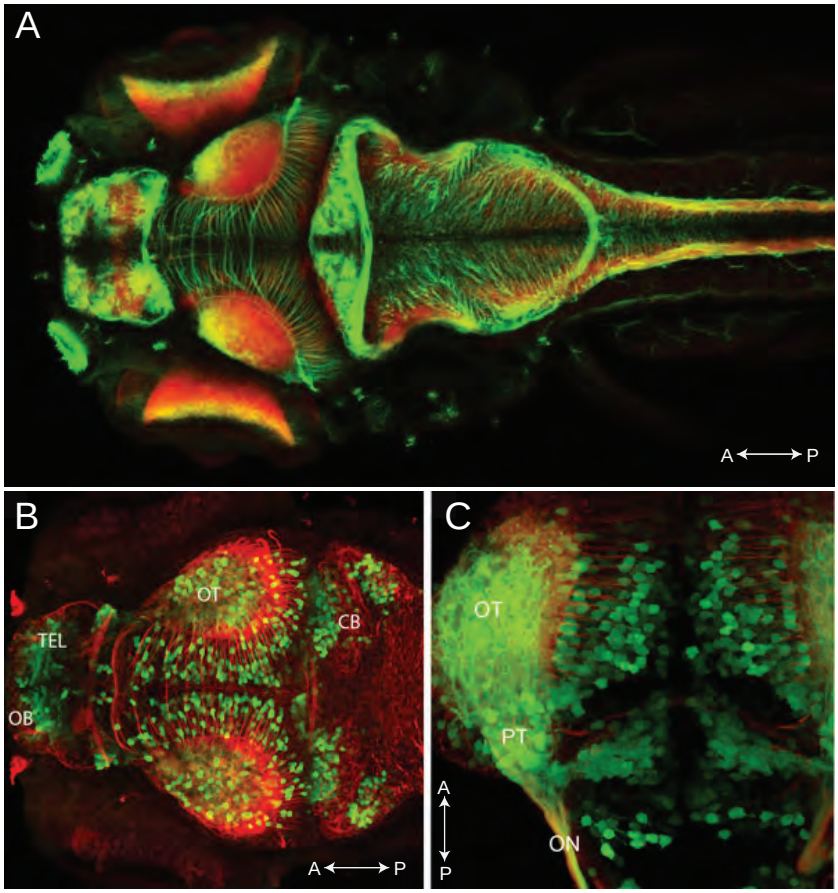

Figure 1.1: Larval zebrafish brain. **(A)** Dorsal view of the 4 dpf zebrafish brain showing axons (green) and neuropil (red). **(B)** Green fluorescent protein labels distinct population of neurons in *Tg(brn3a-hsp70:GFP)* transgenic line. OB: Olfactory bulb, TEL: Telencephalon, OT: Optic tectum and CB: Cerebellum. **(C)** Brain section of a 3 dpf larva expressing calretinin (green) and acetylated tubulin (red) in *Tg(1.4dlx5a-dlx6a:GFP)* transgenic line at the forebrain-midbrain boundary. PT: Pretectum and ON: Optic nerve. (**A** adapted from Zebrafish Brain Atlas, Jay Patel (http://zebrafishbrain.org/), **B** and **C** adapted from Steve Wilson Group webpage, UCL (http://www.ucl.ac.uk/zebrafish-group/research/neuroanatomy.php). A = anterior, P = posterior.

whole retina and are responsible for regeneration in case of any damage (Dyer and Cepko, 2000; Robel et al., 2011).

The retinal neurons are ordered by three nuclear and two synaptic (plexiform) layers, which makes the study of connectivity between neurons easy (Figure 1.2). The outermost layer, called outer nuclear layer (ONL), is populated by photoreceptors. Then comes the

outer plexiform layer (OPL), which builds the synaptic layer between the photoreceptors and inner nuclear layer (INL), where the horizontal, amacrine and bipolar cells (retinal interneurons) reside. Finally, the inner plexiform layer (IPL) forms the synaptic layer between the INL and the ganglion cell layer (GCL). The retina matures enough by 68 hpf to support the earliest visually mediated behavior, the startle response, in zebrafish (Kimmel et al., 1974; Easter and Nicola, 1996).

Photoreceptor cells are the primary light detecting elements in the retina that convert light into a chain of electrical signals. The zebrafish retina contains one type of rod photoreceptors and four types of cone photoreceptors with distinct spectral sensitivities as well as morphologies. Rod photoreceptors function at low light conditions whereas cone photoreceptors are adapted to bright light conditions. The peak spectral sensitivity for rods is approx. 500 nm whereas for cones they are approx. 410 nm for short-, approx. 480 nm for middle-, approx. 560 nm for long- and approx. 360 nm for ultraviolet-wavelength cones (Cameron, 2002). Therefore, including sensitivity to ultraviolet light, zebrafish have tetrachromatic vision as opposed to the trichromatic vision of humans. By 55 hpf, rod and cone photoreceptor outer segments become visible (Schmitt and Dowling, 1999) and by 70 hpf, photoreceptor synaptic terminals start to form on bipolar cells (Fleisch and Neuhauss, 2006). Visual information flows from photoreceptors to the retinal interneurons and by 5 dpf signal transmission becomes fully functional (Biehlmaier et al., 2003). Since rods develop later than cones in the zebrafish retina, larval vision is largely dominated by cones (Bilotta et al., 2001). Although Orger and Baier (Orger and Baier, 2005) showed that red and green cones contribute to the optomotor response (see section 1.3.2), while short-wavelength cones provide strong input to the phototaxis in larvae, behaviorally specific roles of different types of photoreceptors largely remain to be explored.

The retinal interneurons, namely horizontal, bipolar and amacrine cells, can be subdivided into several subtypes, based on their morphology, physiology and molecular specificity in the mammalian retina (Masland, 2001; Wässle, 2004; Sanes and Zipursky, 2010). In zebrafish, description and especially functional classification of these interneuron subtypes is not complete. Advances in transgenic methods has enabled labeling of specific

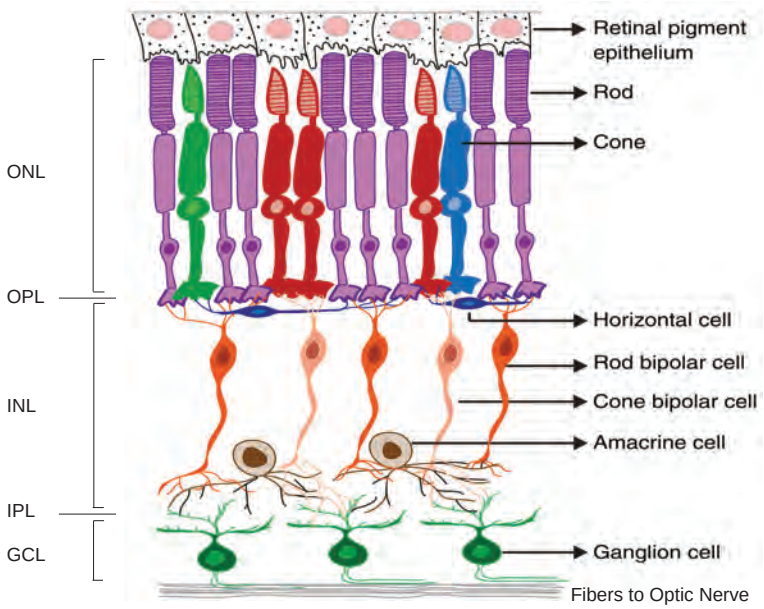

Figure 1.2: Top-to-down, apical-basal scheme of the vertebrate retina. Light travels from basal (lens down) to apical side. Main cell types are organized in three nuclear layers: the outer nuclear layer (ONL), the inner nuclear layer (INL) and the ganglion cell layer (GCL). Two synaptic layers, namely the outer plexiform layer (OPL) and the inner plexiform layer (IPL), interconnect the cells in nuclear layers. (Figure adapted from Ratnapriya and Swaroop (2013).)

cell types using, for example, cell type specific promoters (Cederlund et al., 2011); however, molecular markers only rarely label a single cell type. Thus, cellular morphology including the stratification pattern in the IPL is commonly used as a classification criteria. Jusuf and Harris (Jusuf and Harris, 2009) showed that there are at least 28 amacrine cell morphologies present in the larval zebrafish retina. Horizontal cells have been found to be of 4 types in zebrafish; large field rod-specific, large field UV responsive and two types of small field cone-specific horizontal cells, based on their connectivity and light sensitivity (Li et al., 2009; Connaughton and Nelson, 2010). Finally, 17 morphologically distinct bipolar cells have been recognized in zebrafish, which can be divided further into three subclasses based on their stratification pattern; ON, OFF and multistratified ON- and OFF type (Connaughton and Nelson, 2010; Connaughton et al., 2004; Ott et al., 2007). The exact number of retinal neuron subtypes are not known but speculated to be approx. 120 in the tetrachromatic teleost fish retina (Baier, 2013).

In the IPL, synapses between amacrine, bipolar and retinal ganglion cells form around 12 anatomically distinguishable sublaminae in zebrafish (Marc and Cameron, 2001; Yazulla and Studholme, 2001). While horizontal cells adjust the system's response to overall illumination by providing lateral inhibition to photoreceptors (Masland, 2001), amacrine cells together with bipolar cells innervate specific sublaminae and convey specific visual information, such as color, form, direction of motion or contrast, to the connected RGCs (Roska and Werblin, 2001; Azeredo da Silveira and Roska, 2011). Amacrine cells are the most diverse of the retinal cells (Masland, 2001). They shape and control RGC responses, although, for most of them, it is not known how specifically they function (Masland, 2001; Azeredo da Silveira and Roska, 2011). We do not know whether the larval retina contains most of the functionally characterized mammalian amacrine cells, but there is evidence that motion sensitive starburst amacrine cells exist in zebrafish (Kay et al., 2004; Maurer et al., 2010).

Bipolar cells form the pathway for direct information flow from photoreceptors to RGCs, which deliver the retina's output to the brain (see section 1.2.1.1). Bipolar and ganglion cells make excitatory synapses which are modulated by amacrine cells. Traditionally, the IPL is separated into the OFF sublayer, which is close to the INL and responsive to the offset of light, and the ON sublayer, which is close to the GCL and responsive to the onset of light. However, Odermatt *et al.* (Odermatt et al., 2012) recently showed that in zebrafish, this is not necessarily the case, since the OFF sublayer can also have ON-responsive bipolar cell terminals and vice versa. Perhaps, it is more meaningful to think about these parallel processing units not only as the ON and OFF sublayers but also consider their particular cell types and connectivity patterns that are dedicated to a specific visual feature (Wässle, 2004; Gollisch and Meister, 2010; Azeredo da Silveira and Roska, 2011).

1.2.1.1 Retinal ganglion cells

In 1953, Kuffler first proposed that RGCs are feature detectors rather than mere light detectors (Kuffler, 1953). In his work, he showed that RGCs did respond poorly to overall illumination but robustly to bright and dark edges. For example, some RGCs responded

well to a bright spot surrounded by a dark circle (ON-center RGCs) while others responded to a dark spot surrounded by a bright circle (OFF-center RGCs). These RGCs also extend their dendrites in different layers of the IPL, where they receive lamina-specified synapses from bipolar cells.

Neuroanatomical studies to classify retinal neurons began more than 100 years ago with Cajal (Cajal, 1972), who also suggested that neuronal structure and function are closely interrelated. Since then, identification of neuronal types has a great importance to understand the brain and its specialized circuits. In the context of vision, by identifying RGC types, we can learn about the type of signals that the retina sends to visual areas in the brain.

Everything the brain knows about the outside world visually is conveyed by the RGCs neuronal activity pattern. Each particular RGC type has an afferent circuit formed by a few other retinal neuron types (Azeredo da Silveira and Roska, 2011). So far, morphology (Cajal, 1972; Sümbül et al., 2014; Robles et al., 2014), gene expression (Huberman et al., 2009; Kay et al., 2011), regular spacing between neurons (Reese, 2010; Kay et al., 2012) and physiological properties (Levick, 1967; Roska and Werblin, 2003; Kim et al., 2008; Münch et al., 2009) have been used to classify RGC types. In mice, there are at least 25 RGC types performing specialized computations to encode particular features of the visual scene within their specialized circuit (Zhang et al., 2012; Roska and Meister, 2014) (Figure 1.3). A substantial amount of RGCs are dedicated to analyze motion direction: four ON-OFF RGC types, three ON types and one OFF type report direction of lateral object motion or global image drift (for reviews, see (Berson, 2008; Azeredo da Silveira and Roska, 2011)). More recently, Münch *et al.* (Münch et al., 2009) showed that, in mouse retina, approach motion elicited by looming stimuli is also detected by at least one RGC type. In addition, although the superior colliculus is one of the primary RGC projection areas in mice, different types of RGCs project to different brain areas, producing parallel channels of vision and influencing behavior (Morin and Studholme, 2014; Dhande and Huberman, 2014). For example, intrinsically photosensitive RGCs project their axons to two brain nuclei that control the hypothalamic circadian clock and pupillary light reflexes (Hattar et al., 2006;

Güler et al., 2008) while direction selective RGCs axons target superficial layers of superior colliculus, the brain structure involved in orienting behaviors (Kim et al., 2008).

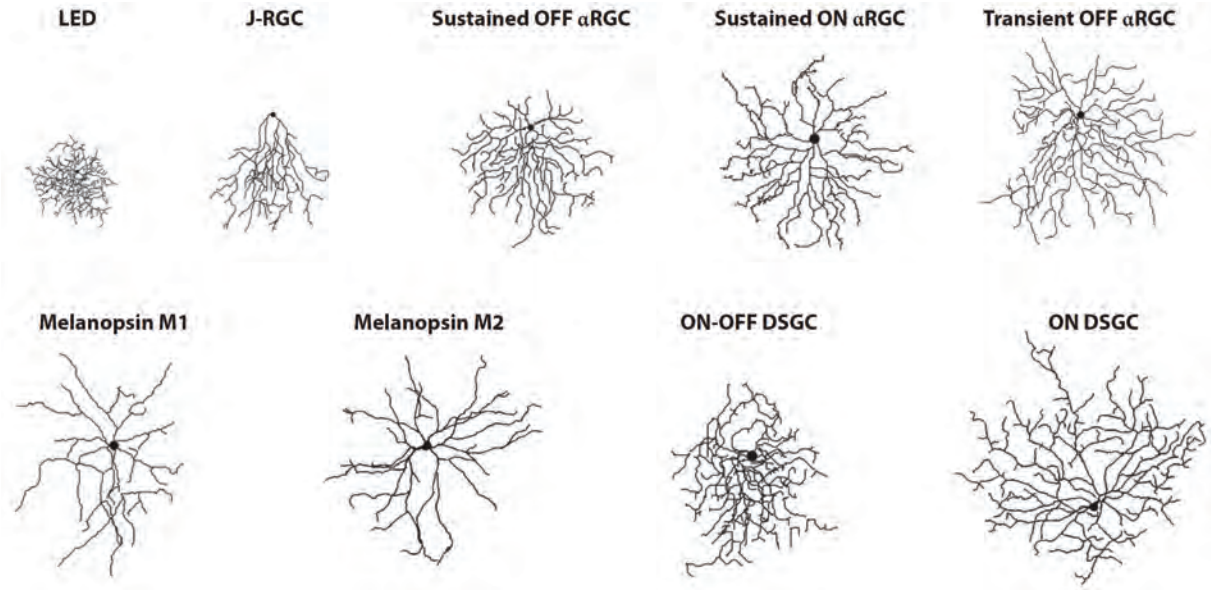

Figure 1.3: A selection of mouse retinal ganglion cell types. In mouse retina there are over 20 types of RGCs, some of which involve specific behaviors. While melonopsin RGCs regulate circadian entrainment, ON DSGCs support optokinetic reflex by projecting to nuclei of the accessory optic system. DSGC: directionally selective ganglion cell, J-RGC: junctional adhesion molecule B-positive RGC, LED: local edge detector. (Figure taken from Sanes and Masland (2015) with permission.)

In zebrafish, RGCs are born first in the retina (around 32 hpf), followed by the IPL interneurons (Schmitt and Dowling, 1999; Kay et al., 2001). Recently, Robles *et al.* (Robles et al., 2014) provided the complete connectivity map between the retina and the target visual areas in zebrafish. They showed that when both dendritic morphologies in the IPL and the axonal projection patterns in the brain are taken into account, at least 50 types of morphologically distinct RGCs exist in the larval zebrafish retina. They found that RGCs with similar dendritic morphologies can have different axonal projections and that many RGCs send axon collaterals to multiple visual areas. The cataloging of features that are encoded by these RGC types and their physiological characterization is an ongoing process. Based on their response properties to full field stimulation, Emran *et al.* (Emran et al., 2007) identified six classes of RGCs, including sustained, transient and ON-OFF charac-

teristics. More recently, it has been shown that direction and orientation selectivity are also implemented in RGCs (Nikolaou et al., 2012; Lowe et al., 2013).

1.2.2 Central projections of RGCs

At the larval stages, the main projection site of RGCs axons is the optic tectum (see section 1.2.2.1), homologous to the mammalian superior colliculus, which constitutes the dorsal aspect of the zebrafish midbrain (Burrill and Easter, 1994). In addition, by intraocular injection of lipophilic fluorescent dye and tracing the RGC axons, Burrill and Easter identified nine more retinorecipient nuclei, called arborization fields (AFs) (Burrill and Easter, 1994) referred to as AF1 to AF10 (Figure 1.4). Specific RGC types project their axons to one of these AFs or multiple AFs, make connections with target cells to establish a representation of the visual field in the brain.

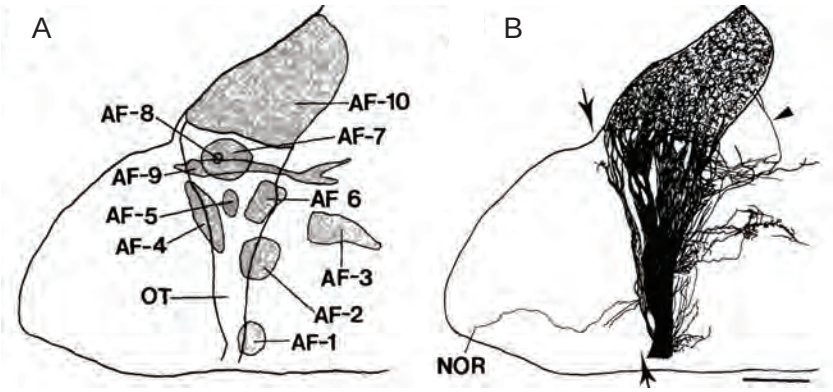

Figure 1.4: Retinal projections in the zebrafish. **(A)** Schematic lateral view of the ten retinorecipient areas (arborization fields) in 6-7 dpf larva, revealed by intraocular injections of DiI. **(B)** Camera drawing of DiI labeled ganglion cell axons and their innervation sites. Dorsal, up; Rostral, left, scale bar represents 50 µm. (Figure adapted from Burrill and Easter (1994).)

So far, little is known about the behavioral functions of extratectal AFs, although it is clear that for the execution of a particular visual behavior, one or few of these nuclei should act together (Ullén et al., 1997; Kubo et al., 2014; Semmelhack et al., 2014). It has been shown that AF7 is predominantly innervated by particular bistratified RGCs that are highly selective in their responses to prey-like visual stimuli (Semmelhack et al., 2014; Robles et al.,

2014). Indeed, ablation of the RGC axons innervating in AF7 impairs the prey-capture behavior in the larval zebrafish. Similarly, neurons surrounding AF9 have been shown to be involved in global optic flow processing (Roeser and Baier, 2003; Kubo et al., 2014).

1.2.2.1 Optic Tectum

The optic tectum, also called AF10, is the biggest retinorecipient area in zebrafish larvae and has been intensively studied. 97% of the RGCs send their axons to the tectum and innervate discrete layers (Robles et al., 2013). Similar lamination of retinotectal axons has been observed in many species from birds to mammals (see review (Huberman et al., 2010)). RGCs project their axons into ten distinct laminae that are stacked on top of each other: the stratum opticum (SO), forming the most superficial layer with its two sublaminae, the stratum fibrosum et griseum superficiale (SFGS), which in turn splits into six sublaminae, the stratum griseum centrale (SGC) and finally the deepest layer stratum album centrale (SAC) and the stratum periventriculare (SPV) (Robles et al., 2013) (Figure 1.5). RGCs usually innervate only one layer, although they may form collaterals in other extratectal visual areas (Xiao and Baier, 2007). Recently, application of the Brainbow (Livet et al., 2007) technique in the zebrafish retina revealed the complexity of precise laminar organization of the RGC axons in the tectum (Robles et al., 2013). Moreover, RGCs project their axons in a retinotopic manner, meaning that RGCs from dorsal retina terminate in the ventral tectum and vice versa, and RGCs from temporal retina terminate in the anterior tectum and vice versa (Robles et al., 2014). In addition, the tectum receives afferent inputs from other sensory modalities (auditory, somatosensory, lateral line, etc.) which form other sensory maps deeper in the tectum (Nevin et al., 2010).

In zebrafish, each tectal lamina is innervated by several RGC types with different dendritic morphologies (Robles et al., 2013). To investigate how this laminar organization of RGC axons relates to the functional specialization in the tectum, several studies employed two-photon *in vivo* calcium imaging in the tectum, using genetically encoded calcium indicators of the GCaMP family (see section 1.4.2). First, Nikolaou *et al.* (Nikolaou et al., 2012) imaged the axon terminals of RGCs, expressing SyGCaMP3, in the retinotectal neuropil

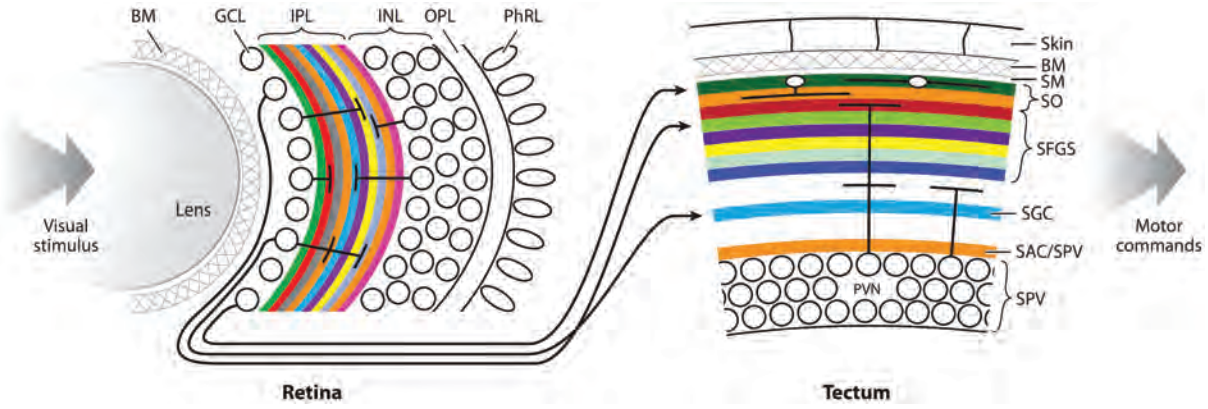

Figure 1.5: Retinal ganglion cell projections to the optic tectum. Schematic depiction of ganglion cell axons receiving input from different layers in IPL and via the optic nerve, project to the optic tectum. RGC axons innervate in the tectal neuropil by forming approximately ten distinct layers. Cell bodies of tectal cells extend their axons and dendrites into the neuropil. BM: basement membrane, GCL: ganglion cell layer, PhRL: photoreceptor layer, SAC: stratum album centrale, SAC/SPV: boundary between SAC and SPV, SFGS: stratum fibrosum et griseum superficiale, SGC: stratum griseum centrale, SM: stratum marginale, SO: stratum opticum, SPV: stratum periventriculare.(Figure taken from Baier (2013) with permission.)

while presenting drifting bars in different directions and orientations in the visual space. By doing so, they discovered that there are three subtypes of direction-selective and two subtypes of orientation-selective retinal inputs to the tectum. Moreover, these two selective responses are organized in a reasonably segregated manner within tectal laminae (Figure 1.6). In a follow-up study, Lowe *et al.* (Lowe et al., 2013) explored these parallel direction and orientation maps further and found that visual experience is not necessary for the establishment of direction maps, yet it is required for the formation of orientation maps. Furthermore, they identified two additional orientation-selective subtypes of RGC inputs to the tectum. Second, Gabriel *et al.* (Gabriel et al., 2012) combined Ca^{2+} imaging of RGC axons terminating in the tectum with targeted patch clamp recordings of genetically labeled tectal neurons. When they compared the tuning of direction-selective retinal inputs with the tuning of postsynaptic tectal neurons, they discovered two types of direction-selective tectal interneurons: one group received direct input from direction-

selective (DS) RGCs and the other group did not receive direct DS-RGC input, although responding direction-selectively.

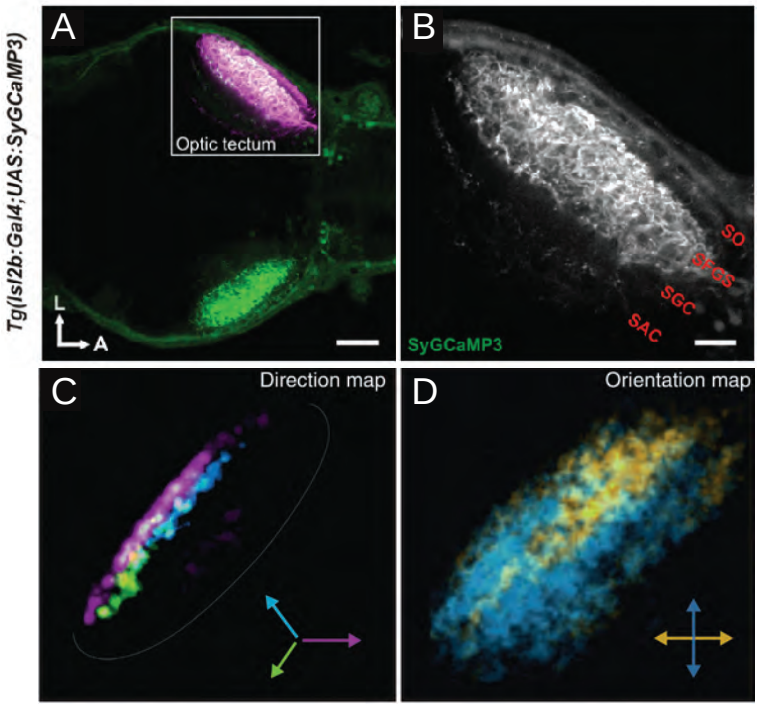

Figure 1.6: Functionally distinct, parallel retinal maps in the tectum. **(A)** 7 dpf transgenic zebrafish larva Tg(Isl2b:Gal4;UAS:SyGCaMP3), expressing SyGCaMP3 in RGC axons and **(B)** magnified view of the boxed region. (Dorsal view) **(C)** Color coded spatial, composite map of direction-selective and **(D)** orientation-selective RGC axons in the tectal neuropil. A = anterior, L = lateral. Scale bars represent 50 µm in **(A)** and 20 µm in **(B)**. (**A** and **B** adapted from Nikolaou et al. (2012), **C** and **D** adapted from Dhande et al. (2013).)

Previously, Niell and Smith (Niell and Smith, 2005) described receptive field sizes, topography, size and direction-selectivity of tectal cell populations and showed that most of these properties are established without a requirement of visual experience. Layer specific tuning of different object sizes was attributed to an inhibitory interneuron type, superficial interneurons (SINs) (Del Bene et al., 2010). Depending on their dendritic target layer in the tectal laminae, SINs process small- and large-size-selective signals, filtered by functionally organized RGC inputs (Preuss et al., 2014). Collectively, RGC axon terminals positioned in distinct tectal laminae can have tuning properties similar to their target postsynaptic partners. Yet, Hunter *et al.* (Hunter et al., 2013) showed that direction tuning properties of retinal input can be transformed by the tectal cells to generate response

properties *de novo*. Combined, all the abovementioned studies suggest that different RGC types convey information about distinct visual features and converge on a specific lamina, generating parallel maps of feature selectivity.

1.3 Zebrafish innate visual behaviors

Remarkably, the visual system of zebrafish matures rapidly and becomes fully functional at 5 dpf (Fleisch and Neuhauss, 2006). At this stage, the larvae are already heavily dependent on vision and perform a plethora of complex visual behaviors (Portugues and Engert, 2009; Fero et al., 2011). For example, they use eye movements to track objects moving in their visual field and stabilize visual flow on the retina.

To elucidate the mechanisms underlying these complex behaviors, zebrafish have been broadly used as a model organism. Little is known about the environmental impact of the laboratory on the zebrafish behavioral repertoire that we can observe, interpret and generalize. However, many of these visual behaviors can be triggered by specific artificial visual stimuli in the laboratory. Among these visually mediated behaviors, the optomotor response (OMR) (Muto et al., 2005), the optokinetic response (OKR) (Easter and Nicola, 1997) and prey-capture (Gahtan et al., 2005) have been widely studied. However, although previous experiments have addressed adult visual escape responses (Dill, 1974a; Li and Dowling, 1997) and acoustic or tactile stimuli mediated escape dynamics (Kohashi and Oda, 2008), the mechanisms of visual escape response in larval zebrafish remain less studied and poorly understood. In the following sections, I will summarize what is known about these behaviors in larval zebrafish and the relevant circuit mechanisms.

1.3.1 Optokinetic response

The optokinetic response (OKR) develops between 73 and 80 (hpf) (Easter and Nicola, 1997) and is one of the most robust behaviors in the larval zebrafish. When a larva is presented with moving objects across the visual field, its eyes follow the object smoothly and reset their position with a quick saccadic movement in the opposite direction after the

object has left the visual field (see Figure 1.7A). Humans also have similar eye movements; for example, when we sit in the car and watch the objects passing by through the window (Schweigart et al., 1997). Zebrafish larvae do not show habituation of this behavior and perform these eye movements as long as the stimulus is presented even when the larva is immobilized. These characteristics make OKR response attractive for quantitative psychophysics and imaging.

OKR has been extensively studied in response to a drifting sine-wave grating of black and white vertical bars (Figure 1.7A). Behavioral genetic screens revealed genes that are essential for visual development and function, and mutations that caused striking OKR deficits (Brockerhoff et al., 1995; Neuhauss et al., 1999). For example, *no optokinetic response* (*nrc*) mutants have synaptic defects in ON retinal ganglion cells and show no OKR, suggesting the necessity of the ON pathway for this behavior (Emran et al., 2007).

Recent studies dissected the brain areas and neural networks that further process this innate reflex (Kubo et al., 2014; Portugues et al., 2014; Schoonheim et al., 2010). Previously, it was shown that unilateral ablation of the optic tectum does not affect the OKR performance in general, except the saccade rate which is lower in the ablated side (Roeser and Baier, 2003). This result shows that the optic tectum is not necessary for the execution of OKR, suggesting an existence of an extratectal visual area essential for the OKR. Optogenetic perturbations in transgenic larvae demonstrated that the area pretectalis (APT) is necessary and sufficient for the OKR (Kubo et al., 2014). Calcium imaging in the APT during the OKR revealed functionally segregated neurons and direction-selective responses that are correlated with the behavior. In addition, whole-brain imaging during the OKR found a bilaterally symmetrical distributed neuronal network (Portugues et al., 2014). The combination of these activity maps from many larvae demonstrates a stereotypical functional architecture localizing sensory and motor signals into defined brain areas. Downstream neurons that generate saccades during OKR have been discovered in the hindbrain, in rhombomere 5 (Schoonheim et al., 2010).

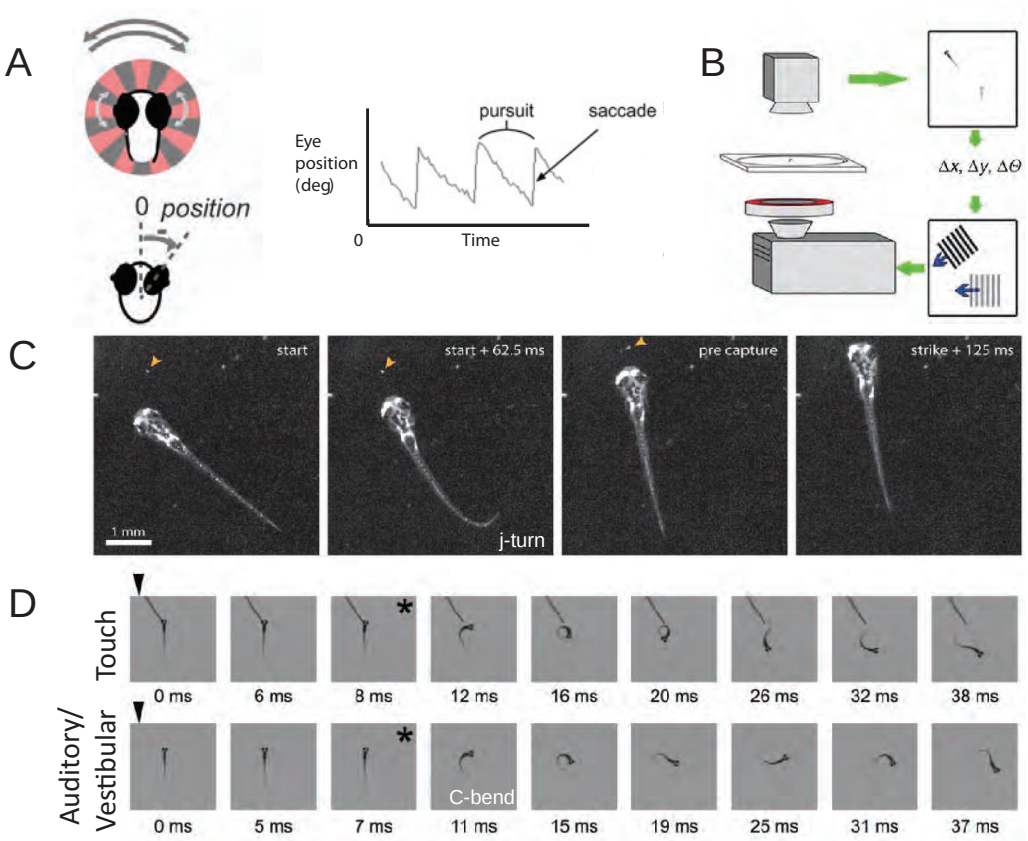

Figure 1.7: Larval zebrafish behaviors. **(A)** Optokinetic response of larval zebrafish to a rotating radial grating, presented below the larva. Eyes follow the direction of motion, quickly resetting their positions with saccades. **(B)** Setup for optomotor response triggered by gratings drifting in different directions in freely swimming larva. The fish reorients its body axis and swims in the direction of visual motion. **(C)** Prey capture behavior divided into multiple phases of actions. Orange arrowhead indicates a paramecium. In the first frame the larva identifies the prey. In the second and third frame, the larva orients itself towards the paramecium with subtle J-turns and accompanying eye convergence movements which are followed by a capture swim in the last frame. **(D)** Escape behavior evoked by head-tactile and auditory/vestibular stimuli in freely swimming larva. Arrowheads and asterisks denote stimulus and behavioral onsets, respectively. For the definition of "C-bend", see section 1.3.4. (**A** adapted from Portugues et al. (2014) and Roeser and Baier (2003), **B** adapted from Orger et al. (2008), **C** adapted from Bianco et al. (2011) and **D** adapted from Kohashi et al. (2012).)

1.3.2 Optomotor response

While OKR is only concerned with the visually induced eye movements, the optomotor response (OMR) is a visually induced locomotion used by the fish to stay stationary in moving water (Figure 1.7B). OMR develops in the larval stages of zebrafish, from 5 dpf on, and can be reliably evoked at 7dpf (Neuhauss et al., 1999). Importantly, the OMR can be triggered in immobilized larvae (Thiele et al., 2014). When the larva is presented with a wide-field motion stimulus from below (similar to OKR stimuli; yet, translational motion instead of rotational), the larva reorients its body axis and starts to swim in the perceived direction of motion. Defective OMR was observed in mutants with specific anatomic phenotypes (Rick et al., 2000; Neuhauss, 2003); however, the underlying neural circuitry processing translational motion stimuli remains largely unknown.

Bilateral ablation of the optic tectum does not affect the OMR performance of the larvae (Roeser and Baier, 2003), suggesting a presence of an extratectal pathway for processing of OMR stimuli. Besides, the chromatic inputs from both red and green cones strongly contribute to the OMR of larval zebrafish (Orger and Baier, 2005). More recent studies focused on the downstream circuitry that generate and control the locomotion behavior during OMR (Orger et al., 2008; Huang et al., 2013; Thiele et al., 2014; Severi et al., 2014). In fish, neurons located in the hindbrain and projecting all through the spinal cord are called reticulospinal neurons. These neurons are primarily responsible for the tail motion during swimming. By backfilling the reticulospinal neurons (approx. 300 neurons) with a calcium indicator dye and *in vivo* two-photon imaging, it was shown that only a small portion of these neurons are responsible for left or right turns during OMR (Orger et al., 2008). In addition, the neurons in the midbrain nucleus of the medial longitudinal fasciculus (nMLF) are involved in eliciting forward locomotion.

1.3.3 Prey capture

One of the most complex behaviors that larval zebrafish perform is prey tracking and capture. It develops as early as 4 dpf as the yolk is slowly degrading and the mouth is pro-

truding for the animal to hunt food, such as paramecia (Kimmel et al., 1995; Budick and O'Malley, 2000; Borla et al., 2002; Gahtan et al., 2005). Prey capture is actually a chain of complex sub-behaviors consisting of identifying prey visually, with possibly an involvement of chemosensation. This behavior consists of movements orienting the body axis towards prey and tracking it with a series of routine turns called J-turns, which are subtle, low-angle turns, and forward slow swims, finally followed by capture (Figure 1.7C). In addition to this series of fine axial locomotion activities, the larva converges its eyes at the beginning of each hunting episode, almost together with J-turns, which are exclusively used to track the prey (Bianco et al., 2011; Patterson et al., 2013).

Prey capture assays developed for freely swimming larvae were initially simple, involving high-speed camera recording of few larvae in a petri dish to quantify the behavior kinematics and counting the paramecia over time as the larvae hunt. Essential function of vision was shown by Gahtan *et al.* (Gahtan et al., 2005). The wild-type larvae in darkness and the *lakritz* (*lak*) mutants, which are known to be blind due to lacking all RGCs (Kay et al., 2001), can not perform prey capture successfully (Gahtan et al., 2005). Unilateral and bilateral ablations of the tectum showed that prey capture primarily depends on an intact optic tectum. This result is not surprising since the tectum has a fine-grained retinotopic organization that is crucial in localizing objects in visual space and thus in orienting movements (Ewert et al., 2001; Doubell et al., 2003) (see section 1.2). Finally, the downstream neurons that coordinate prey capture behavior were found by ablation of two pairs of identified reticulospinal neurons (MeLc and MeLr) in the nMLF. Ablation of MeLc and MeLr impairs the fine orienting turns while leaving spontaneous swims, OKR and OMR unaffected (Gahtan et al., 2005).

Bianco *et al.* (Bianco et al., 2011) developed a virtual reality assay to monitor and quantify the behavior in real time with machine learning algorithms. They found that the zebrafish larvae responds to approx. 1° moving dots on the screen with prey capture while larger size (approx. 10°) moving dots trigger aversive turns. They adapted their assay for head-restrained larvae, in which they left the eyes and tail of the larvae free to move, to record the eye movements during hunting routines. They proposed that convergence of the eyes

enhances the binocular visual space, increasing the chances of a successful hunt. This was the first time that artificial visual stimuli with specific size, speed and contrast properties were shown to trigger the naturalistic prey capture both in freely swimming and head-restrained zebrafish larvae. Later, in a closed-loop virtual reality setup, it was found that prey capture movements can be elicited with a narrow range of size and speed of the stimuli in head-restrained larvae (Trivedi and Bollmann, 2013).

Behavioral experiments demonstrate that size is an important parameter for an object to be perceived as a prey or predator (Colwill and Creton, 2011; Trivedi and Bollmann, 2013). How does the larvae detect prey-like stimuli? What are the building blocks of this size selectivity in the visual system? In their seminal work "What the Frog's Eye Tells the Frog's Brain", Lettvin and his colleagues (Lettvin et al., 1959) described how complex visual features are extracted by the output neurons of the eye, the RGCs. They introduced the concept of 'feature-detection' in the visual system, meaning that the behaviorally most relevant features are filtered and extracted by specialized visual channels. For example, they found a subset of RGCs that respond best to small moving stimuli on a stationary background, the so-called 'bug-detectors'. These RGCs would then trigger downstream circuits to generate prey capture movements. Although we know that small moving objects (such as paramecium) trigger prey capture behavior whereas large moving (predator-like) objects trigger aversive turns in zebrafish larvae, the neural substrates of size perception remain elusive.

Recently a study combined a virtual reality setup with *in vivo* electrophysiology and two-photon calcium imaging, and showed that a subset of RGCs provides size-selective responses into the tectum (Preuss et al., 2014). Intriguingly, the responses to prey-like stimuli targeted superficial layers of the tectum, while the responses to predator-like, large size stimuli were mostly restricted to the deeper layers. In addition, size-selective responses in tectal neurons are shaped by intratectal circuitry (Del Bene et al., 2010). A subset of postsynaptic tectal cells, the superficial interneurons (SINs), processes size-selective responses depending on their dendritic position in the tectum (Preuss et al., 2014). This study is the first to show that the retina can filter size information in the visual system of larval ze-

brafish. However, a set of behavior experiments which proves that the visual stimuli used in the study can efficiently evoke approach or aversive turns is missing.

Two recent studies focused on the neural circuit underlying prey recognition in zebrafish larvae (Semmelhack et al., 2014; Bianco and Engert, 2015). Two-photon calcium imaging of RGC axons in head-restrained larvae revealed that a small extratectal visual area, AF7 (see section 1.2), is specifically activated by the optimal prey stimulus or real prey, paramecia (Semmelhack et al., 2014). The RGCs projecting to AF7 belong to two types and have collaterals in the tectum (Robles et al., 2014). Moreover, laser targeted loss of function experiments in AF7 result in impaired prey capture, suggesting that AF7 acts as a hub for prey recognition. In addition, it was shown that a subset of postsynaptic neurons with arbors in AF7 projects to the nMLF and to the hindbrain as well as to the optic tectum. Another study proposed the optic tectum to be the area that underlies visual prey recognition (Bianco and Engert, 2015). Combining a virtual prey capture assay with two-photon functional imaging in the optic tectum during naturalistic behavior, Bianco and Engert showed that highly selective tectal neurons appear to link the prey perception to hunting responses.

1.3.4 Startle and escape responses

Visual startle and escape responses are evolutionary conserved, adaptive behaviors in zebrafish but remain less studied and poorly understood especially in larval stages. Visual startle response is defined as immediate, rapid locomotor responses of the larvae to aversive stimuli, such as sudden luminance changes in the environment (Kimmel et al., 1974; Easter and Nicola, 1996; Burgess and Granato, 2007; Liu and Hale, 2014). This response can be observed in the larvae as early as 3 dpf (Easter and Nicola, 1996). For most aquatic vertebrates, startle response patterns can be classified into three distinct body-bending axial movements: the C-bend, withdrawal, and S-bend (Liu and Hale, 2014). Withdrawal is often seen in elongate species with more vertebrae such as larval lamprey (Currie and Carlsen, 1988) and has not been reported in zebrafish. While the S-bend often involves small head rotation angles with S-shaped body bend and triggered by caudal aversive

stimulation, the C-bend turn is described as the rapid body bend into a C-shape with head rotating away from the stimulus, followed by a fast-burst swim and often triggered by rostral stimulation (Liu and Hale, 2014). Both C-bend and S-bend escape responses are reported in zebrafish (Burgess and Granato, 2007; Liu et al., 2012).

Kinematic analysis of visually evoked turns in the larvae in response to abrupt light increment and decrement revealed that turns that are evoked by increased luminance resembled the large amplitude C-bend turns (Burgess and Granato, 2007) (Figure 1.7D) that can also be seen in acoustic or tactile stimuli triggered startle responses in zebrafish larvae (Kohashi and Oda, 2008). The direction of C-bend turns is always away from the stimulus (here, a sudden light flash), probably to propel the fish away from the disturbance. In contrast, dark flashes induce O-bend turns, producing near circular body bend, which are directed towards the dark flash stimulus (Burgess and Granato, 2007). Moreover, ablation of both Mauthner cells, i.e. two pairs of reticulospinal neurons in the hindbrain of teleost fish that are known to be excited by visual stimuli in adult goldfish fish (Zottoli et al., 1987), does not affect the O-bend turns.

Zebrafish not only hunt prey but they can be on the menu themselves too. Escaping (or avoiding) approaching predators is another innate visual behavior of zebrafish. In nature, predators of zebrafish include adult fish and avian predators (Engeszer et al., 2007). It was shown that a behavior setup where a freely swimming adult zebrafish is placed in the middle of a cylindrical arena and a dark paper swept around a cylinder as a threatening object, is sufficient to evoke robust avoidance responses (Li and Dowling, 1997). Moreover, a display of large spots that oscillate back and forth below the swim chamber of freely swimming larvae also induces avoidance responses (Colwill and Creton, 2011). Approaching objects induce an expanding dark spot growing on the retina. A looming stimulus, which is an expanding dark object on a bright background, thus mimics the approach of a predator or an impending collision. We do not know how larvae respond to looming stimuli. A previous study by Emran *et al.* showed "dimming detectors"-like OFF RGCs in the zebrafish retina by 5 dpf (Emran et al., 2007). However, their involvement in visually evoked escape behavior, e.g. by looming stimuli, is not known. The importance of

avoiding collision and predation suggests the evolution of a hard-wired dedicated neural pathway for the detection of looming.

In a classic study with adult zebrafish, Dill (Dill, 1974a) showed that artificial model predators approaching with a constant speed towards the fish can trigger the same defensive escape responses as the real predators. The rate of change of the visual angle that is subtended by the predator at the prey's eye is found to be the threshold parameter (approx. $25°/s$) for the zebrafish to flee (Dill, 1974a). In addition, Dill (Dill, 1974b) showed that repetitive presentation of looming stimuli to the adult zebrafish evokes quicker escape responses, suggesting the existence of a sensitization mechanism in looming-triggered escape responses. It would be interesting to know whether this is also true for the larval zebrafish and whether the same looming stimuli parameters can evoke escape responses in zebrafish larvae too. Finally, in other species, neurons that detect looming stimuli were found in retina (Münch et al., 2009), optic tectum (Nakagawa and Hongjian, 2010; Liu et al., 2011) and thalamus (Sun and Frost, 1998). However, the behavioral responses to looming stimuli and the mechanisms underlying looming mediated escape in larval zebrafish remain to be explored.

At the downstream level, electrophysiological recordings showed that the Mauthner cells and its homologues are strongly correlated with the C-bend escapes in adult goldfish in response to looming stimuli (Preuss et al., 2006). It was also shown that the Mauthner cells play a crucial role in short-latency, fast escapes in response to tactile or acoustic stimuli in larval zebrafish (Kohashi and Oda, 2008). While the Mauthner cells receive tectal inputs (Zottoli et al., 1987), it is still unknown whether the looming response in zebrafish is mediated by the Mauthner cells. Specifically, light flashes have been shown to prime the Mauthner cells (Mu et al., 2012), although they do not evoke startle responses themselves.

1.3.5 Phototaxis

The other known visual behavior relevant to luminance changes in the environment is phototaxis (Brockerhoff et al., 1995; Burgess et al., 2010; Chen and Engert, 2014). Phototaxis (or Photokinesis) is defined as orientation movements in response to light. It can

be either towards the light (positive, a.k.a. Scotophobia) or away from the light (negative, a.k.a. Scototaxis) (Ahmad et al., 2012; Maximino et al., 2011). Both positive and negative phototaxis can be observed in zebrafish larvae after 3 dpf (Orger and Baier, 2005) and persist through adulthood.

Recently, Chen and Engert (Chen and Engert, 2014) addressed whether temporal changes in the luminance without direct spatial information contribute to phototaxis. They developed a virtual circle assay in which an invisible circular boundary is defined within a uniformly illuminated arena. Whenever the larvae crossed this invisible border, they turned off the lights in the arena. They found that despite the absence of direct spatial cues, trajectories of the larvae were very well confined in the virtual circle, suggesting a mechanism relying on temporal integrations. A previous study in frogs showed that phototaxis is mediated by the thalamus (Kicliter, 1973), suggesting the existence of an extratectal pathway for this behavior. Indeed, Fernandes *et al.* (Fernandes et al., 2012) described a light-seeking behavior in the blind zebrafish larvae through deep brain photoreceptors; however, differences in locomotor kinematics suggest that these two phototactic behaviors are different. The neuronal substrates of phototaxis still remain to be explored.

1.4 Tools to dissect neuronal circuits and function

Over the past several years of zebrafish research, many tools have been developed for dissecting neural circuits and are continuously improved. These tools include:

- Transgenic approaches that have enabled us to target and visualize particular cell types (Kawakami et al., 2004; Asakawa and Kawakami, 2008; Scott and Baier, 2009; Clark et al., 2011).

- Genetically-engineered, fluorescence-based Ca^{2+} indicators to probe different cellular functions (Higashijima et al., 2003; Ahrens et al., 2012; Chen et al., 2013; Berlin et al., 2015; Fosque et al., 2015).

- High resolution neural activity imaging (Denk et al., 1990; Kerr and Denk, 2008; Vladimirov et al., 2014) and reconstruction techniques (Helmstaedter et al., 2008).

- Light-activated molecular tools to switch ion-channels and pumps on and off in behaving animal (Fenno et al., 2011; Packer et al., 2013).

- Other chemical or photo-inducible probes to permanently silence neurons (Bulina et al., 2006; Curado et al., 2008; Koide et al., 2009).

All these methods are increasingly exploited in translucent zebrafish larvae to establish a causality between patterns of neural activity of specific cell populations, the function of the neural circuits and the behavior. Below, I will focus on the tools that I used for my project and provide a brief introduction.

1.4.1 Transgenesis tools

Perhaps, one of the most important steps in circuit neuroscience is the development of targeted gene expression systems that enable us to express transgenes in specific subsets of neurons (Luo et al., 2008). Stable transgenic lines labeling selected cell types are usually generated by injection of DNA constructs including promoter sequences into the embryo at one-cell stage (Nüsslein-Volhard and Dahm, 2002; Detrich et al., 2004). Thanks to the Tol2 transposon system introduced by Kawakami *et al.* (Kawakami et al., 2004), generation of transgenic zebrafish lines has become efficient. Transposon-mediated transgenesis methods are followed by enhancer trap (ET) and gene trap (GT) screens, in which a promotor sensitive to enhancer/gene regulatory elements, is linked to a marker gene and randomly inserted into the genome (Trinh and Fraser, 2013). Combining ET and GT approaches with the two-component Gal4/UAS system allowed more flexible targeting of transgenes and produced several zebrafish transgenic lines expressing Gal4 in restricted neuronal populations (see below, section 1.4.1.1). Other methods for generating gene expression pattern libraries in zebrafish include TeT (Zhu et al., 2009), LexPR/LexA (Emelyanov and Parinov, 2008), Cre/LoxP (Boniface et al., 2009) systems, bacterial artifi-

cial chromosome (BAC) transgenesis (Suster et al., 2011) and more recently CRISPR/Cas systems (reviewed in (Sander and Joung, 2014) and (Hisano et al., 2015)).

1.4.1.1 The Gal4/UAS system

Targeted gene expression by the Gal4/UAS system was first introduced in *Drosophila* (Brand and Perrimon, 1993) and quickly became one of the most powerful techniques for analyzing the function of cells *in vivo* in zebrafish (reviewed in (Asakawa and Kawakami, 2008)). This two component system utilizes independent activator/driver (Gal4) and responder (UAS) lines. By crossing Gal4 zebrafish lines harboring various driver genes to zebrafish with a responder gene downstream of UAS, the transgene is expressed specifically in a defined set of cells (Figure 1.8). Combining this approach with hundreds of gene/enhancer trap lines that have been generated by the zebrafish community allows a flexible targeting of defined circuits (reviewed by (Baier and Scott, 2009; Kawakami et al., 2010)).

Previous studies have successfully exploited this combinatorial system along with the large-scale enhancer trap screens to express any genetically encodable probe linked to UAS in any defined pattern, expressing Gal4. For example, in one of the early studies, Scott *et al.* (Scott et al., 2007; Scott and Baier, 2009) made use of a photoconvertible fluorophore Kaede linked to UAS in order to characterize the expression pattern of the Gal4-driven trapped enhancers. In the same manner, genetically encoded calcium indicators (Naumann et al., 2010; Muto et al., 2013), chemical probes (Davison et al., 2007; Koide et al., 2009), and ion channels (Thiele et al., 2014) or receptors (Wyart et al., 2009) can be easily inserted into defined neural populations to perturb and explore the function of a desired circuit in an intact zebrafish.

The use of the Gal4/UAS system in enhancer trapping has also its drawbacks. First of all, finding tissue or cell type specific promoters can still be challenging. Secondly, Scott *et al.* (Scott et al., 2007) reported that Gal4 toxicity may cause lethality, although it was observed only in a small proportion of the generated patterns. Importantly, the expression of various marker proteins often varies, resulting in mosaic expression. It has been previously

shown that UAS-driven transgenes are susceptible to variegation due to their tendency to methylation (Goll et al., 2009). Finally, background expression, for example in muscles, may interfere with the expression of trapped enhancers. This can be improved by identifying a basal trapping promoter with minimal background expression (Scott et al., 2007).

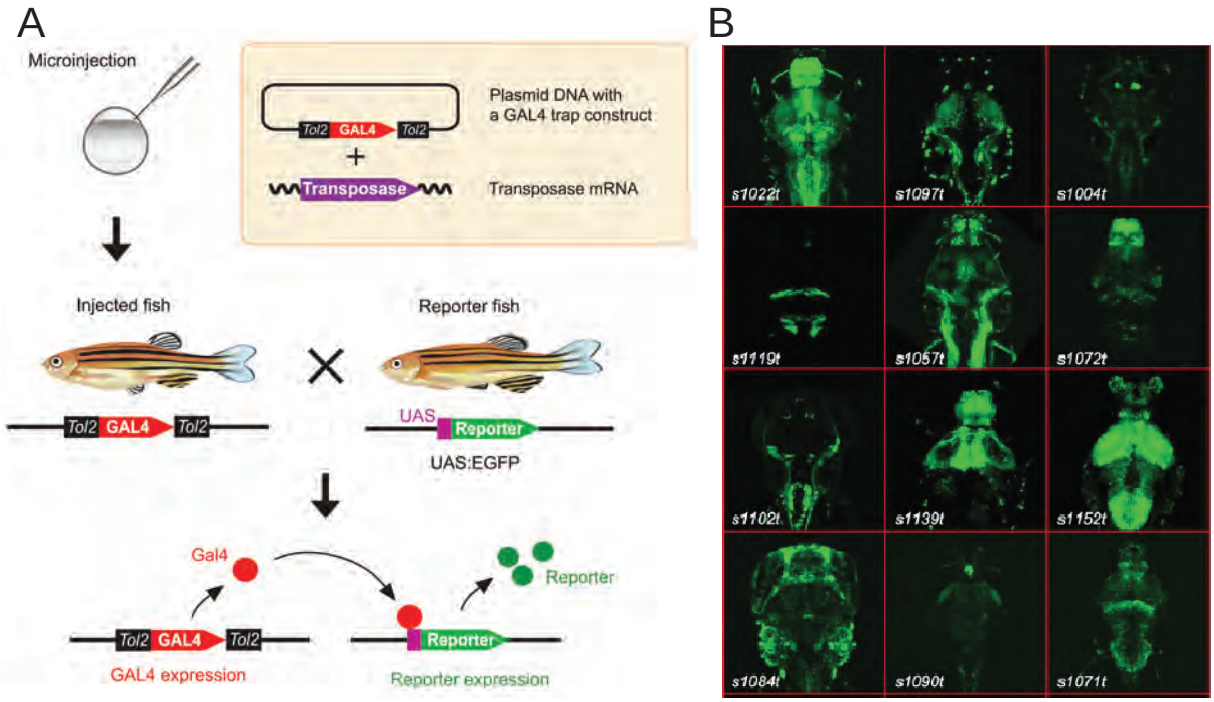

Figure 1.8: Generation of transgenic zebrafish using the Gal4/UAS system. **(A)** Gal4 trap DNA constructs containing specific promoter elements are injected into fertilized zebrafish eggs at single cell stage. This construct is integrated in the genome and a growing embryo will express the gene of interest. When this transgenic fish carrying the Gal4, which is expressed only in a specific subset of neurons, crossed with the UAS-reporter fish carrying the effector gene X, here EGFP, their offspring will express gene X in Gal4 defined subset of neurons. **(B)** Examples of Gal4-VP16 driver lines with UAS:Kaede expression from an enhancer trap screen (5-6 dpf larvae, dorsal view). (**A** adapted from Asakawa and Kawakami (2008), **B** adapted from Scott and Baier (2009).)

1.4.2 Two-photon microscopy functional imaging

Understanding how dynamic activity in neuronal populations give rise to perceptual states and appropriate actions is crucial for understanding the brain (Yuste, 2015). Electrophysiological methods provide a direct measure of neural activity with high temporal

resolution. However, these methods are limited to recording from small subsets of neurons at best; in addition, they are invasive and often blind to the genetic identity of the recorded neurons. Furthermore, recording in freely behaving animals is still a challenge. Two-photon microscopy was introduced in 1990s (Denk et al., 1990) and together with genetically encoded calcium indicators (1.4.2.1) opened a new era for imaging neural activity *in vivo* from genetically defined groups of neurons during behavior (reviewed in (Kerr and Denk, 2008)).

In principle, optical sectioning in a two-photon microscopy is achieved by a femtosecond-pulsed infrared (IR) laser light, leading to the simultaneous absorption of two photons on the specimen containing fluorescent proteins, such as GCaMP (see below, section 1.4.2.1). Therefore, only the neural tissue on the focal plane is excited, minimizing out of focal plane photo damage and bleaching. Furthermore, using an IR light is advantageous: it scatters less in the tissue enabling deep tissue imaging, it is less energetic hence causing less photodamage and, most importantly, it is invisible to the zebrafish, allowing visual stimulation with visible light while imaging simultaneously (Renninger and Orger, 2013). Many studies have routinely exploited and refined the two-photon functional imaging method to understand various aspects of sensory and motor processing in behaving zebrafish (Ramdya and Engert, 2008; Dreosti et al., 2011; Odermatt et al., 2012; Thiele et al., 2014; Kubo et al., 2014; Lacoste et al., 2015).

New technologies have been derived from two-photon microscopy, which opened new possibilities for imaging and manipulating the circuit activity with improved spatial and temporal resolution. For example, spatial light modulators (Nikolenko et al., 2013) have been implemented in two-photon microscopy, enabling simultaneous scanless imaging and photostimulation with structured light patterns, such as holograms (Lutz et al., 2008; Dal Maschio et al., 2010). A method based on temporal beam focusing has been developed to shape two-photon excitation and, combined with optogenetics, to stimulate single neurons (Papagiakoumou et al., 2010). More recently, by using SLM based methods, Quirin *et al.* (Quirin et al., 2014) managed to image the brain-wide calcium transients

in three dimensions simultaneously *in vivo*, in larval zebrafish expressing GCaMP5G (see section 1.4.2.1).

Altogether, these functional imaging and photostimulation tools allow a visualization of population activity and non-invasive neuronal manipulation in intact behaving animals, enabling the functional dissection of neural circuits.

1.4.2.1 Genetically encoded calcium indicators

The arrival of action potentials at the synapse opens voltage-gated calcium channels, increasing the intracellular [Ca^{2+}] level. This increase can be used to predict the timing of spiking activity (Grienberger and Konnerth, 2012). Over thirty years ago, Roger Tsien and his colleagues (Tsien, 1980) synthesized one of the most powerful tools to visualize intracellular Ca^{2+} by using highly calcium-selective chelators, such as BAPTA, with a fluorescent chromophore. These indicators change their fluorescence depending on the intracellular [Ca^{2+}] level allowing neuronal activity to be assessed with imaging. Since then, various calcium indicators, from dextran-conjugated indicators to acetoxymethyl (AM) ester dyes have been developed and used to measure neuronal activity *in vivo* in zebrafish (O'Malley et al., 1996; Ramdya et al., 2006; Yaksi and Friedrich, 2006; Orger et al., 2008; Sumbre et al., 2008). However, these synthetic indicators are often loaded with invasive methods and they indiscriminately fill different cell types. Furthermore, it is difficult to control the amount of dye loaded, which in return, affects the sensitivity especially in high-affinity indicators (Renninger and Orger, 2013).

The next breakthrough was the engineering of genetically encoded [Ca^{2+}] indicators (GECIs) (Miyawaki et al., 1997). These indicators are based on fluorescent proteins fused to Ca^{2+} buffer proteins, such as calmodulin, which undergo conformational changes in response to Ca^{2+} binding. GECIs' most important advantage over synthetic calcium indicators is that they can be coupled to cell-specific promoters to target various neuronal subtypes and be stably expressed in neurons by using, for example, the Gal4/UAS system (1.4.1.1). Moreover, they allow non-invasive Ca^{2+} measurements over long periods of time. Previously, a bioluminescent version of GECIs, green fluorescent protein (GFP)

coupled aequorin (GFP-aequorin), was used to study neuronal activity during natural behaviors in larval zebrafish (Naumann et al., 2010). However, the majority of the GECIs are GFP derived with a prime representative of them being the GCaMP family (Nakai et al., 2001), especially for *in vivo* Ca^{2+} imaging of the nervous system (review by (Looger and Griesbeck, 2012)). These indicators are constantly improved for better signal-to-noise ratio, faster temporal dynamics and higher sensitivity (Akerboom et al., 2012; Chen et al., 2013).

In zebrafish, Dreosti *et al.* (Dreosti et al., 2009) generated syGCaMP2 by fusing GCaMP2 with synaptophysin to target the synapses of spiking neurons in the retina and the tectum, which enabled imaging of hundreds of terminals simultaneously *in vivo*. Del Bene *et al.* (Del Bene et al., 2010) expressed GCaMP1.6 and GCaMP3 in the larval zebrafish tectum to monitor neuronal activity during the presentation of visual stimuli. GCaMP-HS (GCaMP-*hy*per sensitive) was used to record activity from the spinal motor neurons in larval zebrafish (Muto et al., 2011). GCaMP5G was expressed under the control of the pan-neuronal *HuC* promoter (Park et al., 2000) to record the activity from the entire volume of the larval zebrafish brain *in vivo* (Ahrens et al., 2013). The engineering of red and blue fluorescent GECIs opened the doors to optogenetic manipulations of neural function in combination with calcium imaging (Akerboom et al., 2013; Walker et al., 2013). Very recently, Fosque *et al.* (Fosque et al., 2015) engineered a novel fluorescent protein CaMPARI that converts from green to red when the neuron fires, permanently marking the active neurons in a large tissue volume. They showed that this technology enables neural activity to be visualized in freely moving zebrafish larvae, eliminating the necessity of a restrained preparation for imaging.

1.4.3 Light as a tool to establish causality

For the causal analysis of neural circuits underlying behaviors, it is necessary to perform loss and/or gain of function experiments. This can be done, for example, by permanently removing genetically labeled, neuronal types, neuropil regions or brain areas with femtosecond laser pulses while testing the behavioral phenotype afterward. A more sophisti-

cated way is to manipulate the neural activity while observing behavior. By doing so, the necessity and sufficiency of distinct neural populations for the behavior can be assessed. Particularly in the translucent zebrafish, light can be transferred deep into the brain very efficiently, offering a promising future for genetically encoded optical tools to induce reversible and controlled perturbations.

1.4.3.1 Targeted laser ablation

Nonlinear absorption of ultra-short laser pulses in UV or IR regime can induce highly localized damage in transparent living organisms when focused through a high numerical aperture objective (Galbraith and Terasaki, 2003; Vogel et al., 2005). The small focal volume on which the laser pulses are applied conforms high photon density which, in return, enhances the probability of simultaneous multiphoton absorption. Furthermore, this process generates a plasma (an ionized gas) in the focal volume, resulting in plasma-mediated ablation (reviewed in (Vogel and Venugopalan, 2003)). So far, several applications of this laser-induced ablation method have been used in zebrafish to study the neural basis of behaviors. For example, laser ablation of particular hindbrain neurons indicated their necessity for escape behavior (Liu and Fetcho, 1999) or for execution of visually evoked swimming patterns (Orger et al., 2008), while laser ablation of the retinotectal neuropil resulted in selective impairment of prey-capture behavior in the larval zebrafish (Roeser and Baier, 2003; Gahtan et al., 2005). More recently, by utilizing two-photon ablations of specific cerebellar neurons, Aizenberg and Schuman (Aizenberg and Schuman, 2011) showed the selective involvement of cerebellum in memory acquisition in zebrafish larvae. Thus, the laser ablation method in combination with the labeling of targeted neurons can be effectively used to assess the necessity of the ablated component for the behavior.

An important drawback of this method is its variability. First of all it is a manual procedure, having the risk of damaging neighboring areas. Second, depending on the expression level of genetically encoded fluorescent markers, the total deposited energy into the larva may vary, affecting the efficiency of ablations. Additionally, the physical effects underlying the

ablation change considerably depending on the laser pulse frequency (Vogel and Venugopalan, 2003). Lastly, it is an irreversible process. Nevertheless, laser targeted ablation is still a powerful technique that can be applied to the larval zebrafish in order to elucidate whether the targeted neurons are necessary for a particular behavior.

1.5 Thesis objectives

A key function of an animal's visual system is to extract ecologically relevant information from the environment in order to initiate appropriate behavior. A looming stimulus is a two dimensional representation of an object approaching on a collision course, which may represent a predator or an obstacle (Schiff et al., 1962). The behavioral response to looming stimuli is remarkably conserved across animal species (Holmqvist, 1994; Sun and Frost, 1998; King et al., 1999; Preuss et al., 2006; Fotowat and Gabbiani, 2007) including humans (Ball and Tronick, 1971), and usually involves stereotyped defensive responses, such as freezing or escape. Given the importance of avoiding predation, we would expect that evolution has selected a fast, hardwired neural pathway for the detection of looming. Indeed, specialized looming-sensitive neurons have been found in visual areas in locusts (Hatsopoulos et al., 1995; Gabbiani et al., 1999), *Drosophila* (de Vries and Clandinin, 2012), amphibians (Nakagawa and Hongjian, 2010) and pigeons (Sun and Frost, 1998). The visual parameters that are commonly used to detect looming threats include estimated time to collision (Sun and Frost, 1998) and a specific angular size of a looming object on the retina (Gabbiani et al., 1999; Yamamoto et al., 2003; Fotowat et al., 2009).

This study aims to investigate the neural basis for visually-evoked escape in zebrafish larvae. Based on the rapidly expanding size of looming stimuli, a looming detector would require a large receptive field, in which inputs from an array of smaller units are pooled. The smaller units might be detectors of luminance change (e.g. dimming) or of sweeping edges. Their activation in a center-to-periphery sequence would mirror an expanding disk and thus signal looming. It is unclear where along the visual pathway the smaller units and the looming detectors reside. Retinal ganglion cells (RGCs) that respond specifically

to moving edges or to dimming have been described. Their inputs might be integrated at the level of the tectum, the largest retinorecipient area of the vertebrate brain. Alternatively, RGCs themselves might function as looming detectors by sampling from an array of OFF bipolar cells, which would serve as dimming units. Indeed, consistent with the latter scenario, in mice, at least one type of RGC that is specialized for detecting approach motion has been described (Münch et al., 2009), although it is not known how specific this cell type is for looming stimuli, and whether it is involved in defensive behavior (Yilmaz and Meister, 2013).

My first step was to develop a visual paradigm to explore the behavioral responses to looming stimuli in head-restrained larvae. Thereby, I made use of an already existing behavioral setup and modified it to record the induced behavioral responses with a high-speed camera. In response to an approaching object (or to a looming stimulus as its two-dimensional simulation on the screen), the larval zebrafish would start a C-bend escape swim (see section 1.3.4) to put the greatest possible distance between itself and the perceived threat. After I could evoke robust escape behavior in head-embedded larvae, I aimed at categorizing the essential features of escape tail movements in head-restrained larvae. Then, I intended to determine the characteristics of the looming stimulus (e.g. angular size, speed of expansion, contrast, luminance, direction of motion, etc.) that are optimal for eliciting escape responses. I anticipated that this would provide information on the tuning properties of the looming detection pathway and on the receptive fields of the underlying neurons.

My next goal was to identify the visual areas in the zebrafish brain that receive the retinal input generated by the looming stimuli. Previous studies have shown that the genetically encoded calcium indicator GCaMP can be used in combination with two-photon imaging to monitor calcium dynamics in retinal ganglion cells in response to a visual stimulus (Del Bene et al., 2010; Nikolaou et al., 2012). To determine which visual areas respond to looming stimuli, I designed and performed imaging experiments in RGC axon terminals. I used the Gal4/UAS reporter system fused to GCaMP in the retinal axons of transgenic fish to localize the responses to the known visual areas.

Finally, to identify the circuit components that are necessary for looming-triggered escape, I performed targeted laser ablations in the tectal neuropil, where I observed selective retinal responses for looming stimuli. Then, to confirm the importance of an intact tectum in looming-triggered escape, I performed a series of psychophysics experiments. Altogether, this work has defined the visual stimulus parameters that evoke escape responses in the larval zebrafish and established the retinotectal neuropil as the likely site of looming computation in the zebrafish brain.

2 Materials & Methods

2.1 Fish care and transgenic lines

Adult zebrafish were maintained and bred at 28° C on a 14/10, light/dark cycle. Embryos were raised in Danieau's solution (17 mM NaCl, 2 mM KCl, 0.12 mM $MgSO_2$, 1.8 mM $Ca(NO_3)_2$, 1.5 mM HEPES). All animal procedures were in accordance with the institutional guidelines of the Max Planck Society and the local government (Regierung von Oberbayern).

Wild type TL (Tupfel long-fin) larvae were used for behavioral experiments (in Results, sections 3.1, 3.2, 3.3, 3.4, 3.5, 3.6). 6-8 day-old blind *lakritz/atoh7* mutant larvae, in which retinal ganglion cells do not form (Kay et al., 2001), were used in the control behavioral experiments (see section 3.1). TLN (Tupfel long-fin nacre) larvae (*mitfa-/-*), which lack pigment in the skin but retain wild type eye pigmentation, were used for two-photon imaging experiments for the convenience (in Results, sections 3.7, 3.8, 3.9, 3.10).

The following transgenic lines were used: *Tg(Atoh7:Gal4-VP16)s1992t* (a.k.a. Ath5:Gal4), *Tg(Isl2b.2:Gal4-VP16), Tg(UAS:Dendra-Kras)s1998t* and *Tg(UAS: GCaMP6s)*. Transgenic lines were kept in either TL or TLN background.

2.2 Behavioral assays and data analysis

2.2.1 Escape behavior assay

6-8 day-old TL larvae were used for behavioral experiments. Larvae were fed with baby powder (Sera Microns) at 5 dpf and embedded in 2.6% low melting point agarose (Invitro-

gen) 24h prior to the experiments. For embedding, the lid of a 35 mm Petri dish (Corning, Sigma-Aldrich) was used and larvae were positioned 2 - 3 mm away from the edge of the dish. After the agarose solidified, the dish was filled with Danieau's solution and agarose around the tail below the swim bladder was cut away using a scalpel, leaving the tail free to move. Embedded larvae were kept at 28° C in a chamber where behavioral experiments were conducted.

Visual stimuli were generated in Python using the VisionEgg psychophysics library (Straw, 2008), as custom-written comma-separated values (csv) files. Stimuli were displayed at 60 Hz on a 12 x 9 mm monochrome organic-light-emitting-diode (OLED) screen (eMagin) spanning over approximately 62° (horizontally) and 50° (vertically) of the larva's visual field and controlled by a NVIDIA Quadro FX 3500 graphics card. The screen was covered with three magenta Wratten filters (Edmund Optics) and positioned 10 mm from the larva. The stimuli were presented in the center of the screen except for Figure 3.2B, in which different stimuli positions on the screen were used to investigate directionality in initial escape bends. A custom-built infrared light source, formed by an array of six infrared (850 nm) light-emitting diodes (Osram GmbH), equipped with a diffusive screen (Thorlabs) illuminated the larvae from below. The lid of the petri dish with an embedded larva was placed on a clear glass platform. Tail movements were recorded from above with a high speed CMOS camera (Photonfocus), attached to a Sigma 50 mm F2.8 EX DG Macro-objective, at 648 fps, with a spatial resolution of 380 x 400 pixels. Behavioral experiments were performed with the room lights on, and screen brightness at maximum. The luminance of the dark screen was 0.07 cd/m^2 and the one of the white screen was 122.5 cd/m^2.

Looming stimuli expanded from 2° to 48° unless stated otherwise. The visual angle of the approaching disk was updated approximately every 17 ms. For the constant approach speed looming stimuli, visual angle is determined by the equation:

$$\tan\left(\frac{\theta(t)}{2}\right) = \frac{l}{x(t)} = \frac{l}{vt} \tag{2.1}$$

where $t = 0$ corresponds to the collision time and $t < 0$ before collision, l is the half-width (radius) of a three-dimensional object, v is the approach velocity towards the larva which is $v < 0$ when the object is approaching and $x(t)$ is the distance between the larva and the approaching object, given as a function of time with $x = 0$ at collision. l and v are constant values during approach. The angular size can be obtained by rearranging Eq. 2.1,

$$\theta(t) = 2\tan^{-1}\left(\frac{l}{vt}\right) \tag{2.2}$$

The first derivative of $\theta(t)$, $\dot{\theta}(t)$, gives the angular edge speed of the looming stimulus (see Figure 2.1).

The stimulus shall simulate a predator approaching with constant speed towards the larva. However, in the experimental setup, the distance between the larva and the disk on the screen is constant. Hence, the disk radius is set to increase over time according to Eq. 2.3 to mimic the constant speed approach:

$$\frac{r(t)}{d} = \tan\left(\frac{\theta(t)}{2}\right) = \frac{l}{vt} \tag{2.3}$$

where $r(t)$ is the radius of the disk projected on the screen, increasing over time to simulate the approach of an object with a constant l/v value and d is the constant distance between the larva and the screen, which is 10 mm in my setup.

By varying the approach velocity, for a disk expanding from 2° to 48° on the screen, I tested five l/v conditions 30, 60, 90, 120 and 150 ms, with expansion durations (or stimulus durations) of ≈ 1.65, 3.3, 4.9, 6.5 and 8 s, respectively. These l/v values correspond to 0.03 mm initial virtual disk radius $r(t)$, and five approach velocities 1, 0.5, 0.33, 0.25 and 0.2 mm/s (see Figure 2.1). For the experiments testing behavioral responses to a range of stimuli (Figures 3.1 to 3.9), stimuli were presented in a random order. In addition, to avoid habituation, intervals of at least 3 minutes separated successive trials.

To analyze behavior videos, I digitized the tail by assigning approximately 50 points along the tail and extracted swim bouts as described previously (Thiele et al., 2014). In brief,

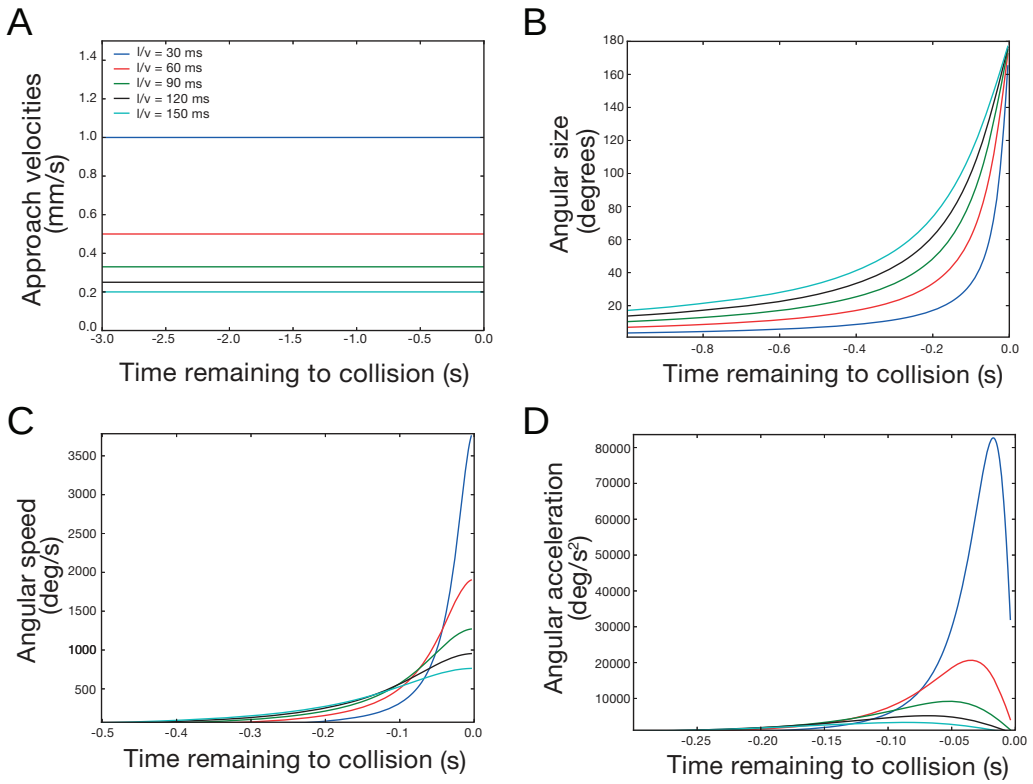

Figure 2.1: Kinematics of visual looming stimuli. **(A)** Schematics of the stimulus approach speeds over time. **(B)** Stimulus angular size expands nonlinearly over time for five different size-to-speed ratios. **(C)** Stimuli angular edge speeds and **(D)** acceleration for five size-to-speed ratios. Time t = 0 corresponds to collision time where stimuli angular size reaches 180°. For convenience, time flows toward t = 0. Colors mark the correspondence to different (l/v) values.

Python based custom-written software employs the OpenCV computer vision library to load videos and implements a tail tracking algorithm to quantify tail position in each frame, as a series of points along the midline of the tail. For this, first the user selects the start point, which was taken right below the swimbladder in all experiments. Then the software iterates through the tail by taking a cross-section of the luminance profile of the tail and convolves it with a tail-like kernel, where the maximum corresponds to the points on the tail midline. (For this tail tracking algorithm based on a luminance change threshold, the best tracking results were obtained when the contrast between the tail and the background was high.) This procedure is then repeated for each video frame. The swim bouts were detected with another custom Python script. A swim bout was detected when

an absolute value of the first derivative of the tail angle over time is bigger than a threshold value.

In Figure 3.3, the spontaneous swim video was flipped vertically before any analysis, so that the example escape and spontaneous swims would start in the same direction. Detailed analysis of the tail kinematics were performed offline using Python, based on the digitized tail data. In Figure 3.4, the tail bend angle was calculated by measuring the angle between two vectors: 1. a baseline vector measured in the still larva, 2. a vector describing the instantaneous tail position in the moving larva. In both cases, the vector is defined as a straight line from the first point near the beginning of the tail to the mean position of three points at the end of the tail (to reduce noise).

Tail beat frequencies were calculated as a ratio of number of tail flips per bout to overall bout duration. To distinguish spontaneous and escape swims, I first checked that the initial turn direction was away from the looming stimulus. Then I used two criteria to define escapes: maximum tail bend angle $\geq 70°$ or average tail beat frequency ≤ 35 Hz (see Figure 3.4). Positives and false negatives were identified as the red dots within the red dashed lines surrounding the blue dots area being false negatives. I chose the maximum tail angle and frequency thresholds so that there were no false positives within the test dataset. Data were further compiled and visualized using Python.

For the experiments in Figure 3.5, the size-to-speed ratio was $l/v = 60$ ms. Looming stimuli sometimes triggered more than one escape per trial, and in these cases only the first escape was analyzed. Temporal dynamics of the dimming stimulus was matched with the dark looming stimulus. For the linear dimming stimulus, I kept the initial and final luminance level and overall stimulus duration same with the dark looming stimulus. Decrease of luminance per unit time was linear. In Figure 3.7, for the calculation of escape onset timing, I detected the frame of first tail movement and subtracted a delay of 35 ms as a sum of the delays in central processing in visual information (≈ 25 ms) (Zottoli et al., 1987; Canfield, 2003) and motor output (≈ 10 ms) (Zottoli, 1977) from the escape onset as an approximation of total delay. For the computation of the angular size threshold, I used the equation (Gabbiani et al., 1999):

$$\theta_{\text{thresh}} = 2\tan^{-1}\left(\frac{1}{\alpha}\right) \tag{2.4}$$

where α is the slope of the linear regression line in Figure 3.7A. In the absence of neural delay adjustment (meaning the total delay of 35 ms) for the escape onset timing, the linear regression fit (y = -5.033x + 15.98) gives an angular size threshold of 22.5°. In Figure 3.7A, when the two outlier data points from l/v = 120 ms and l/v = 150 ms (corresponding to the values when t < -1200) are excluded, the linear regression line (y = 4.823x - 28.04 with p-value = $2.1x10^{-12}$, R^2 = 0.59) gives an angular size threshold of 23.2°. Behavior data were averaged within larvae first and then averaged as a population to calculate the escape probabilities.

2.2.2 Optomotor assay

To test OMR, I embedded 6 dpf larvae in the same manner as for escape behavioral experiments and waited 24 hours to test the pre-ablation OMR. Post-ablation larvae were re-embedded at 7 dpf and were allowed to recover for 24 hours. The experimental setup and the software to control the visual stimuli were previously described (Schoonheim et al., 2010). In brief, embedded larvae were placed in the middle of an arena with a LCD screen (Miller Technologies), covering an area of 5.5 x 7.5 cm on the right side of the larvae. Gratings moving from caudal to rostral at speeds ranging from 16 - 29°/s were displayed to evoke a forward optomotor response. The same grating speeds were used before and after ablations. Stimulus presentation was controlled with a custom LabVIEW script, and tail movements were recorded at 250 fps using a high-speed camera (Pike F032B, Allied Vision Technologies) and StreamPix software (Norpix). Each stimulus was presented for 10 seconds. The number of OMR forward swim bouts was averaged for each larva from at least three trials (Figure 3.20C).

2.3 Two-photon calcium imaging and data analysis

Calcium imaging was performed using a movable objective two-photon microscope (Sutter Instruments) with a 40x water-immersion objective (Olympus). Excitation light was tuned to 920 nm (Chameleon Ultra, Coherent). Scanning and image acquisition were controlled using ScanImage software (Pologruto et al., 2003). Time series were recorded with spatial resolution of 128 x 128 pixels (for extratectal AF imaging, see Figure 3.10 and 3.11) or 256 x 256 pixels (for tectal neuropil imaging, see Figure 3.12 and 3.13) at a frame rate of 3.62 Hz.

To prevent motion artifacts arising from movement in response to looming stimuli during imaging, most 6-8 dpf *Tg(Isl2b.2:Gal4-VP16)* and *Tg(UAS: GCaMP6s)* larvae were anaesthetized with 0.02% tricane (MS-222, tricaine methane-sulfonate; Sigma Aldrich) and then paralyzed by injection of alpha-bungarotoxin (4 µl of 10 mg/ml; Invitrogen), 1 µl Phenol Red and 1 µl 5X Danieau's solution to the spinal cord. The tricaine was washed out prior to experiments. Larvae were embedded as for behavioral experiments, except that the agarose around the tail was not removed to prevent any movement artifacts. The imaging chamber was heated to 28° C. Stimuli were displayed on the same type of OLED screen as for behavior, also covered with three magenta filters.

The looming stimuli used for imaging consisted of five types, as for the behavior experiments (Figure 3.5A: dark looming, dimming, bright receding, dark receding and bright looming, l/v = 60 ms). To prevent saturation of the photomultiplier tubes from green screen light that was able to pass through all three filters, I used a grey instead of white background for the dark looming stimulus, and changed all other stimuli to match. The luminance of the grey screen was 19.75 cd/m^2. I note that a grey/black looming stimulus was highly effective in triggering escapes in the behavior setup (data not shown). Visual stimuli were presented three times each, in pseudorandom order, with intervals of 3-5 minutes between trials.

Calcium imaging analysis was done by custom-written Python-based codes. SIMA was used for motion correction (Kaifosh et al., 2014). For extratectal AF calcium imaging anal-

ysis, AFs were identified anatomically as in Figure 3.10A. For the tectal neuropil analysis, ROI covered all 4 retinorecipient zones (SO, SFGS, SGC, SAC/SPV). A Fast Fourier Transform (FFT) based automated alignment was performed to align across all trials for each fish (http://www.lfd.uci.edu/ gohlke/code/imreg.py.html). Minor filtering (median with a kernel size of 3, Gaussian with sigma = 0.2) was performed to reduce noise. Background subtraction linearized the luminosity over the slow axis of the microscope, which was then heavily filtered to extract the low frequency luminance changes affecting the whole image. $\triangle$F/F was calculated per pixel from the background subtracted image. Pixels corresponding to image background were filtered out by a threshold set by observation of the histogram of $\triangle$F values. The threshold was set just to the right of the first peak of this distribution. Values above half of the threshold were linearly derated to provide a smooth threshold since some pixels can be shared by both the background and the signal, and values below half of the threshold were discarded.

The peak $\triangle$F/F values were extracted using a 95th percentile filter. In Figures 3.10B, 3.11A and 3.14A peak responses were taken over a time window from just after stimulus start to after the stop of the stimulus but before its removal ($\approx$ 5 seconds). The responses were averaged over trials (for individual trials see Figure 3.14B) for a single fish and pseudocolored. In the scatter plots for pixel responses (Figures 3.13 and 3.17B), data from all larvae with good pixel alignment across all trials (n = 4 for each region) was plotted, using the maximum of each pixel's response during the mentioned time window. The pixel analysis for all planes was performed at a resolution of 128 x 128 pixels. Individual pixel areas were 0.34, 0.57 and 1.44 μm^2 for AF6, AFs 7, 8 and 9, and the tectum, respectively. For the tectum, functional time-series were acquired at three depths. Stimuli were presented in a pseudorandom order unique to each plane in each larva. Data from each plane were pooled across larvae to generate scatter plots for pixel activation for each stimulus.

2.4 Two-photon laser ablations

Larvae were treated with 0.1 mM PTU (Sigma Aldrich) from 1 dpf on to prevent excessive tissue damage during ablations. A few hours prior to ablations, larvae were embedded completely in the center of a 35 mm Petri dish with an oblique angle to visualize the RGC axon bundles entering the tectal neuropil (see Figure 3.14A). Ablations were performed using a two-photon microscope (Femtonics, Hungary) with a laser system (Chameleon Ultra II, Coherent) in *Tg(Atoh7:Gal4-VP16)s1992t* and *Tg(UAS:Dendra-Kras)s1998t*, 7 dpf TLN larvae. A 20x water-immersion objective with a large back-aperture (Olympus, 1.0 NA) was used for ablations. Laser power after the objective was approximately 150 mW at 850 nm. Axons were ablated by scanning a focused pulsed laser beam for 1 s over a 62 µm x 28 µm rectangular area at three planes (ventral, middle and dorsal) within the tectal neuropil. Ablations were performed unilaterally (only in the left tectal neuropil) and for each plane, after scanning the entering axon bundles, 3-4 additional scans were performed randomly across the neuropil surface to lesion the neuropil (see Figure 3.19A). 24 hours after the ablations, an image stack of an ablated neuropil was acquired to ensure that fluorescence did not recover and eliminate photobleaching factor. After ablations, larvae were freed from the agarose and allowed to recover for 3-6 hours before being re-embedded for post-ablation behavioral experiments.

I waited 24 hours after embedding to test the escape behavior. To test the ablated fish escape responses, I presented a constant approach speed looming stimulus at l/v = 60 ms and a linearly looming stimulus 20°/s (Figure 3.20A-B) at least three times. For post-ablation behavior experiments, I used transgenic siblings of ablated larvae and subjected them to the same treatment ('sham operation') as experimental larvae except laser ablations. In Figure 3.20A, ablated larvae's escape probability on the ablated side is compared with the transgenic siblings escape probability after 'sham operation' and with the ablated larvae's escape probability on the intact side. In Figure 3.20B, after ablations, n = 2 larvae did not perform any escape on the ablated side while they performed escapes in each trial on the intact side and, before the ablations, on the to-be-ablated side (Pre-ablation).

If the ablated larvae did not perform any escape on the intact side, they were excluded from the analysis (8 larvae out of 22). I discarded the ablated larvae that failed to respond on the intact side because I could not conclude that it was the ablation that reduced the escape probability in these larvae, as opposed to other factors. Control siblings that did not perform any escapes in response to the looming stimuli for three to four consecutive trials were also excluded from the analysis (3 larvae out of 17). In few cases (Figure 3.20B), I could perform pre- and post-ablation behavioral experiments within the same larvae (n = 2). However, using this protocol did not allow larvae for enough recovery from several embedding treatment (embedding procedure differs between for the behavioral experiment and for the ablation experiment), thus decreased the survival rates of the operated animals.

2.5 Lipophilic labeling of retinofugal projections

I used lipophilic dye labeling to assess the extent of the ablations through the entire retinofugal projection as previously described (Ben Fredj et al., 2010). Briefly, ablated larvae at 8 dpf after post-ablation behavior experiments were fixed overnight at 4° C in 4% paraformaldehyde in PBS, pH7.4. The carbocyanine dye DiI (Invitrogen) was diluted to 1% solution in chloroform (wt/vol) and pressure-injected (Eppendorf FemtoJet) into the left and right eyes, between the lens and the retina, of fixed larvae embedded in 2% low melting point agarose. After an overnight diffusion period, DiI labeling was visualized with two-photon microscope (Femtonics, Hungary) with excitation light tuned to 1020 nm (Chameleon Ultra II, Coherent), using a 20x objective (Olympus, 1.0 NA).

2.6 Statistics

Statistical analysis was performed in R and Python. For analysis involving the measure of escape responses (where for each condition a fish is subjected to multiple trials and for each trial the response is binary, and thus can be thought of as Bernoulli trials) Gener-

alized Estimating Equations (GEE) with a binomial link function were implemented and used, as in (Preuss et al., 2006). Standard errors (S.E.) were extracted from the GEE modeled population coefficient estimates. For other group comparisons, trials within each fish and condition were averaged and then pooled to eliminate any bias from larvae that contributed more data points than others. Then they were analyzed with ANOVAs to assess the statistical similarity between groups. Bootstrap 95% confidence interval error bars were calculated using SciPy module of Python. Multiple comparisons were corrected with Tukey HSD (ANOVA) or Bonferroni-Holm (all others) method when necessary. For all figures n.s. > 0.05; * = p-value ≤ 0.05; ** = p-value ≤ 0.005; *** = p-value ≤ 0.0005.

3 Results

This chapter is taken from my publication (Temizer et al., 2015) with permission.

3.1 An expanding disk triggers escape in zebrafish larvae

To investigate the escape behavior evoked by looming stimuli, I made use of a head-restrained behavioral assay in which larvae were embedded in agarose and their tails were freed so that swimming behavior could be recorded with a high-speed camera (Figure 3.1A) (see section 2.2 for details). Initial experiments showed that binocular presentation of a looming dark disk, which starts as a small dot and expands until it fills the whole screen, is an effective escape stimulus. In this stimulus configuration, I found that larvae performed the typical C-bend fast starts that were previously described in response to acoustic or head-tactile stimuli (Kohashi and Oda, 2008; Liu et al., 2012) (Figure 3.1B). The C-bend turns the larva away from the aversive looming stimulus, and is followed by an immediate fast forward swim, another kinematic feature of escape (Budick and O'Malley, 2000), which propels the larva away from the looming object. The time from the onset of tail bending to the moment of maximum tail curvature varied between 9 ms and 18 ms (Figure 3.1B), similar to the timing that has been reported in freely swimming larvae escaping from tactile stimuli (Budick and O'Malley, 2000). This C-bend and forward swim sequence was also observed in freely swimming larvae when presented with the looming stimulus (data not shown, experiment conducted by J. Semmelhack, described in Temizer et al. (2015)).

To verify that the visually evoked escape I observed involves the retina, rather than alternate pathways such as deep brain photoreceptors or the pineal organ (Roberts, 1978; Fernandes et al., 2012), I tested the escape response of lakritz mutants, which lack RGCs

(Kay et al., 2001). I observed that lakritz mutants did not perform any escapes in response to looming stimuli (Figure 3.2A), confirming that looming-triggered escapes require the retina. Notably, lakritz mutants are still capable of escapes in response to tactile cues (data not shown, experiment conducted by J. Semmelhack, described in Temizer et al. (2015)).

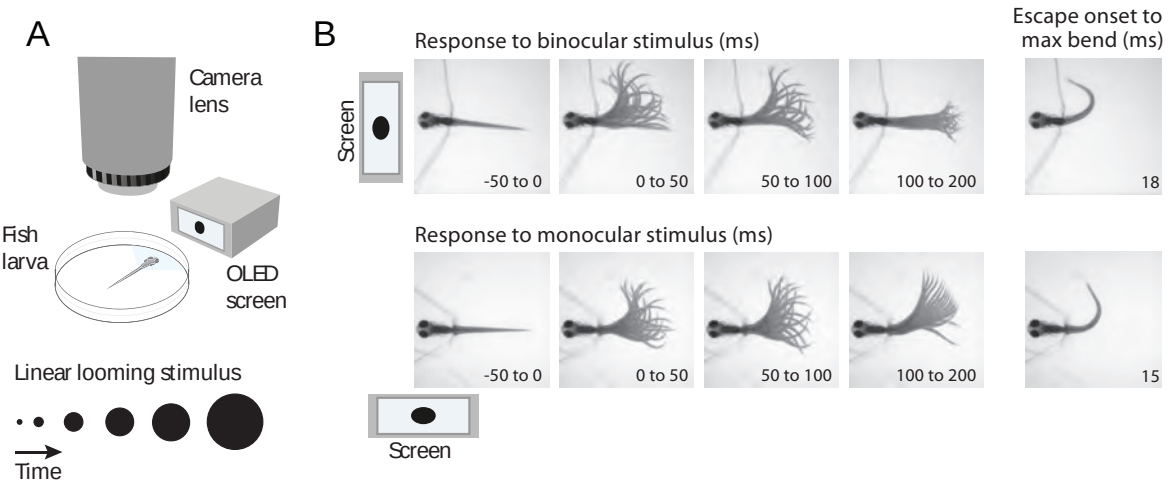

Figure 3.1: Visual assay for looming-mediated escape. **(A)** Schematic of the behavioral setup showing a larva embedded in agarose with its tail freed, with the screen positioned head-on (binocular orientation) or to the side (monocular orientation). **(B)** Examples of binocularly and monocularly evoked escape swims a in 8-dpf (days post-fertilization) Tupfel long-fin wild type larva. On the right, the frame showing the tail position at the point of maximum bending is displayed.(Figure adapted from (Temizer et al., 2015) with permission.)

3.2 Monocular stimulation evokes escapes away from the looming disk

Next, I asked whether larvae are able to direct their escape swim away from an approaching object, by investigating the relationship between escape direction and stimulus position within the visual field (Figure 3.2B). Looming stimuli were presented binocularly, in the center 0°, 16° to the left, and 16° to the right of the larva's visual field. Moving looming stimuli, which started on center-left and moved to the center-right while looming (or vice versa), were also presented (Figure 3.2B). Quantification of initial escape bend directions demonstrated a strong preference of the larvae to swim away from the looming stimulus.

For example, both the stationary looming stimulus on the right and a left to right moving looming stimulus reliably evoked leftward escapes (Figure 3.2B). I observed an overall preference for leftward escape bends in these larvae. Behavioral laterality in zebrafish was documented previously (Miklósi et al., 2001; Miklósi and Andrew, 2006) and could be an explanation for this bias. However, studies in behavioral lateralization in the larval zebrafish provided inconsistent results (Barth et al., 2005; Facchin et al., 2009).

The responses to lateral stimuli suggested that purely monocular stimuli might be able to induce escape behavior. Predators approaching from the side are likely to be observed by only one eye, so monocular detection should be a useful property of the visually-induced escape circuitry. To address this question, looming stimuli were presented with the screen to the side of embedded larvae, and analyzed in the same manner as above (Figure 3.1B). Monocular looming stimuli evoked escape responses that were kinematically similar to those evoked by binocular looming stimuli (see Figure 3.1B). When the right eye was presented with the looming stimulus, the larva typically performed an escape with the initial bend to the left. The time between escape behavior onset and maximum bend curvature of the tail was similar to that of binocularly triggered escapes (Figure 3.1B). However, monocularly triggered escapes tended to have a lower maximum bend angle than binocular escapes. This result is not surprising since a monocular looming object is approaching from the side (as opposed to the front for a binocular looming object), meaning that the larva does not need to make as sharp a turn to swim away from the object. This experiment also showed that an increase in angular size detected by one eye gives sufficient information to the brain to trigger an escape. The use of monocular stimuli allows the contralateral side to be used as a within fish control for imaging or unilateral ablation experiments. Thus, for the remainder of this work, I focus on monocularly induced escapes.

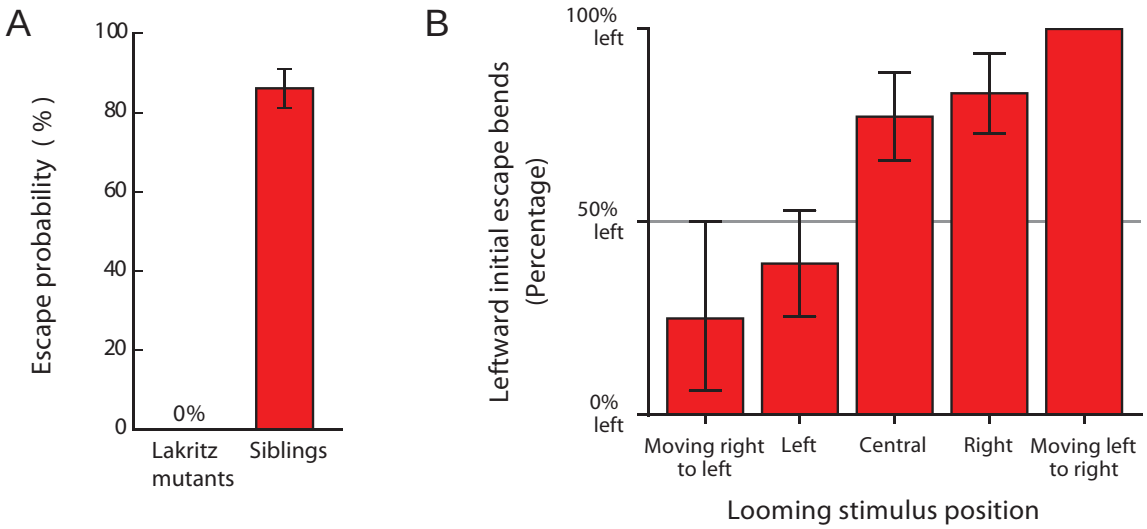

Figure 3.2: The looming-evoked escape response is mediated by the retina and depends on the stimulus position in the visual field. **(A)** Escape probability in *lakritz* mutants lacking RGCs (n = 7 larvae) and in heterozygotes control siblings (n = 12 larvae). *Lakritz* mutants could not perform any escapes in response to looming stimulus. **(B)** The direction of the initial bend of the escape response varies depending on the position of the binocularly presented looming stimulus. Data pooled from n = 14 larvae. Error bars indicate 95% bootstraps. (Figure adapted from (Temizer et al., 2015) with permission.)

3.3 Escape swims are kinematically distinct from spontaneous swims

In the absence of visual stimuli, larvae occasionally perform spontaneous swims. Comparison of the two types of behaviors showed that escape swims are characterized by movement of more rostral tail segments and a higher tail beat frequency than spontaneous swims, as revealed by dynamic bend angle plots (Figure 3.3). I used a quantitative thresholding approach to objectively distinguish spontaneous and escape swims. First, the tail was digitized as previously described (Semmelhack et al., 2014). To calibrate the thresholding parameters, I extracted tail shape and kinematics from 350 swimming bouts performed in the presence (escape swims) or absence (spontaneous swims) of looming stimuli. The two parameters of maximum tail bend and average tail beat frequency revealed a clear separation between spontaneous and escape swims (Figure 3.4). Escape swims had larger tail bend angles (escape: 61.0°, spontaneous: 38.3°, Mann-Whitney U

test, p-value < 1.0x10^{-5} and higher tail beat frequencies (escape: 45.5 Hz, spontaneous: 24.6 Hz, Mann-Whitney U test, p-value < 1.0x10^{-5}) (spontaneous swims data provided by J. Semmelhack).

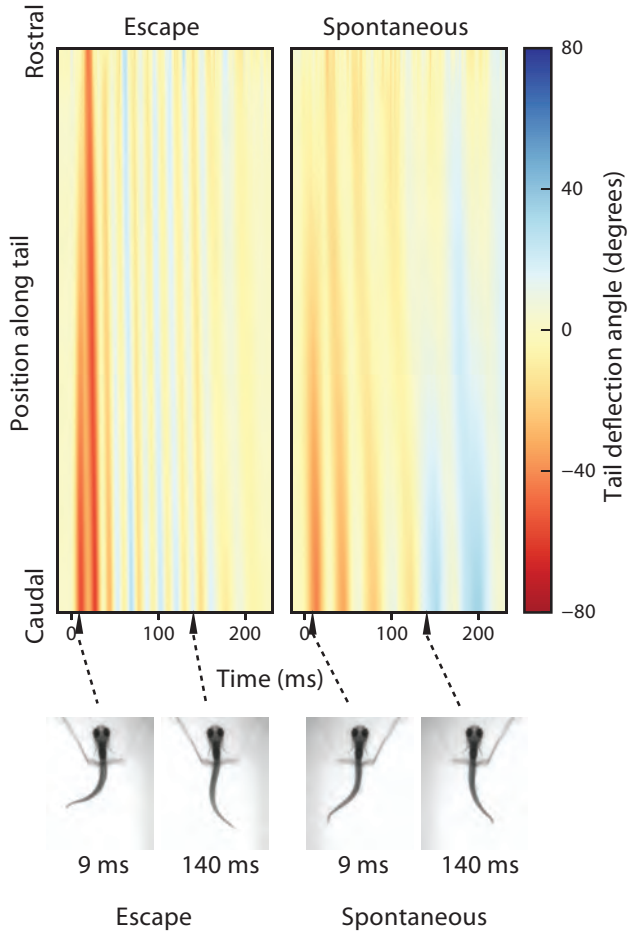

Figure 3.3: Escape and spontaneous swims bend angle plots. Bend angle plots showing the evolution of the tail shape during spontaneous and escape swims for a 7-dpf larva. Tail deflection angles, indicating the overall bend angle from the baseline for each digitized tail point, are color coded in each column. (Figure adapted from (Temizer et al., 2015) with permission.)

I classified as escape any swim bout that met the following three criteria: 1) initial escape bend direction away from the stimulus; 2) average tail beat frequency ≥ 35 Hz or maximum bend angle ≥ 70°; 3) occurring before the anticipated collision time with the approaching object (when angular size reaches 180° visual angle). This conservative set of thresholding criteria allowed classification of escape swims with high accuracy (false

positive rate 0%, false negative rate 7.2%). Looming-evoked escapes are probabilistic and habituate over repeated display of the stimulus in many species (Holmqvist, 1994; Fotowat et al., 2009; Yamamoto et al., 2003). In line with this, I also observed that zebrafish larvae, when exposed to the repeated looming stimuli, would habituate and cease responding. To compensate for the habituation effect, I excluded the trials including and following the fourth consecutive unsuccessful trial.

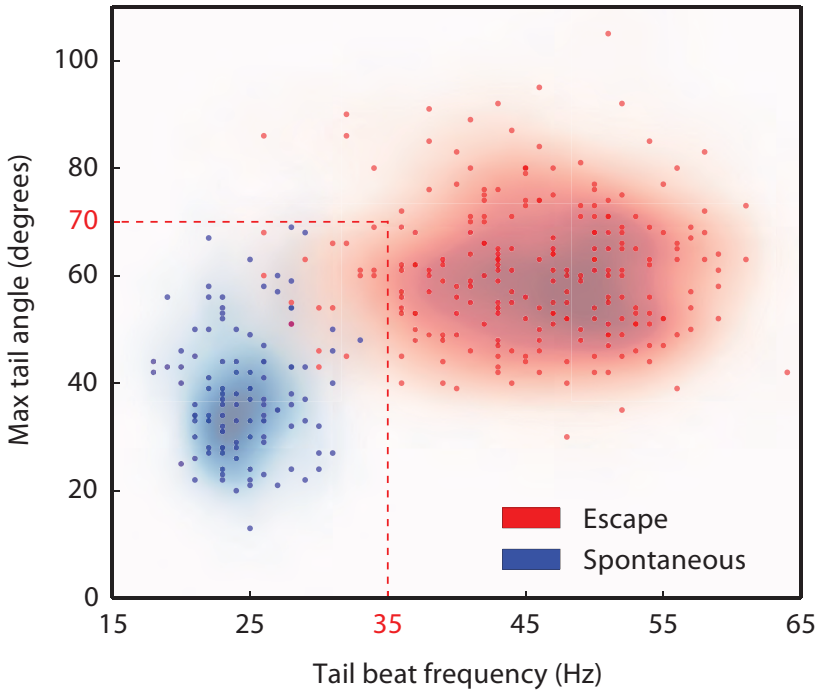

Figure 3.4: Escape swims are kinematically distinct from spontaneous swims. Two tail metrics (maximum tail bend angle and average tail beat frequency) were extracted and used to identify escape swims. Data were pooled from 114 spontaneous swim bouts (n = 15 larvae) and 236 escape swim bouts (n = 21 larvae). The intensity of the shading depicts the mean value of each group. (Figure adapted from (Temizer et al., 2015) with permission.)

3.4 Escape responses are most effectively elicited by a dark looming disk on a bright background

Which parameters of the looming stimulus elicit escape behavior? I systematically tested five different stimulus conditions; a looming dark disk on a bright background, a looming bright disk on a dark background, a receding bright disk on a dark background, a receding dark disk on a bright background and a uniformly dimming stimulus (Figure 3.5A).

A dark disk that expands from 2° to 48° of the visual field (hereafter referred to as dark looming) is the most effective stimulus, evoking escapes in more than 80% of the trials. I asked whether the luminance change alone of such a stimulus was sufficient to evoke an escape. A constant size (48°) disk, that dimmed with the identical overall luminance change of the dark looming disk (dimming), did not elicit escapes. The same was true for a disk that dimmed more slowly, with constant luminance decrements over time (linear dimming). Similarly, a bright receding disk (receding bright) was largely ineffective to evoke escapes. This suggests that dimming alone, or a combination of dimming and moving edges, are insufficient to induce escape behavior (Figure 3.5B). I next tested whether a looming bright disk on a dark background (bright looming) would trigger escapes. This stimulus contains an inverted luminance profile compared to both the dimming and dark looming stimuli used before. Such a stimulus evoked escapes in about 25% of the trials, suggesting that there are mechanisms that extract global expansion from a visual scene, regardless of the sign of stimulus contrast (Figure 3.5B). However, a bright-on-dark expanding disk is substantially less potent in eliciting escape behavior than its dark-on-bright equivalent. Finally, I tested a receding dark disk on a bright background (dark receding) to determine whether a decrease in the size of a dark spot would trigger the behavior. I did not observe any escapes in response to a receding dark disk (Figure 3.5B), suggesting that expansion is an important parameter of the looming stimulus.

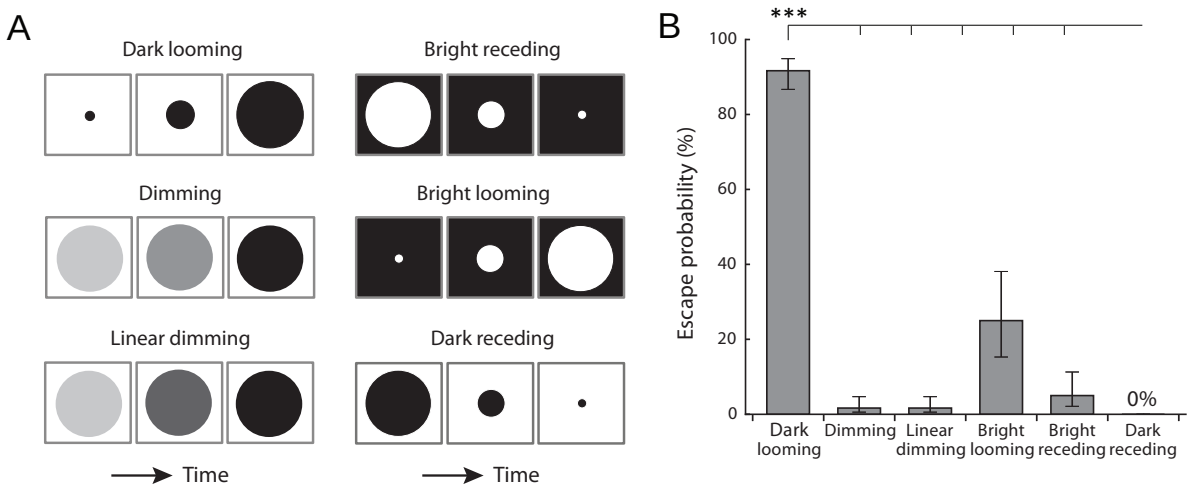

Figure 3.5: Escape probability with respect to stimulus parameters. (A) Schematics of the stimuli over time. **(B)** Escape probability of larvae in response to the six stimuli above. Dark looming was the most effective in triggering escapes (n = 20 larvae, GEE, p-value < $1x10^{-7}$ for dark looming vs. all the others, p-value ≤ 0.04 for bright looming vs. each of all the others, multiple comparison corrected by Bonferroni-Holm). The dark receding stimulus did not trigger any escapes. Stimuli generated from l/v = 60 ms stimulus (see section 2.2.1). Error bars indicate ±S.E. (Figure adapted from (Temizer et al., 2015) with permission.)

3.5 Probability of escape is invariant over slow-to-moderate approach velocities

The looming stimulus models an object of constant size approaching at a constant velocity, which is fully described mathematically by the object's size-to-speed ratio (l/v) (explained in section 2.2.1). To further explore the behavioral correlates of the looming stimulus, I systematically changed l/v (Figure 3.6A). Such constant velocity stimuli have been widely used to investigate escape responses in birds, fish and insects (Sun and Frost, 1998; Preuss et al., 2006; Gabbiani et al., 1999; von Reyn et al., 2014). Based on my initial behavioral experiments, I tested a range of l/v values: 30 ms, 60 ms, 90 ms, 120 ms and 150 ms, which correspond to approach speeds of 1, 0.5, 0.33, 0.25, 0.2 cm/s for a virtual object with a radius of l = 0.03 cm. I found that the probability of escapes was consistently high for l/v values above 30 ms. For the rapidly looming stimulus of l/v = 30 ms, however, there

was a decrease in escape probability (Figure 3.6B), suggesting that the expansion speed of this stimulus might exceed the detection limit of the escape circuitry.

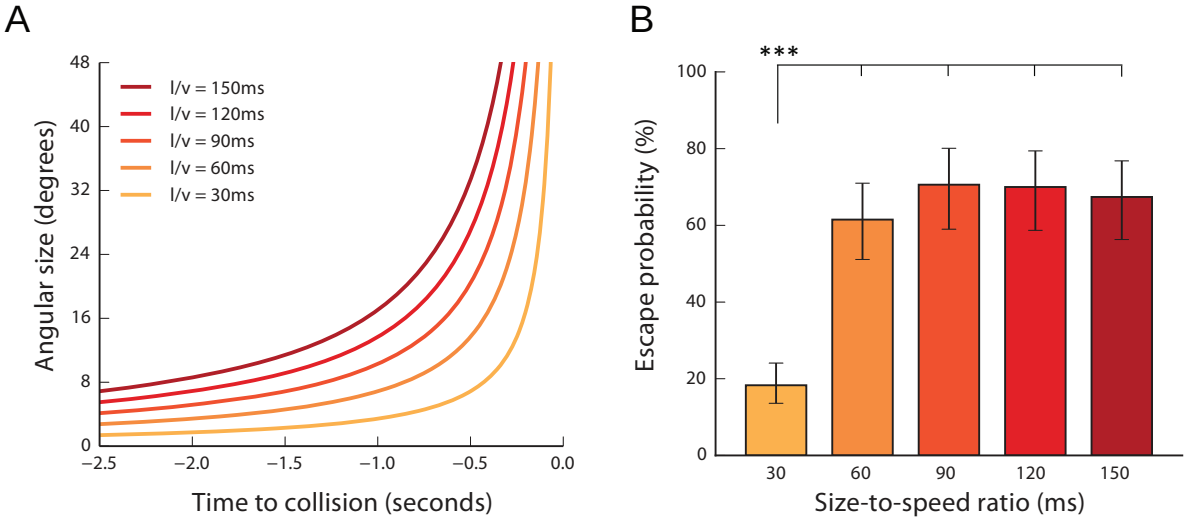

Figure 3.6: Escape probability as a function of size-to-speed ratios. **(A)** Expansion of angular size for constant approach speed looming stimuli in time from 2° to 48°. Time = 0 represents collision time, when the angular size reaches 180°. l: object's radius, v: approach speed. **(B)** Escape probability is consistently high for l/v values above 30 ms (n = 15 larvae, GEE, p-value = $9.32x10^{-6}$ for l/v = 30 ms vs. each of all the others, multiple comparison corrected by Bonferroni-Holm). Error bars indicate ±S.E. (Figure adapted from (Temizer et al., 2015) with permission.)

3.6 Escape is evoked once the disk exceeds a threshold size of approximately 20°

To dissect the looming stimulus parameters that are correlated with escape onset, I looked at the timing of responses for the range of l/v values. Strikingly, examining the remaining time-to-collision at the escape behavior onsets across l/v values (Figure 3.7A) revealed a strong linear relationship. This result has similarities with escape timing correlates from other animals (Sun and Frost, 1998; Gabbiani et al., 1999) and indicates that angular size is a critical parameter extracted by the neural circuit. This linear relationship also suggests that escape is initiated when the stimulus reaches a threshold angular size on the retina,

rather than at a fixed time before collision with the approaching object (Gabbiani et al., 1999). I computed this threshold angular size as $21.7 \pm 2.5°$ (mean ± S.E.) based on the slope of the linear regression in Figure 3.7A (see section 2.2.1, equation 2.4). Similarly, a linear regression on the angular size at escape onset across l/v values (excluding the fastest stimulus, l/v = 30 ms, which does not reliably trigger escape) supports the concept of an angular size threshold of approximately 20° (Figure 3.7B).

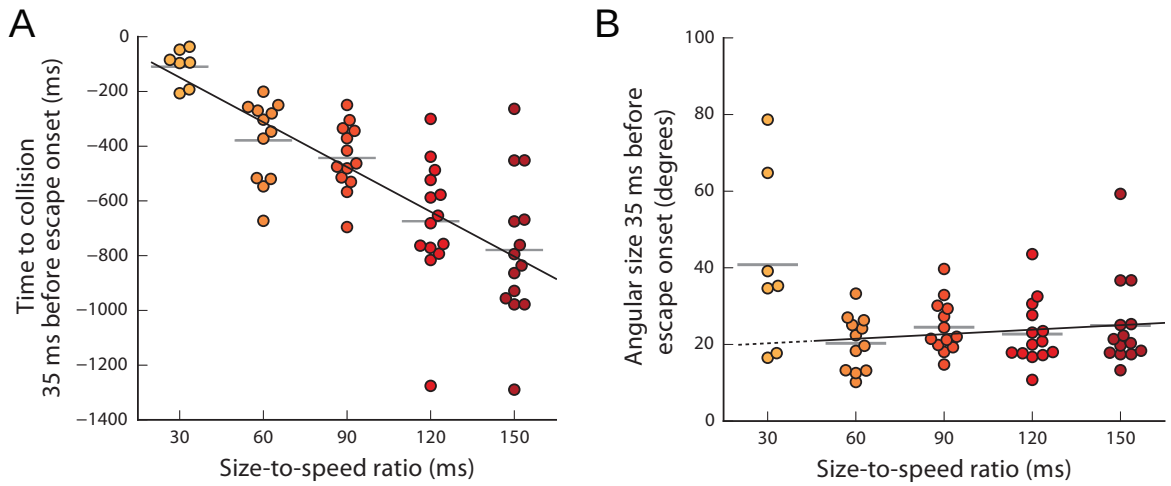

Figure 3.7: The time of escape onsets relative to collision as a function of size-to-speed ratios indicate a threshold angular image size. **(A)** Remaining time to collision at escape onsets as a function of l/v. Same larvae as for Figure 3.6B (least-squares linear regression $y = -5.298x - 3.51$, p-value = $1.4x10^{-11}$, R^2 = 0.55, from 60 responses across all l/v values). **(B)** Value of the average stimulus angular size at a fixed neural delay preceding escape onset (35 ms, see Materials and Methods, section 2.2.1) over l/v values from 60 ms to 150 ms is 23.13°. Gray bars indicate the mean values. (n = 15 larvae, least-squares linear regression $y = 0.039x + 19.11$, p-value = 0.286, R^2 = 0.02). (Figure adapted from (Temizer et al., 2015) with permission.)

To directly test this angular size threshold, I devised another set of experiments with truncated looming stimuli, which expand until a certain size is reached and then stop. Looming stimuli truncated to 9°, 13° or 15° were relatively ineffective at triggering the behavior, but did occasionally elicit an escape (Figure 3.8). However, stimuli with final angular sizes above ≈ 20° induced escape with a higher probability. I fitted the data with a sigmoid, and confidence intervals placed the center of the sigmoid, (or point of maximum slope),

between 17.5° and 20.7° (Figure 3.8, dashed red lines). These data support the idea that the angular size of the stimulus is a critical parameter for computing approach, and that a substantial change in escape probability occurs when the stimulus angular size surpasses ≈ 20°.

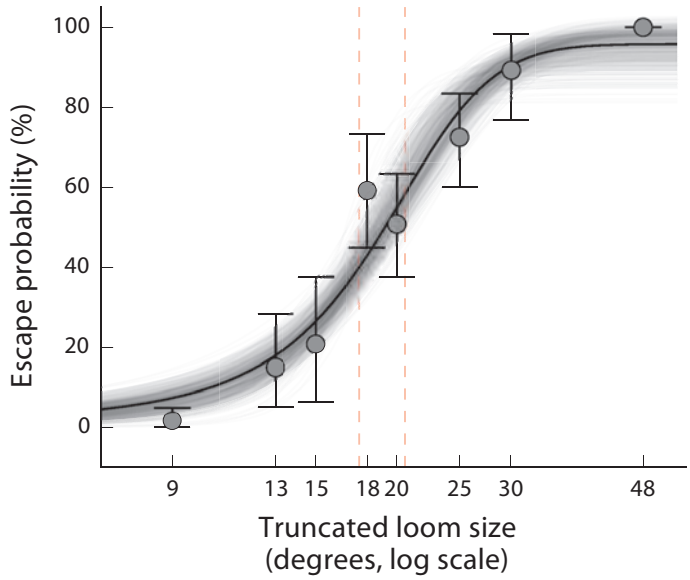

Figure 3.8: Escape probability as a function of final angular image size. Truncated looming stimuli were generated from the l/v = 60 ms stimulus. The tuning curve was fitted by a sigmoidal function ($y = 1/(1+e^{-k(x-x_0)})$ with x_0 = 18.8°). Bootstrap 95% confidence intervals computed to be 17.5° to 20.7° for the middle of the sigmoid which corresponds to the point of maximal slope, 0.25. Data points are mean probabilities across larvae (n = 20 larvae). Error bars indicate 95% bootstraps. (Figure adapted from (Temizer et al., 2015) with permission.)

For stimuli that approach with constant speed, angular size and speed are interrelated and thus difficult to disentangle. To directly explore the speed-tuning properties of escape responses, I generated a linearly expanding stimulus in which angular expansion was constant, unlike the constant approach speed stimuli (e.g. Figure 3.6A) in which the angular size expands nonlinearly. Such a stimulus expands linearly in angular size over time, thus, toward the end of the stimulus, the angular expansion is not as fast as the constant approach speed looming. I used five linear looming speeds; 2°/s, 10°/s, 20°/s, 100°/s and 200°/s. The higher angular speeds of 100°/s and 200°/s had a lower probability of trigger-

ing escapes. This could be because of the fact that, at the beginning of the stimulus, the linear looming is faster than the constant approach speed looming. Thus, for these high speeds, it is possible that the animal cannot identify looming initially, thus, fail to initiate escapes reliably. The 20°/s looming stimulus triggered more escape responses than the slower or faster stimuli (Figure 3.9). This suggests that the relevant circuitry can initiate escapes most reliably at an optimal angular expansion speed of around 20°/s. Moreover, this indicates that the expansion speed of the looming stimulus is an important factor in evoking escapes.

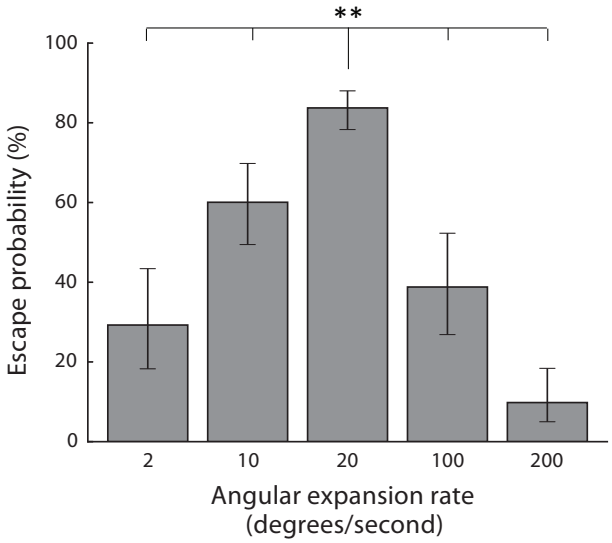

Figure 3.9: Escape probability as a function of constant angular expansion rate. (n = 23 larvae, GEE, p-value = $4.2x10^{-3}$ for 20°/s vs 10°/s. For 20°/s vs. all the other speeds, p-value < 0.0005, multiple comparisons were corrected by Bonferroni-Holm). Error bars indicate ±S.E. (Figure adapted from (Temizer et al., 2015) with permission.)

3.7 Visual areas AF6 and AF8 respond to looming as well as dimming stimuli

Next I used functional imaging to determine whether there are RGCs that respond to looming stimuli. RGC axons innervate nine distinct arborization fields (AFs) in the larval brain, in addition to the optic tectum (Figure 3.10A) (Burrill and Easter, 1994; Robles et al., 2014). I performed two-photon calcium imaging of RGC axon terminals in larvae

expressing the calcium indicator GCaMP6s under control of the RGC-specific promoter Islet2b. I presented a dark looming stimulus that had a relatively short stimulus duration (≈ 3.3 s, see Materials and Methods, section 2.2.1) but was effective in triggering escapes reliably (l/v = 60 ms). While displaying the looming stimulus monocularly to the larvae and scanning through the contralateral AFs, I detected robust responses in only two extratectal areas, AF6 and AF8 (Figure 3.10B-C and Figure 3.11). To assess the stimulus selectivity of these areas, I presented the array of stimuli used for the behavior experiments. Additionally, to compare the responses to a looming stimulus with different kinematics, I also tested a linearly looming stimulus (linear looming) which robustly triggered the escape behavior (20°/s angular expansion; see Figure 3.9). During each trial, there was first a blank screen, followed by the appearance of the stimulus (Figure 3.10C, "Stim on"), then the expansion, contraction, or dimming of the object ("Start") until the stimulus ceased changing ("End") and finally disappeared ("Stim off").

I found that AF6 RGC axons responded robustly to the dark looming stimulus (Figure 3.10B). AF6 RGCs were also activated by a linear looming stimulus (Figure 3.10B), which might be expected as this stimulus also evokes escape and is distinct from dark looming only in its temporal evolution. In addition, AF6 RGC axons responded to the dimming stimulus (Figure 3.10B). For these three decreasing luminance (OFF) stimuli, the peak AF6 response occurred during the expansion or darkening of the dark disk (Figure 3.10C). I also observed a slight response to the dark receding stimulus, but the plot of the time course of the response shows that the AF6 RGC axons were responding to the initial appearance of the dark stimulus, not its receding motion (Figure 3.10C). I also investigated the response of AF6 to a bright looming stimulus, which occasionally evoked escapes (Figure 3.5B), and found that AF6 was not responsive to this stimulus (Figure 3.10B).

I also observed responses to the looming stimulus in a more dorsal plane containing AFs 7, 8, and 9 (Figure 3.11A). Like AF6, AF8 axons responded to both looming dark and dimming (OFF) stimuli. Interestingly, AF9 RGCs responded vigorously to only looming bright and receding bright (ON) stimuli. For the receding bright stimulus, the time course of the response shows that the AF9 axons were activated by the appearance of the bright stimulus,

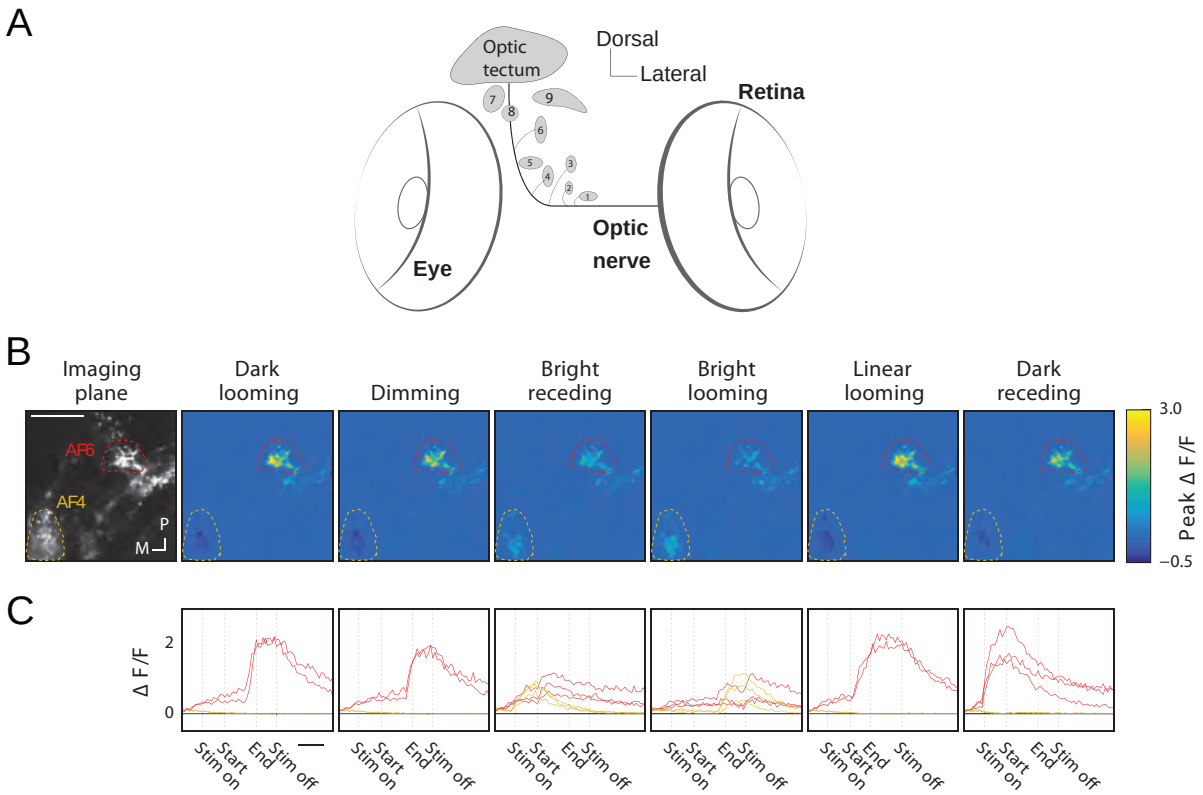

Figure 3.10: RGC axons that project to AF6 respond to looming and dimming stimuli. **(A)** Schematic frontal view of the larva denoting AFs in the midbrain and forebrain. **(B)** *Isl2b:Gal4, UAS:GCaMP6s* transgenic larvae were presented with a set of looming and control stimuli, and RGC axons in the plane containing AF6 and AF4 were imaged. The peak pixelwise stimulus response ($\triangle F/F$) over the stimulus time window is plotted for each stimulus. Responses are averaged across all trials for a single fish. **(C)** Temporal dynamics of the AF6 responses to each stimulus as traces of individual trials. The peak pixelwise stimulus responses ($\triangle F/F$) are given as 95 percentile values. AF6: red, AF4: yellow colored dashed lines. In (C), scale bar is 3 seconds and black colored traces indicate background. In (B), scale bars = 30 µm; P = posterior, M = medial. (Figure adapted from (Temizer et al., 2015) with permission.)

not the receding motion (Figure 3.11B). Some AF9 axons were activated by dark looming and dimming stimuli, but this response was relatively weak. The third AF in this plane, AF7, was only weakly activated by bright looming stimuli and did not respond to any of the darkening stimuli (Figure 3.11A).

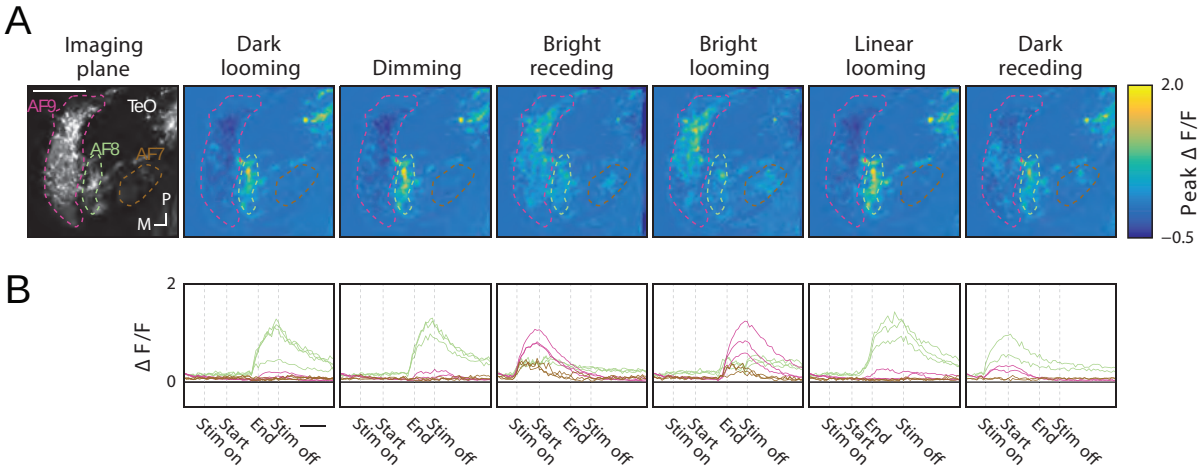

Figure 3.11: RGC axons that project to AF8 respond to looming and dimming stimuli. **(A)** Shows the same stimuli set as in Figure 3.10B, but in a more dorsal plane that includes AF7, AF8 and AF9. Responses are averaged across all trials for a single fish. **(B)** Temporal dynamics of AF8 and 9 responses are given per stimulus as traces of individual trials. The peak pixelwise stimulus responses ($\triangle$F/F) are given as 95 percentile values. AF7: orange, AF8: light green and AF9: magenta colored dashed lines. In (B), scale bars is 3 seconds and black colored traces indicate background. Scale bars = 30 µm; TeO = Optic Tectum, P = posterior, M = medial. (Figure adapted from (Temizer et al., 2015) with permission.)

3.8 Pixelwise analysis reveals a generalized OFF response of RGCs innervating AF6 and AF8

To determine whether individual RGC axons in these AFs are selective for any of the stimuli, we further analyzed the responses of single pixels within the imaging data. Each pixel corresponds to an area of 0.3 to 0.6 µm^2, which is in the range of single presynaptic boutons of RGC axons (Nikolaou et al., 2012). We compared the pixel responses to dark vs. bright looming by subtracting each pixel's bright looming response from its dark looming response. This revealed that most AF6 and AF8 pixels responded to the dark looming stimulus, whereas AF9 pixels were activated by bright looming (Figure 3.12A). An analysis of the temporal dynamics of six example pixels (two from each AF) showed that responses to the dark looming and dimming stimuli occurred during the darkening (OFF) phase of

the stimulus (Figure 3.12B), while the responses to the receding stimuli occurred at the initial appearance of the stimulus ("Stim on", Figure 3.12B).

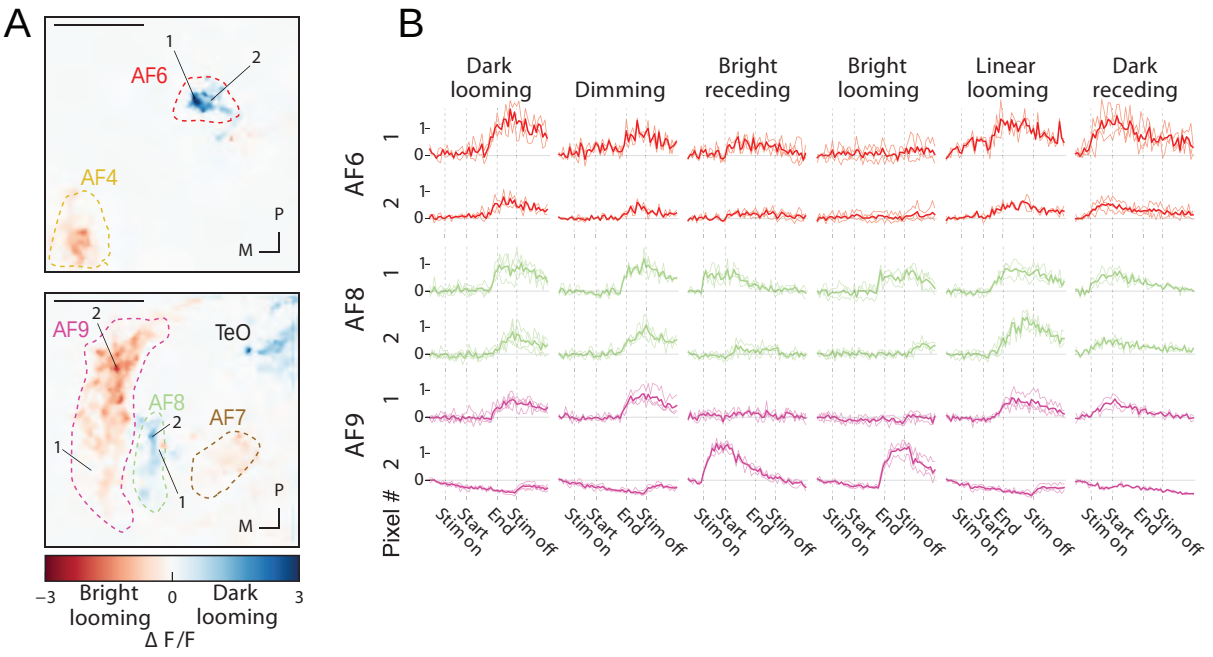

Figure 3.12: Pixelwise analysis of responses to looming vs. control stimuli reveal functional specialization in extratectal AFs. **(A)** Comparison of pixelwise responses to dark vs. bright looming stimulus. Each pixel's bright looming response is subtracted from its dark looming response. Pixels with positive values (larger response to dark looming) are blue, and negative values (larger response to bright looming) are red. **(B)** $\triangle$F/F traces of individual example pixels from corresponding AFs (confined with dashed lines) for each stimulus. Responses from individual trials per pixel are shown as colored traces and the mean is indicated by a bold colored trace. 95 percentile values were used as the pixel peak $\triangle$F/F values. Scale bars represent 30 µm; TeO = Optic Tectum, P = posterior, M = medial. (Figure adapted from (Temizer et al., 2015) with permission.)

We next plotted the individual pixel responses to dark looming vs. all other stimuli to assess whether this more fine-grained analysis would reveal selectivity for different stimulus features. Comparing the responses to dark looming and dimming for AF6 and AF8, we observed that pixels that responded to dark looming also responded to dimming stimuli, since the pixels are concentrated along the y = x unity line (Figure 3.13, panels 1, 6).

Similarly, we found that most AF6 pixels responded equally to dark looming and linear looming stimuli (Figure 3.13, panel 4).

Interestingly, two scatter plots of pixel responses in AF9 (Figure 3.13, panels 12 - 13) do not show a high pixel concentration along the straight unity line, but a bent distribution pointing in both horizontal and vertical directions. This may be caused by the presence of two functionally distinct populations of RGCs projecting to this area; one responding to decreasing luminance stimuli, and a larger population activated by the increases in luminance that occurred during the looming and receding bright stimuli. Indeed, recent study showed that AF9 receives input from ON and OFF-RGCs with distinct morphologies (Robles et al., 2014). Based on our analysis, AF6 and AF8 seem to be predominately innervated by RGCs that respond to decreases in luminance, rather than behaviorally relevant parameters such as the expansion of the looming object.

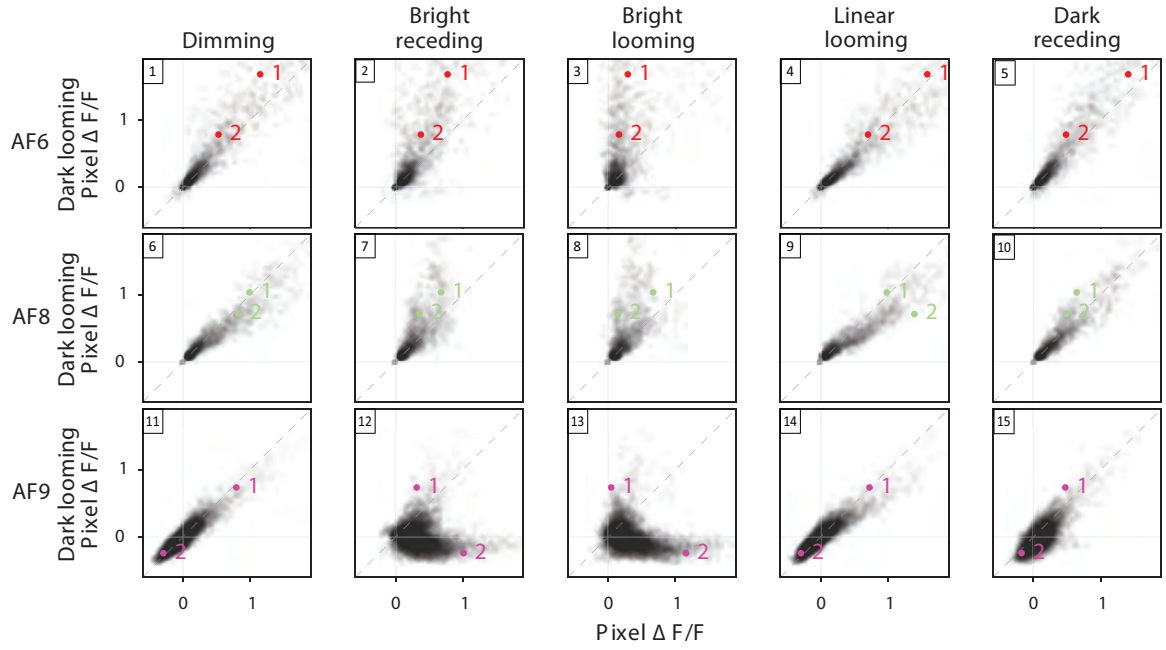

Figure 3.13: Scatter plots comparing peak response for each pixel in AF6, AF8 and AF9, to looming dark vs control stimuli. Pixels that are close to the unity line x = y, respond similarly for both compared stimuli (n = 4 larvae). Pixel # 1 and 2, marked red, are the same pixels as in Figure 3.12B. 95 percentile values were used as the pixel peak $\triangle F/F$ values. Panel labeling from top left to bottom right, 1 - 15. (Figure adapted from (Temizer et al., 2015) with permission.)

3.9 Functional imaging reveals looming-specific subsets of RGC axons in the tectal neuropil

I expanded our analysis of looming-responsive RGCs by performing imaging experiments in the optic tectum. The tectum receives highly organized RGC input, with each axon arborizing in one of the ten layers of visual neuropil (Robles et al., 2013). In response to the dark looming and linear looming stimuli, I saw robust activation in several layers of the stratum fibrosum et griseum (SFGS; Figure 3.14A) and often the stratum griseum centrale (SGC; Figure 3.15). The dimming stimulus also activated some SFGS axons, but this response was confined to the deepest layer of SFGS, SFGS6 (Figure 3.14A). All of these stimuli primarily evoked responses in the central (rather than the more anterior or posterior) SFGS (Figure 3.14A). This confined response could be due to the fact that the screen spanned over 62° of the monocular visual field. The looming stimulus therefore did not sweep across the most nasal and most temporal regions of the retina, which provide input to posterior and anterior tectum, respectively. In contrast, the two bright stimuli, bright receding and bright looming, both activated a larger swath of the tectum throughout the anterior/posterior axis (Figure 3.14A). This broad response could be due to the activation of RGCs that have very large receptive fields, or respond to overall luminance. Indeed, in the case of the receding bright stimulus, the response occurred at the appearance of the large bright object, not during the receding motion, indicating that these RGCs are likely to be activated by the increase in luminance (Figure 3.14B). The bright looming stimulus had similar temporal response dynamics to the dark looming stimulus since it differs from the dark looming stimulus only in its background-to-disk contrast (reversed contrast stimulus) (Figure 3.14B). This result might be related with the bright looming stimulus triggered escape responses (Figure 3.5B). However, the bright looming and the dark looming stimuli had much less spatial overlap in their activation (see Supplemental Figure 6.2). In addition, we imaged the tectal neuropil responses to the dark receding stimulus and a dark flashed disk of 48° (Figure 3.16), which induced similar activation patterns to the bright receding and dimming stimuli, respectively (experiment conducted by J. Semmelhack).

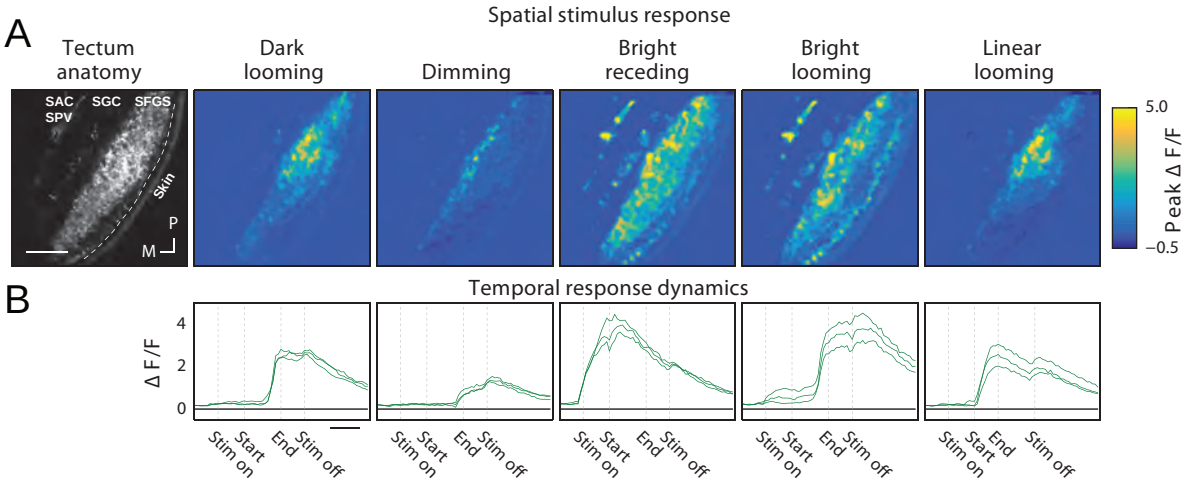

Figure 3.14: Differential activation of tectal RGC axons by looming vs. dimming. **(A)** Looming dark and control stimuli are presented monocularly to 6 to 8 dpf *Isl2b:Gal4, UAS:GCaMP6s* transgenic larvae while imaging the response of RGC axons within the contralateral tectal neuropil. Baseline fluorescent image from the *Isl2b:Gal4, UAS:GCaMP6s* transgenic larva showing tectal anatomy (SO, stratum opticum; SFGS, stratum fibrosum et griseum superficiale; SGC, stratum griseum centrale; SAC, stratum album centrale). The peak pixelwise stimulus response ($\triangle$F/F) over the stimulus time window is plotted for each stimulus. Responses are averaged across all trials for a single fish. **(B)** Temporal dynamics of tectal neuropil responses are given per stimulus as traces of individual trials. In (B), scale bars represents 3 seconds and black colored traces indicate background. 95 percentile values were used as the pixel peak $\triangle$F/F values. Scale bar represents 30 µm; P = posterior, M = medial. (Figure adapted from (Temizer et al., 2015) with permission.)

Pixelwise analysis of the tectal imaging data revealed populations of pixels that responded to decreasing or increasing luminance stimuli (Figure 3.17A), as in AF6, AF8 and AF9. However, unlike in the extratectal AFs, many dark looming-responsive pixels had a negligible response to dimming (e.g. Figure 3.17A, pixel #1). Indeed, the majority of looming-responsive pixels in the tectum had a weaker response to dimming than to looming (Figure 3.17B, panel 1). (For comparisons between control stimuli, see Supplemental Figure 6.3). We calculated the ratio of the responses to looming over dimming for each pixel, and found that this ratio was significantly higher for tectal pixels compared to extratec-

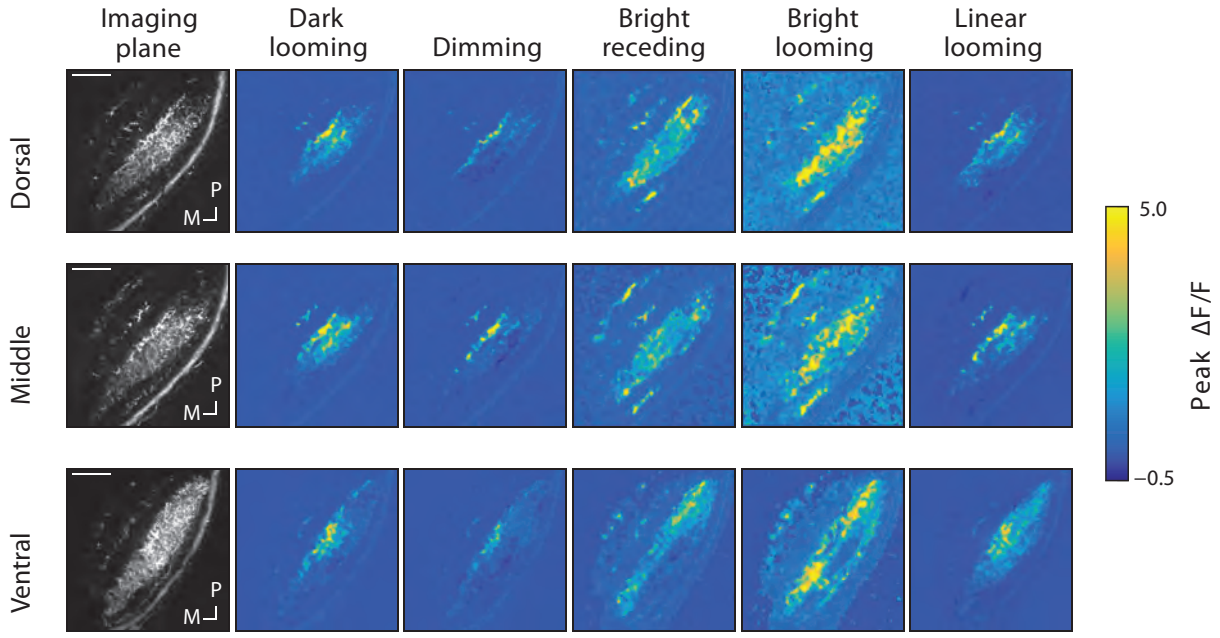

Figure 3.15: Spatial pattern of tectal neuropil responses to looming vs. control stimuli from individual larvae. Baseline fluorescent images (panel 1) and pseudocolored peak pixelwise stimulus responses (△F/F) from the three tectal planes imaged (n = 3 larvae). Responses during the stimulus time window are averaged across all trials and plotted for each stimulus. The peak △F/F's are given as 95 percentile values. Scale bars represent 30 µm; P = posterior, M = medial. (Figure adapted from (Temizer et al., 2015) with permission.)

tal AF pixels (Mann-Whitney U test, p-value = $6.9x10^{-4}$, p-value < $1x10^{-10}$, and p-value = $1x10^{-10}$ for tectum vs. AF6, AF8 and AF9 respectively.)

Finally, we visualized the location of dark looming-selective pixels within the tectum by subtracting each pixel's dimming response from its dark-looming response (Figure 3.18). This analysis confirmed that many of the pixels in the SFGS responded selectively to the expansion of the dark object, rather than to the change in luminance. When we plotted dark looming-selective pixels in the extratectal AFs with the same scale, we saw only a few pixels in AF6 with a slight preference for looming (Figure 3.18). These results imply that, unlike AF6 and AF8, the tectum receives looming-selective input.

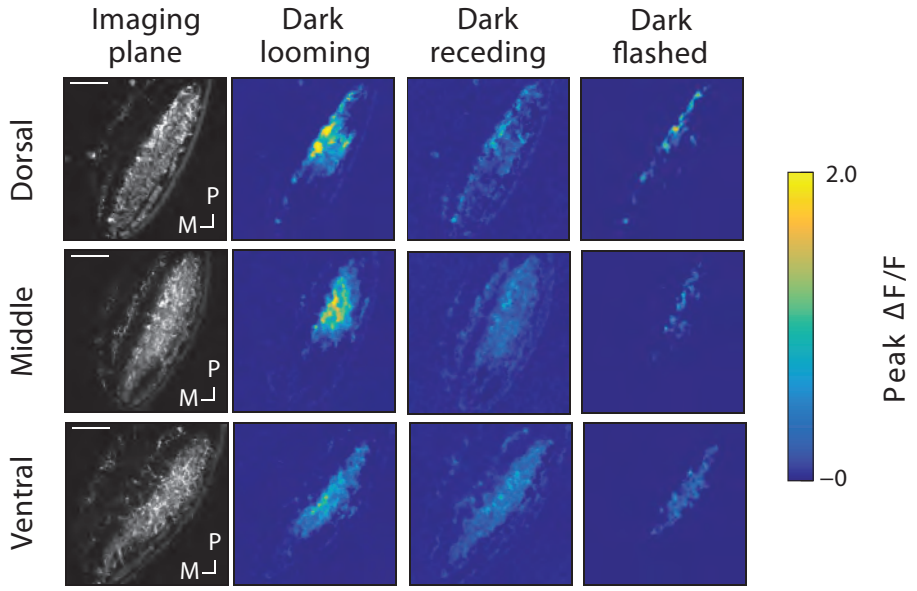

Figure 3.16: Differential tectal neuropil responses to dark looming, dark receding and dark flashed stimulus. Baseline fluorescent images (panels 1, 5, 9) and pseudocolored peak pixelwise stimulus responses (△F/F). Responses during over the stimulus time window are averaged across all trials per larva and plotted for each stimulus (n = 3 larvae). The peak △F/F's are given as 95 percentile values. Scale bars = 30 µm; P = posterior, M = medial. Panel labeling from top left to bottom right, 1 - 12. (Figure adapted from (Temizer et al., 2015) with permission.)

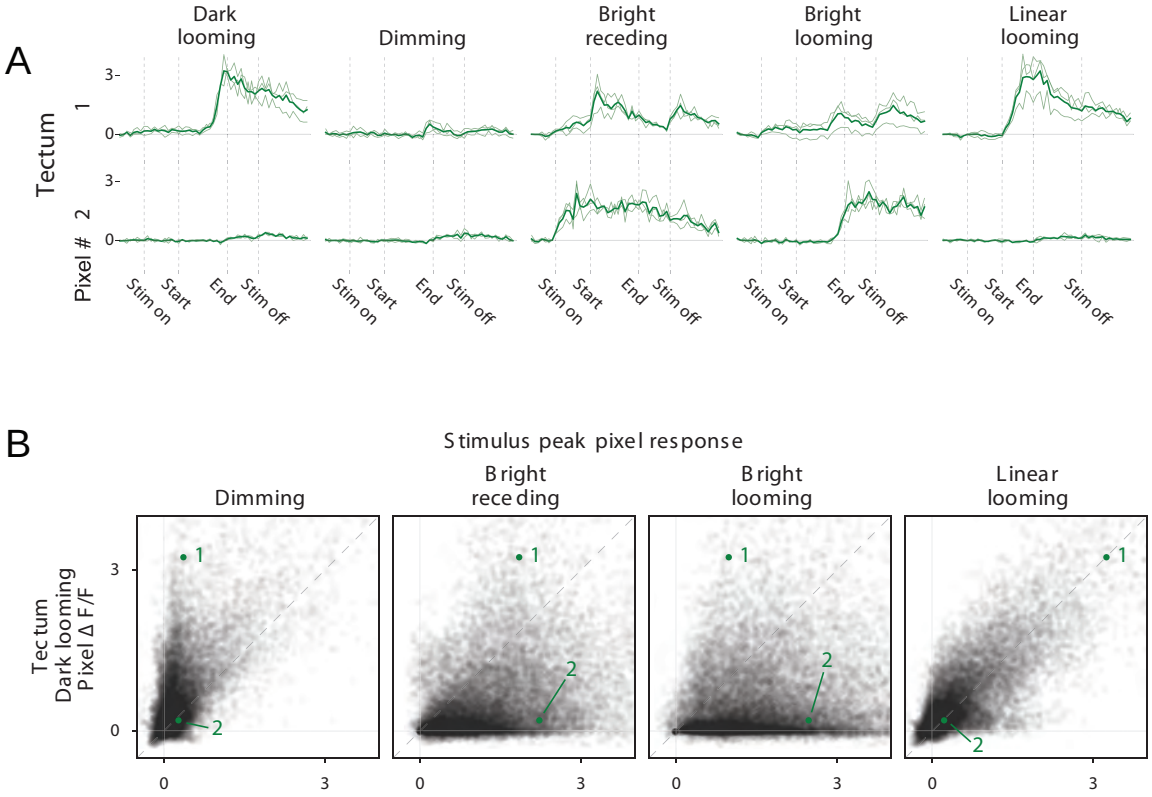

Figure 3.17: Pixelwise responses of tectal RGC axons. **(A)** $\triangle F/F$ traces from individual example pixels for each stimulus. **(B)** Scatter plots comparing peak pixel responses for looming dark vs. control stimuli. Pixels that are close to the unity line (x = y) respond similarly to both compared stimuli (n = 4 larvae). (For comparisons between control stimuli, see Supplemental Figure 6.3) 95 percentile values were used as the pixel peak $\triangle F/F$ values. Scale bars = 30 µm; P = posterior, M = medial. (Figure adapted from (Temizer et al., 2015) with permission.)

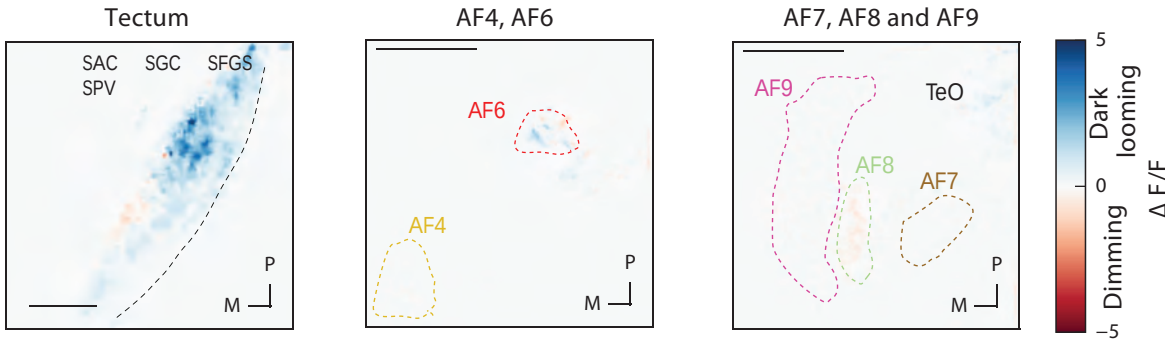

Figure 3.18: Comparison of pixelwise responses to dark looming vs. dimming stimulus in AFs. Each pixel's dimming response is subtracted from its dark looming response. Pixels with positive values (larger response to dark looming) are blue, and negative values (larger response to dimming) are red. 95 percentile values were used as the pixel peak $\triangle$F/F values. Scale bars = 30 µm; TeO = Optic Tectum, P = posterior, M = medial. (Figure adapted from (Temizer et al., 2015) with permission.)

3.10 Lesions of the tectal neuropil impair looming-evoked escapes

Since the imaging experiments identified tectal RGC axons that responded specifically to the behaviorally relevant looming stimuli, I focused on the tectum as the potential neural substrate for escape behavior. To test the necessity of retinotectal projections for looming-evoked escape, I performed laser ablations of the tectal neuropil. Ablations were performed unilaterally (always in the left tectum) in larvae expressing the fluorescent protein Dendra in RGCs. I selectively targeted the RGC axon bundles entering the tectum (Figure 3.19A; pre-ablation). Since I presented the stimuli monocularly (to the right eye of the larvae) and, in zebrafish, the retinal projections from each eye to the optic tectum cross completely at the optic chiasm, the contralateral tectum (the right tectum) served as an intrinsic control. Lesioning of axons subsequent to targeted ablations was immediately detectable (Figure 3.19A; post-ablation). All larvae were imaged 24h after the ablations to verify the persistence of the lesions. I confirmed that the ablations were restricted to the tectum by assessing the integrity of other AFs with DiI injections to the eye to label RGC axons (Figure 3.19B).

I found that larvae with tectum lesions were significantly impaired in their ability to escape in response to a looming stimulus (Figure 3.20A). To confirm that the tectal neuropil ablations did not have a generally adverse effect on visual function or swimming behavior, I tested the optomotor response (OMR), before and after ablation, by presenting a moving grating to the ablated side. In line with previous work (Roeser and Baier, 2003), the OMR was unaffected by ablation of the tectum (Figure 3.20C). In a few experiments, I recorded the behavior of individual larvae before and after the ablation (Figure 3.20B). The lesions completely abolished escape responses on the ablated side, while behavior was unaltered on the control side (n = 2 larvae). Together, these data indicate that the tectum plays an important role in looming-evoked escape behavior.

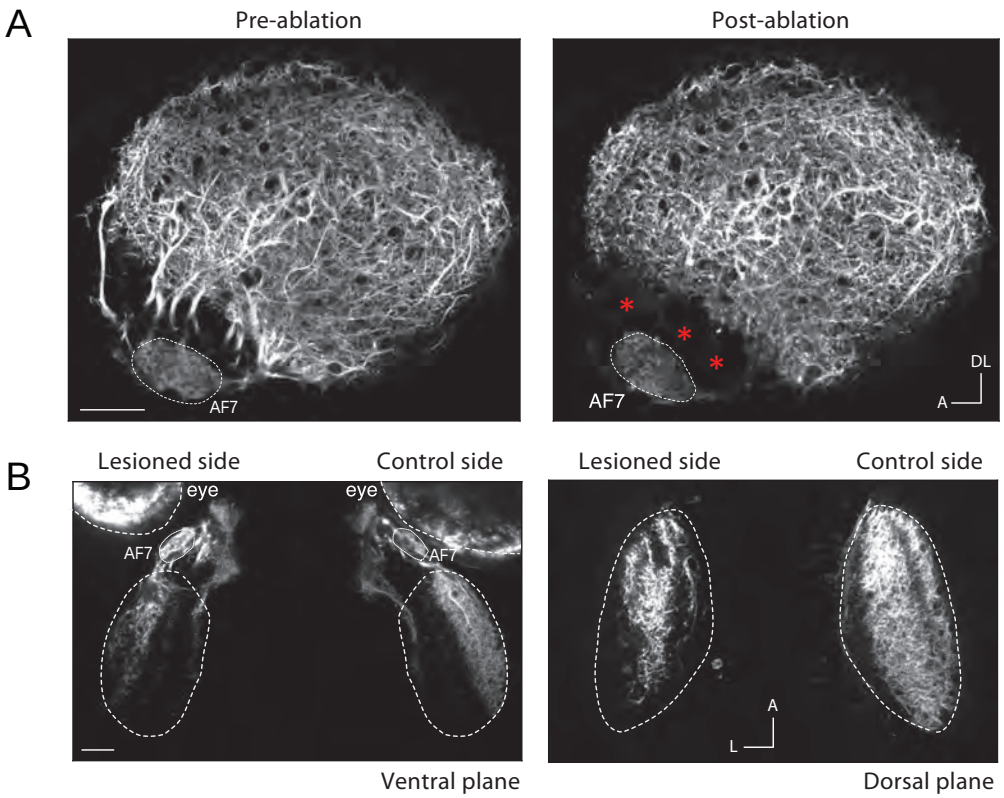

Figure 3.19: Targeted laser ablations of RGC axons innervating in the tectal neuropil. **(A)** Side view of a 7 dpf *Ath5:Gal4, UAS:Dendra* transgenic larva with intact left tectal neuropil (left panel) and immediately following ablation of left tectal neuropil (right panel). **(B)** DiI injection of the same larva as in (A). DiI images are given in two example z planes (left panel = ventral; right panel = dorsal) to show the extent of lesions through tectal neuropil. Asterisks denote lesion sides. Scale bars = 30 µm; A = anterior, L = lateral, DL = dorsa-lateral. Hatched white lines indicate tectal neuropil and AF7 for each image in (A) and (B). (Figure adapted from (Temizer et al., 2015) with permission.)

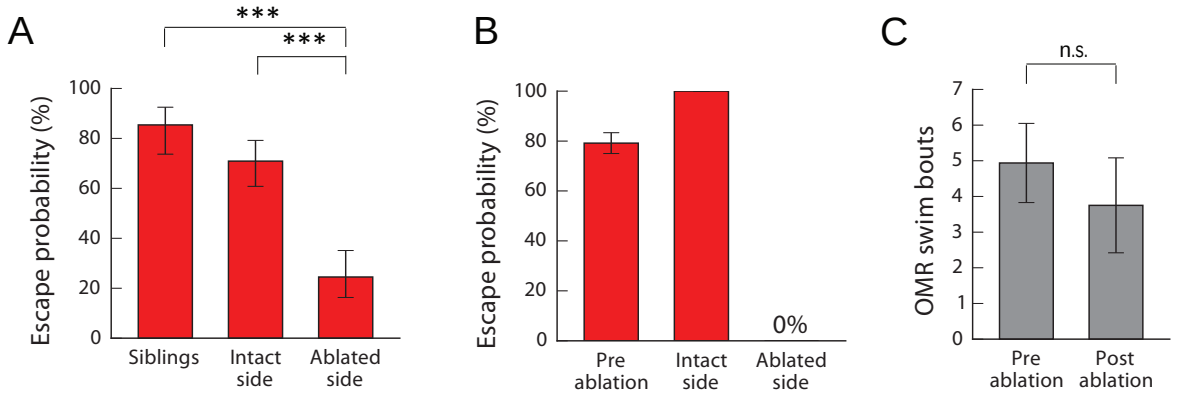

Figure 3.20: Intact tectal neuropil is necessary for the looming-evoked escape response. **(A)** Escape probability in control larvae (transgenic siblings, n = 13 larvae) and ablated larvae to the intact and ablated side (n = 12 larvae, GEE, p-value = $6.8x10^{-6}$ for siblings control vs ablated side and p-value = $9.2x10^{-5}$ for intact side control vs ablated side). **(B)** Escape probability before and after ablations (n = 2 larvae). Pre-ablation behavioral experiments were performed on the to-be-ablated side. No escape was observable to the ablated side. **(C)** Optomotor response triggered by moving gratings presented to the ablated side was unimpaired by tectum ablation (n = 5 larvae, dependent t-test, p-value = 0.44). Intact side in ablated larvae was used as an intrinsic control for behavior experiments. For details, see Materials and Methods, section 2.4. (Figure adapted from (Temizer et al., 2015) with permission.)

4 Discussion

In this work, I have established a behavioral paradigm to study the previously unknown escape behavior of zebrafish larvae in response to looming stimuli. I determined the specific parameters of the stimulus that effectively triggered escape responses and partially dissected the neural circuit underlying the escape response. Thereby, I used functional imaging to identify a subset of RGC axons that respond to looming. Two retinorecipient brain areas, AF6 and AF8, were shown to respond robustly, although not exclusively, to looming stimuli. RGCs innervating these two areas also responded to overall dimming. However, a looming-specific pattern of excitation was detected only within the retinorecipient layers of the optic tectum. This suggests that looming-selective RGCs project only to the tectum. Moreover, I demonstrated that ablation of RGC axons in the tectal neuropil markedly reduced the escape behavior, establishing the importance of this area for visually-evoked escapes. Taken together, the collected data expand the repertoire of interesting sensorimotor tasks that the fish larva can perform and are compatible with the presence of a specialized RGCs population, involved in detection and transmission of looming-specific visual information into the tectum.

4.1 Looming-triggered escapes in zebrafish

I have described strong, robust and immediate responses of zebrafish larvae to looming stimuli, to the best of my knowledge, for the first time. These looming-triggered responses mainly consist of two phases: the initial high amplitude contralateral bend of the tail and the following fast burst swim (see Results, sections 3.1, 3.2). The bend during the first phase of the escape normally turns the larva away from the stimulus, so that the subsequent forward burst swim serves to propel the larva away. This fixed action pattern

can be observed during looming-evoked escape in freely swimming fish (data not shown) and is maintained under open-loop conditions when the animal is immobilized. Previously, whole-field dark flashes-induced startle turns, called O-bends, were described in zebrafish (Burgess and Granato, 2007; Chen and Engert, 2014). These turns differ from the escape maneuvers that I describe here in several aspects: first, the turn direction is independent of stimulus origin in the case of an O-bend, whereas in escapes, it is usually away from the stimulus origin. Second, O-bend swims are not followed by burst swims as in the case of escape. Third, the swim direction of O-bend turns induced by dark flashes can be towards the stimulus. Thus, looming-triggered escapes comprise a novel class of visually evoked behaviors in the larval zebrafish.

In the head-restrained preparation, the eyes were not freed from the agarose, and typically become fixed in a neutral position during the embedding process (the eye positions of the larvae in Figure 3.1B are representative). Previously, it was estimated that, for larvae with unconverged eyes, visual objects 1.4 mm in front of the larva should be visible to both eyes (Bianco et al., 2011). Since the screen was 10 mm away, it can be assumed that objects in the center of the screen were viewed binocularly when larvae were placed facing directly toward the screen. This binocular stimulation of the larvae with looming stimuli revealed sharp, immediate C-bend turns with a high amplitude. Binocular stimulation results mostly in sharp C-bend escapes to either side. Monocular stimulation of the larvae occasionally resulted in S-bend escapes (Liu and Hale, 2014), with a lower turn angle than C-bend turns. This could be due to the stimulus position in the visual field: in monocular stimulation the looming was presented to the side of the larva. In this case, a smoother turn may already be enough to direct the larva away from the threat. In experiments with binocular stimulation, I observed a lateralization in the behavior (Figure 3.2A): the larvae had a tendency to initialize leftward turns.

I used an open-loop behavioral setup with a head-restrained preparation of the larvae. This may alter behavior response compared with free swimming. I chose a head-restrained preparation to have a better control over the stimulus parameters that I presented to the larvae as well as for the functional imaging afterward. My results show that

the behavior kinematics I observed overlap with the kinematics of the acoustic or tactile stimuli triggered C-bend escapes in the freely swimming larvae (Budick and O'Malley, 2000; Kohashi and Oda, 2008). Moreover, the looming stimulus evokes escape behavior in freely swimming larvae that are near the screen when the stimulus is displayed, with a similar locomotion pattern to the escapes that are evoked in head-restrained larvae (data not shown). Thus, the tethered preparation produces comparable behaviors to the innate, natural behavior of the zebrafish larvae.

4.2 Looming detection across species

Previous studies in visual looming-mediated escape behaviors in locusts (Hatsopoulos et al., 1995), flies (Holmqvist, 1994; de Vries and Clandinin, 2012; von Reyn et al., 2014), pigeons (Sun and Frost, 1998), adult teleost fish (Preuss et al., 2006; Dill, 1974a), amphibians (Nakagawa and Hongjian, 2010; Ishikane et al., 2005), mice (Yilmaz and Meister, 2013; Wei et al., 2015; Shang et al., 2015) and primates (Schiff et al., 1962) showed that the behavioral response is highly conserved, and that animals utilize similar neurobehavioral strategies to gauge the approach of a threatening stimulus.

Among vertebrate species, looming-sensitive cells are best described in the pigeon (Sun and Frost, 1998). These cells, found in the midbrain nuclei along the tectofugal pathway, in nucleus rotundus. They were classified into three distinct types (τ, ω and η cells), defined by thresholds for distinct optimal parameters of the looming stimuli: time to collision, angular speed and angular size of the looming object. Similarly, electrophysiological and behavioral studies in the locust have identified a looming-sensitive cell, the lobula giant movement detector (LGMD) neuron. These neurons robustly respond to looming stimuli in a contrast and luminance invariant manner (Simmons and Rind, 1997; Gabbiani et al., 2001). The time of peak firing rate of this cell relative to collision varies linearly with the looming stimulus size-to-speed ratio (l/v), (Hatsopoulos et al., 1995; Gabbiani et al., 1999). This linear relationship means that the peak response of these cells occurs at a fixed time delay after the stimulus reaches an angular size threshold on the retina. As a result,

escapes in response to fast-looming stimuli (small l/v) occur later than to slow-looming stimuli (large l/v) relative to collision. The firing rate of these neurons can be described with a nonlinear function of the stimulus angular size, called *eta*, which was introduced by Hatsopoulos *et al.* (Hatsopoulos et al., 1995):

$$\eta(t) = \dot{\theta}(t)\left(\mathrm{e}^{-\alpha\theta(t)}\right) \tag{4.1}$$

where $\theta(t)$ is the angular size, $\dot{\theta}(t)$ is the angular edge speed, α is a constant related to the angular size threshold (see Materials and Methods, section 2.2). This function increases with angular speed (excitation) at the beginning of looming and eventually decreases with angular size as implemented with negative exponential (inhibition).

Interestingly, my findings indicated a similar linear relationship between the timing of escape onsets, the anticipated time of collision and the value of l/v (Figure 3.7A-B). Furthermore, the threshold angular size that was observed in my psychophysics experiments, ($\approx$ 20°; Figure 3.7B) is remarkably similar to the angular size thresholds in other species such as locusts ($\approx$ 24°) and bullfrog ($\approx$ 25°) (Gabbiani et al., 1999; Nakagawa and Hongjian, 2010). It is quite possible that the zebrafish brain combines the excitation provided by angular speed and inhibition provided by angular size in a nonlinear manner as in $\eta(t)$ function, which uniquely reproduce the characteristic linear relation between l/v and the response onset time relative to collision (Gabbiani et al., 1999).

The behavioral experiment with the constant angular speed looming stimuli was designed to investigate the dependency of escape responses on the speed of the looming (Figure 3.9). In terms of an approaching object, this stimulus corresponds to a decelerating approach, meaning that the true speed of the object is decreasing over time. The plot of the angular sizes at escape onsets for constant angular speed looming stimuli did not yield a clear threshold angular size (see Supplemental Figure 6.1) as in constant approach speed looming stimuli (Figure 3.7B). Although the angular sizes at escape onsets are statistically indistinguishable for the stimuli from 2°/s to 20°/s ($\approx$ 27.2°, least-square regression y = 0.05755x + 26.76, p-value = 0.79, R^2 = 0.002), for higher angular speeds this

value increases significantly (Supplemental Figure 6.1). These two looming stimuli sets (constant approach speed looming and constant angular speed looming) differ in their kinematics, representing different object approaches. For example, in locusts, while the constant approach speed looming stimuli trigger escape responses, the constant angular speed looming stimuli fails to elicit responses that are comparable to those of constant approach speed looming (Rind and Simmons, 1992; Simmons and Rind, 1992; Simmons et al., 2013). Although the constant angular speed looming stimuli can trigger escape responses in zebrafish, it is difficult to interpret the angular size threshold in the context of constant angular speed looming.

Interestingly, if we assume a longer sensory-motor delay ($\approx$ 180 ms) for the constant angular speed looming stimuli triggered escapes, we reach a threshold angular size ($\approx 25^{\circ}$) which is fairly similar to the one observed in the constant approach speed looming stimuli triggered escapes. From this point of view, if there is one fixed threshold angular size, one can hypothesize that these two stimuli sets simply activate different (maybe parallel) escape pathways with different neural delays, that finally converge on escape. In this case, the larvae select one of these escape pathways to trigger escape responses at different delays, depending on the looming stimuli statistics. Further experiments are necessary to elucidate the precise details of the escape responses that are elicited by statistically distinct looming stimuli.

4.3 Responses to looming stimuli in RGC axons

My experiments showed that looming-triggered escapes occur as an innate response in the naïve animal and that the escape latency strongly depends on the expansion speed of the looming stimulus (Figure 3.7A). Given the importance of detecting an approaching threat for survival and the rapid, robust responses that were observed, one would expect the existence of a dedicated neural circuit driving this essential behavior. Since the RGCs constitute one of the earliest stages in visual processing and some distinct subtypes support specific innate responses, I hypothesized that the first opportunity for the zebrafish

brain to detect an approaching object might emerge at the RGC level. These looming-detecting RGCs then would hypothetically project to particular, dedicated visual area(s) that drive escape responses.

I showed that, although a mere dimming of a disk of constant size is not sufficient to evoke escapes (Figure 3.5), the most effective looming stimulus has a dimming component (Figure 3.5), implying a role for the OFF-RGCs. However, since the bright looming stimulus can also trigger escapes, although much rarely than the dark looming stimulus (Figure 3.5B), the ON-OFF direction selective RGCs can also be involved in looming detection. Furthermore, the speed tuning of the behavior responses (Figure 3.9) suggests involvement of transient OFF-RGCs and/or ON-OFF direction selective RGCs which are sensitive to rapid changes (Weng et al., 2005), rather than the sustained OFF-RGCs, which have a broader speed tuning covering slower speeds (Pang et al., 2003). Such a highly approach-sensitive type of a retinal ganglion cell was described in mice previously (Münch et al., 2009), although it is not known whether its activation results in a behavioral change.

I found that ganglion cells in two retinorecipient areas, AF6 and AF8, as well as several layers of the tectum, were robustly activated by dark looming stimuli. It is worth noting that an expanding stimulus sweeps across a large part of the visual field and therefore activates a substantial population of neurons. This feature makes it inherently difficult to identify the neurons that are directly involved in encoding the escape-triggering stimulus. While a pan-RGC imaging approach can detect RGC subtypes, there is a chance of missing a rare subtype that has its axons, and therefore the calcium signal, mixed in with other broadly responding RGC subtypes.

To identify the neural substrate of the behavior, I used a variety of stimuli that shared important parameters with the looming stimulus, but did not evoke the behavior. I found that individual RGC axons in AF6 and AF8 generally responded to a decrease in luminance, rather than to the behaviorally relevant parameter of expansion. These AFs have been shown to receive input predominately from RGCs with dendrites in the OFF layer of the IPL (Robles et al., 2014), which is consistent with their responses to dark looming and dimming. Moreover, AF6 is mostly innervated by dorsal RGCs whereas AF8 is preferen-

tially innervated by ventral RGCs (Robles et al., 2014), possibly covering the visual space important for triggering defense against ecologically relevant threats. Interestingly, these RGCs also make collaterals in tectal neuropil, deeper layers of retinorecipient SFGS sublamina, where I observed robust responses to dark looming. In addition, AF6 innervates also in SGC layer in the tectal neuropil.

It is not known whether these RGCs are directly involved in looming-triggered escapes. Imaging and lesioning experiments indicate that the tectum is mediating the behavior (see below, section 4.4). Genetic markers for AF6 and/or AF8 would allow to selectively inhibit the RGCs in these retinorecipient areas. In addition, targeted laser ablations of AF6 and AF8 are technically challenging due to the positions of these AFs. AF6 is relatively deep in the brain and both AF6 and AF8 are very close to the optic tract, making it hard to ablate them without damaging the optic tract. Hence, the functions of AF6 and AF8 have not been isolated yet. They may "alert" the tectum about the presence of a shadow, thus facilitating a looming-evoked escape, or they may be involved in different luminance-sensitive behaviors, such as phototaxis.

4.4 Role of the tectum in escape

The tectum is known to be the main sensory integration and processing unit in teleost fish. It receives direct input from 97% of the RGCs, forming the primary visual center in the zebrafish midbrain. The tectum and its mammalian homologue, the superior colliculus (SC), contain a high-resolution map of visual space and are generally thought to be involved in localizing objects and directing appropriate orienting movements towards or away from salient objects, such as prey or predators (Sahibzada et al., 1986; Sparks and Nelson, 1987; Gahtan et al., 2005; Fajardo et al., 2013). Moreover, it has been shown that pharmacological disinhibition or local stimulation of the tectum can evoke tracking or pursuit and defensive behavior in rodents, goldfish and primates (Dean et al., 1989; Herrero et al., 1998; DesJardin et al., 2013). Furthermore, tectal neurons that respond to looming stimuli have been found in fish (Sajovic and Levinthal, 1983; Niell and Smith, 2005),

tadpoles (Khakhalin et al., 2014), mice (Wei et al., 2015; Shang et al., 2015), cats (Liu et al., 2011) and birds (Wu et al., 2005). Thus, it is conceivable that tectum mediates looming-triggered escapes by integrating looming-selective RGC input and feeding it to the escape-associated reticulospinal circuit.

Within the tectal neuropil, I observed responses to looming and dimming in the SFGS. Interestingly, I found that several layers of the tectum, likely SFGS2-5, appear to respond more strongly to looming than to dimming. These SFGS layers are innervated by RGCs that do not arborize in any other AFs (projection classes 5-8 (Robles et al., 2014)). Thus, looming-selective RGCs, terminating in the SFGS, might underlie the stimulus selectivity of the behavior. However, mapping the looming-selective responses to the SFGS layers of the tectal neuropil via pixelwise analysis has not allowed me to clearly identify a single looming-selective RGC type. From an earlier study (Robles et al., 2014), it is known that these layers of the SFGS receive input from RGCs with many different dendritic morphologies. Therefore, linking the looming-selective RGC axons with dendritic morphology would require systematic single RGC axonal imaging with characterization of dendritic morphology in the retina.

It is possible, however, that additional RGC types are required for the behavior, and that the detection of the looming stimulus occurs in the downstream periventricular neurons of the tectum, perhaps via pooling of the inputs from an array of RGC dimming detectors. Previously, a candidate circuit, filtering responses to objects by size, has been demonstrated in the tectum (Del Bene et al., 2010). By analogy, the angular size threshold that I observed in my psychophysics experiments might be encoded at the level of tectal cells, via a specialized cell population. While the cellular composition of the looming circuit has yet to be revealed, the tectum is the site where spatiotemporal stimulus features are likely to be integrated (see recent study by Dunn et al. (2016)). Once a critical angular size has been reached, a tectum-generated command could then drive escape motor circuits in the hindbrain, such as the Mauthner neuron and its homologues (O'Malley et al., 1996).

My lesioning experiments indicate the relevance of the optic tectum in the looming-evoked escape response. Larvae could occasionally perform escapes on the ablated side,

which could be explained by the incomplete nature of the tectal ablations. I showed that the direction of the escape behavior is dependent on the location of the stimulus within the visual field (Figure 3.2B). Thus, the location of looming-responsive neurons within the tectum could be read-out to generate a directional motor response. Future experiments are required to elucidate the underlying neural circuit.

4.5 Looming computation: single neuron coding or population coding?

Several scenarios are possible for the implementation of looming sensitivity arising from my behavioral and functional imaging data. One possibility would be that the RGCs in AF6 and AF8 encode dimming as an alert function (Franconeri and Simons, 2003) and provide early excitatory input to the optic tectum when appropriate. In parallel, presumably looming-sensitive RGCs that arise from the pixelwise analysis, convey looming selective input to the downstream tectal cells by projecting to the deep layers of the tectal neuropil. The peak activity in RGC axons does not seem to encode the angular size threshold. Hence, alternatively, different RGCs encode different features of the looming stimulus, such as dimming, motion direction, speed, angular size etc. These signals may converge in the deep tectum and the stimulus categorization emerges at the tectal cell level, where all differential inputs are pooled and processed. Previously, looming responsive tectal neurons, with receptive field sizes of up to 30° were found in zebrafish (Sajovic and Levinthal, 1983; Niell and Smith, 2005), but the specificity and spatial extent of these neurons remain unknown. The angular size threshold that I observed in my behavior experiments is in the range of receptive field sizes of the looming responsive tectal cells that were found previously. This suggests that a subset of these cells forms a specialized looming detector class. It is also possible that an expanding OFF edge can be detected through tectal cells, encoding local motion in opponent-direction, center-surround organization, in a distributed tectal network. Summation of the excitation results in a signal exceeding a threshold level which consequently converges on hindbrain descending command circuits to generate appropriate motor output.

In locust and flies, looming-sensitivity is achieved by a pair of wide-field neurons that have a peak firing rate at a fixed delay before the stimulus reaches an angular size threshold and animal takes off (Fotowat and Gabbiani, 2007; Fotowat et al., 2009). These neurons perform a nonlinear computation by combining excitation and inhibition according to the $\eta(t)$ function (Hatsopoulos et al., 1995). Although, there are differences in the anatomical position of these looming-sensitive neurons in locust and flies and the complex neuropil structure of the zebrafish optic tectum, the ultimate computation can be similar. Moreover, this type of nonlinear neural computation facilitates the animal's survival by inducing earlier take-off for larger objects assuming equal speeds, accentuating the salience of a potential threat. However, we need further behavioral and imaging experiments, both pre- and postsynaptically in the tectum, to disentangle the neural computation underlying looming detection.

4.6 Limitations of the methodology

In my current looming stimuli set, I have used two types of looming: first, constant approach velocity looming which triggers an accelerating angular expansion and second, constant angular speed looming, indicating a linear angular expansion. All of the stimuli started from the same initial angular size, 2° and expanded until a maximum of 48°. Although I can trigger escape responses with the current stimuli set, I do not know how much of it relates to the ethologically relevant threat. Further behavior experiments exploring the effect of different stimulus initial sizes and speeds on the behavior separately, are necessary to understand the underlying computation in more detail.

In addition, I could show that mere dimming of a stationary large disk did not evoke any escape responses, indicating the necessity of an edge motion for the behavior. Although in a control experiment we assessed the efficacy of a laterally moving large dark disk (observation by J. Semmelhack), which did not evoke any escape response, I have not tested an iso-luminance looming stimulus. This could be done with a checkerboard looming stimulus in order to check the necessity of pure expansion without dimming. Since the

bright looming stimulus comes second best after dark looming in triggering escapes (Figure 3.5B), I would expect that checkerboard looming evokes escape responses. This would confirm the presence of an expansion computing circuit in the zebrafish brain (see recent study by Dunn et al. (2016)). Previously, it was shown that locust LGMD neurons and fly looming-sensitive neurons both robustly respond to checkerboard looming stimulus (Gabbiani et al., 2001; de Vries and Clandinin, 2012). Stimulus parameter space is large; however, to dissect the responses further, it would also be interesting to design a second-order motion (e.g., motion-defined motion) looming stimuli (Adelson and Bergen, 1985). Since OMR and second-order motion processing do not require the tectum (Roeser and Baier, 2003), this experiment would help to assess the involvement of the extratectal circuits for the escape behavior.

My functional imaging experiments also have limitations in terms of elucidating the identity of putative looming-sensitive RGCs in the tectal neuropil. Unfortunately, we do not yet have transgenic lines that label distinct RGC subpopulations. This led me to perform the calcium imaging in pan-RGC Gal4 line expressing GCaMP6s, which in turn makes it difficult to identify the responding cell types afterward. One way to overcome this problem for now would be a sparse labeling of RGCs by DNA injections of UAS:GCaMP6 into the pan-RGC Gal4 expressing eggs at single cell stage and use transiently expressing transgenic larvae for functional imaging. Alternatively, one could use a BGUG:Gal4 transgenic line (Scott et al., 2007) to label a subset of RGCs. Moreover, the use of faster, newly engineered genetically-encoded calcium or voltage indicators (Chen et al., 2013; Hochbaum et al., 2014; Berlin et al., 2015) and calcium signal acquisition with, for example, a resonant scanner, might help to decode the response kinematics better in the future.

Finally, laser targeted ablations of the RGC axon bundles (Figure 3.19A-B), climbing to the tectal neuropil, were time consuming and since it is a manual surgery, not well-controlled. Although one can confirm the extent of ablations in the AFs overall afterward via DiI labeling, one cannot confirm whether the RGC axons die back at the branch spots or not. Moreover, one cannot confirm whether the ablations also affect the collaterals of ablated RGCs in AF8 and AF6, possibly making them not functional. An alternative approach for

manipulating neural activity would be to use optogenetics to establish causality in the transparent brain of zebrafish in a reversible manner (Fenno et al., 2011). However, the field is currently lacking tools that effectively inhibit neural activity in zebrafish *in vivo*, especially at the axonal level. I have performed proof-of-principle experiments with one of the latest blue-light-sensitive chloride channels, namely Arch (Wietek et al., 2014), to block the AF9 activity during OMR behavior while presenting moving grating, but could not get a positive result, meaning absence of OMR response. If it could work, the idea would be to silence the neural activity in the tectal neuropil unilaterally during looming stimulus presentation and block the escape behavior. Moreover, one could assess more precisely the position of putatively looming-sensitive RGCs in the tectal neuropil by shining light with a fine spatial resolution and moving it across the neuropil.

5 Conclusion and outlook

The zebrafish brain, with its genetic accessibility and homology, provides an excellent model system for neuroscience to link perception to behavior. I have described for the first time a visual looming mediated behavior of zebrafish larvae, which provides a powerful model for studying sensorimotor integration. My results identify the essential features of the looming stimuli psychophysically and point toward a specialized neural circuit for looming detection. Next, I began to characterize neural activation elicited by such stimuli. I found specific responses in defined RGCs. This suggests they encode a threat. Targeted laser ablation experiments in the tectum showed that they were necessary for the escape behavior.

Several open questions remain to be addressed to illuminate the neural basis of looming detection and the circuit components that underlie this vital behavior. One of them is the identity of the RGCs that selectively respond to looming and their postsynaptic partners in the tectum. To tackle these questions diverse RGC markers are required that can target specific subpopulations and dissect the response profile of candidate RGC types with functional imaging. These RGCs are possibly feeding into a tectal network where the further computation of looming is likely to take place. One could perform two-photon calcium imaging in pan-neuronal transgenic larvae, in search of looming-selective tectal cells, although in this case the type of neurons that generates the signals remains ambiguous. From that point, depending on the distribution of selective responses, candidate Gal4 lines that label distinct tectal cell populations can be tested. This will be an essential experiment to understand the representation of looming parameters in tectal cells. Another useful experiment would be utilizing a monosynaptic retrograde tracer (Stepien et al., 2010) by initiating the tracer from the looming-sensitive tectal sites *in vivo* and look at the presynaptic RGC partners. However, this tool is currently not available in zebrafish.

Another open question is the contribution of AF8 and AF6 to the looming-triggered escape, if any. Since I could not perform ablation experiments in these two retinorecipient areas due to their critical anatomical position and since we do not have the tools to selectively silence neural activity at the axonal level, the roles of these areas in behavior, if any, remain to be elusive. One could perform two-photon imaging in postsynaptic AF6 and AF8 neurons to see whether they encode any looming-specific information. Previously it was shown that extratectal neurons process whole-field motion (Kubo et al., 2014), forming dedicated visual channels that support OMR and OKR responses. Although we now know that the looming stimuli selective RGC input feeds to the optic tectum, it will be interesting to see whether these areas are necessary for the behavior.

Finally, it remains unclear what are the neural substrates of the downstream hindbrain circuit that translates looming-specific visual information into motor output. We know that the Mauthner cells (M-cells), a pair of reticulospinal neurons in the hindbrain of teleost fish, and its segmental homologues play a crucial role in fast, high-amplitude C-bend escape turns in response to tactile or acoustic stimuli in larval zebrafish (Kohashi and Oda, 2008; Lacoste et al., 2015). In goldfish, anatomical and physiological experiments demonstrated that M-cells receives direct tectal input from its ventral dendrite (Zottoli et al., 1987); however, currently there is no evidence that this applies to larval zebrafish as well. Previously, electrophysiological recordings also showed that the neural activity in M-cells is strongly correlated with canonical escape maneuvers (the C-bend turns) in adult goldfish, in response to looming stimuli (Preuss et al., 2006). Interestingly, Preuss *et al.* also showed that temporal kinematics of looming-triggered excitatory postsynaptic potentials in the M-cells can be fitted with the scaling function $\eta(t)$, which was described previously (see section 4.2). In preliminary experiments, I performed two-photon functional imaging in the M-cells backfilled with dextran-conjugated calcium indicator, OGB-1, and did not receive any signal in response to looming. Moreover, I performed laser targeted ablations of M-cells and tested whether this would cause any dramatic effect on the behavior. While ablation of M-cells did not abolish or cause any obvious defect in the behavior (data not shown), it is still possible that certain parameters of the behavior, such as bend-amplitude, speed and latency of escape are affected (see recent study by Dunn et al. (2016)). Future

experiments are needed to dissect the role of M-cell and its segmental homologues in visually-mediated escapes and to confirm the putative direct, anatomical link between the tectum and the M-cell in zebrafish. Understanding the complete neural circuit that filters salient sensory cues and transforms them into an innate behavior will provide fundamental insights into how the vertebrate brain makes complex evaluations, for example, when facing impending threats.

Other future directions include dissecting the behavior further by high-speed camera recordings to observe sub-behaviors, preparatory phases and accompanying eye movements of the looming-triggered escapes. In combination with functional imaging and correlation analysis, each of these details may provide information about the underlying neural circuit. In addition, one can look at other brain areas, such as nucleus isthmi, that was shown to respond to looming stimuli in teleostean fish (Gallagher and Northmore, 2006), especially in the presence of two competing stimuli in owls (Asadollahi et al., 2010). Little is known about how the saliency decision is made when larva is presented with both a prey- and predator-like stimuli simultaneously. To map the whole-brain looming-triggered escape circuit, one can utilize CaMPARI, a new calcium indicator (Fosque et al., 2015), to label active neurons during the escape behavior depending on their calcium activity level in freely swimming larvae. Such technological advances in tools and methods enable us to genetically target, monitor, manipulate, trace and model the neuronal circuits. I believe that the zebrafish model organism, in combination with these advances, will continue to provide us a better understanding of the general working principles of vertebrate brain and perhaps in future, will help us to better describe the neural basis of 'simple' innate behaviors in humans.

6 Appendix

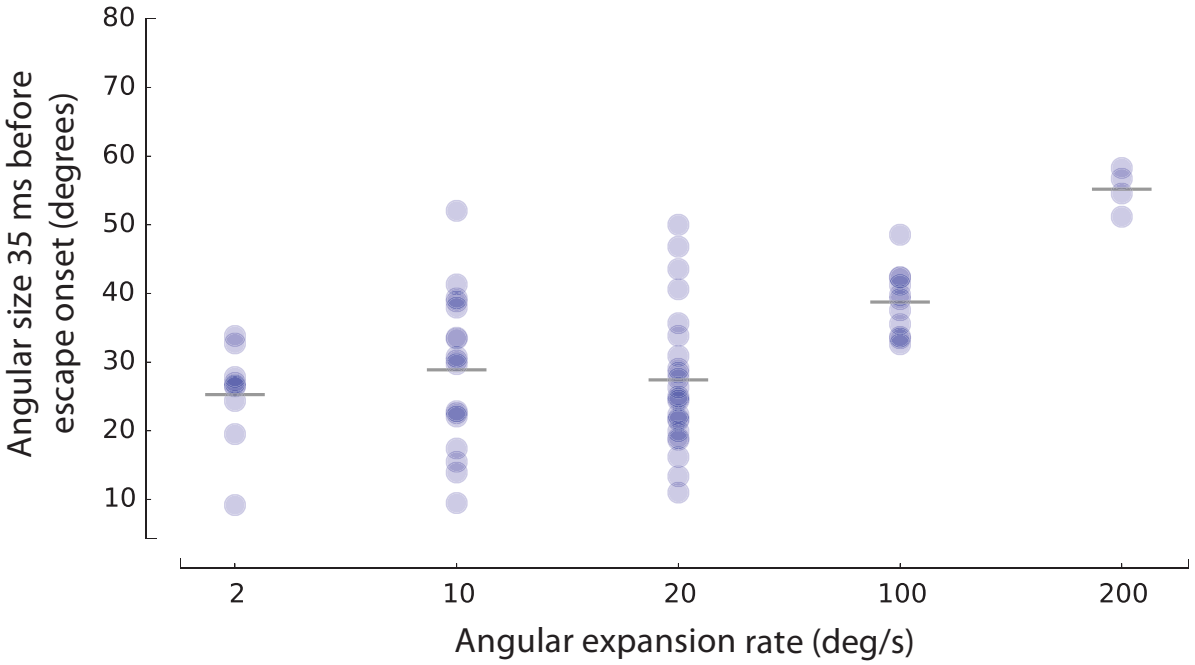

Figure 6.1: Angular size 35 ms before escape onset for constant angular speed looming stimuli. Stimulus angular sizes at a fixed neural delay preceding escape onset (35 ms, see Materials and Methods, section 2.2.1) vs. constant angular speed stimuli from 2°/s to 200°/s. Each dot represents the angular size value averaged within larva (n = 23 larvae). Overlapping dots (dark color) show the intensity of escape events. Gray bars indicate the mean values.

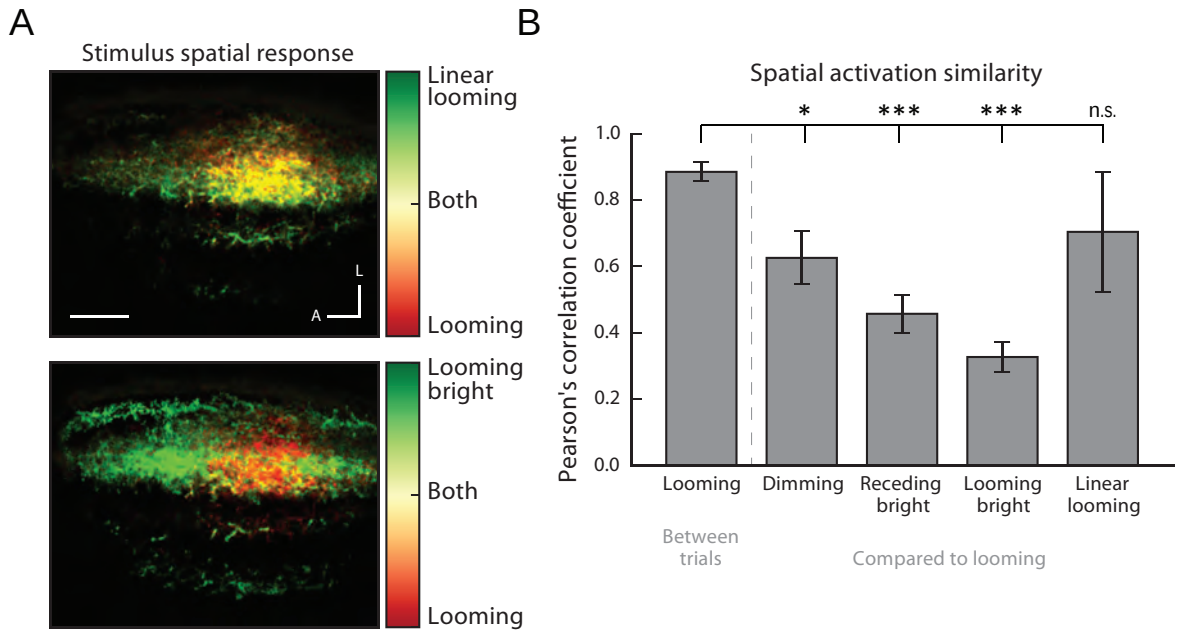

Figure 6.2: Stimulus spatial response overlap in the tectal neuropil. **(A)** Spatial overlap between the response to the linear looming and bright looming stimuli. Yellow indicates a robust response to both stimuli, while red and green denote areas that were responsive to a single stimulus. **(B)** Quantification of the spatial similarity of activation by looming vs. other stimuli. Pearson's correlation coefficient was computed per fish for the response to each stimulus vs. looming. A value of 1 would indicate an identical response. Between different trials of looming stimuli, the response was highly correlated. Dimming, receding bright, and looming bright stimuli all had significantly different response correlations. Dependent t-test within fish (n = 5 larvae), Bonferroni corrected p-values of $2.7x10^{-2}$, $2.4x10^{-4}$, $1x10^{-4}$, and $4.3x10^{-1}$, respectively. Scale bars = 30 µm; A = anterior, L = lateral.

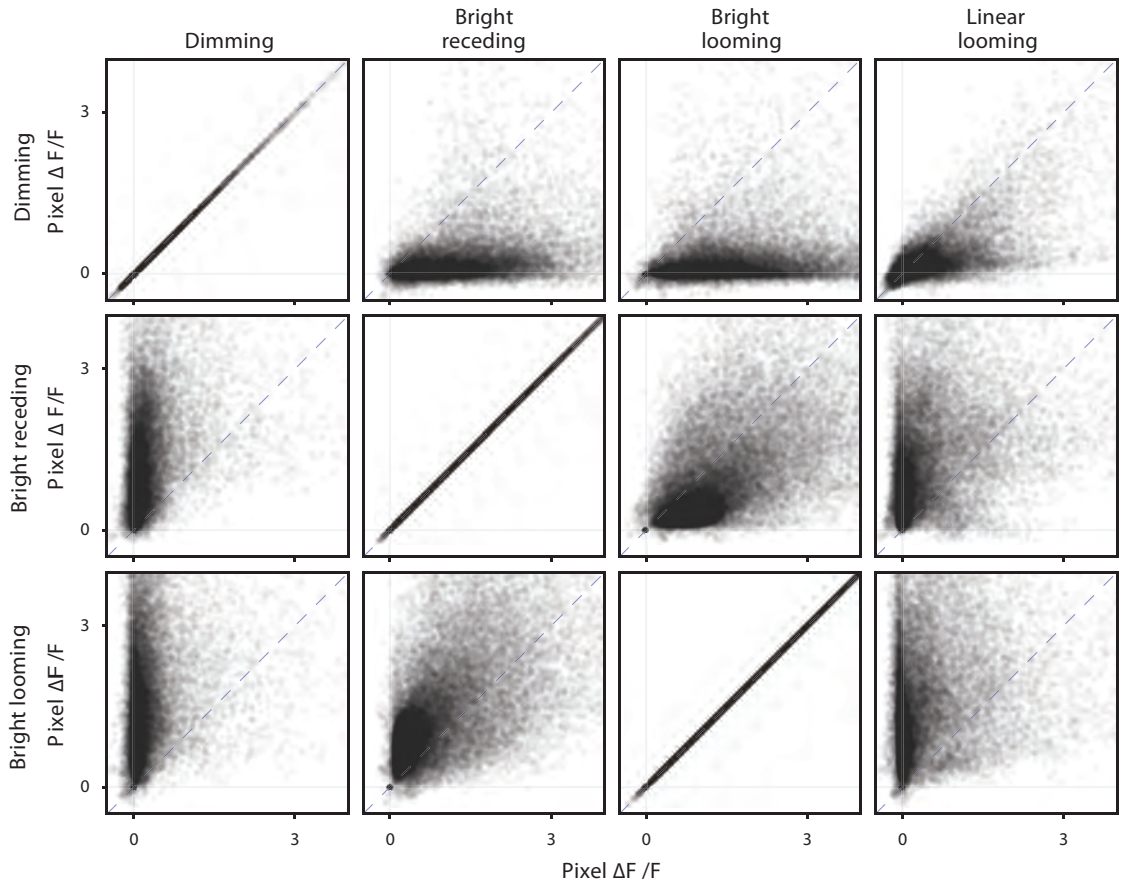

Figure 6.3: Comparisons of pixelwise tectal responses between control stimuli. Scatter plots comparing peak pixel responses between control stimuli. Pixels that are close to the unity line (x = y) respond similarly to both compared stimuli (n = 4 larvae). 95 percentile values were used as the pixel peak △F/F values. Scale bars = 30 µm; P = posterior, M = medial.

References

Adelson, E. H. and Bergen, J. R. Spatiotemporal energy models for the perception of motion. *Journal of the Optical Society of America*, 2(2):284–299, 1985.

Ahmad, F. , Noldus, L. P. J. J. , Tegelenbosch, R. A. J. , and Richardson, M. K. Zebrafish embryos and larvae in behavioural assays. *Behaviour*, 149(10-12):1241–1281, 2012.

Ahrens, M. B. , Li, J. M. , Orger, M. B. , Robson, D. N. , Schier, A. F. , Engert, F. , and Portugues, R. Brain-wide neuronal dynamics during motor adaptation in zebrafish. *Nature*, 485 (7399):471–477, 2012.

Ahrens, M. B. , Orger, M. B. , Robson, D. N. , Li, J. M. , and Keller, P. J. Whole-brain functional imaging at cellular resolution using light-sheet microscopy. *Nat Methods*, 10(5):413–420, 2013.

Aizenberg, M. and Schuman, E. M. Cerebellar-dependent learning in larval zebrafish. *The Journal of Neuroscience*, 31(24):8708–8712, 2011.

Akerboom, J. , Chen, T. W. , Wardill, T. J. , Tian, L. , Marvin, J. S. , Mutlu, S. , Calderón, N. C. , Esposti, F. , Borghuis, B. G. , Sun, X. R. , Gordus, A. , Orger, M. B. , Portugues, R. , Engert, F. , Macklin, J. J. , Filosa, A. , Aggarwal, A. , Kerr, R. A. , Takagi, R. , Kracun, S. , Shigetomi, E. , Khakh, B. S. , Baier, H. , Lagnado, L. , Wang, S. S. H. , Bargmann, C. I. , Kimmel, B. E. , Jayaraman, V. , Svoboda, K. , Kim, D. S. , Schreiter, E. R. , and Looger, L. L. Optimization of a GCaMP calcium indicator for neural activity imaging. *The Journal of Neuroscience*, 32(40):13819–13840, 2012.

Akerboom, J. , Carreras Calderón, N. , Tian, L. , Wabnig, S. , Prigge, M. , Tolö, J. , Gordus, A. , Orger, M. B. , Severi, K. E. , Macklin, J. J. , Patel, R. , Pulver, S. R. , Wardill, T. J. , Fischer, E. , Schüler, C. , Chen, T. W. , Sarkisyan, K. S. , Marvin, J. S. , Bargmann, C. I. , Kim, D. S. , Kügler, S. , Lagnado, L. , Hegemann, P. , Gottschalk, A. , Schreiter, E. R. , and Looger, L. L. Genetically encoded calcium indicators for multi-color neural activity imaging and combination with optogenetics. *Frontiers in Molecular Neuroscience*, 6:2, 2013.

Asadollahi, A. , Mysore, S. P. , and Knudsen, E. I. Stimulus-driven competition in a cholinergic midbrain nucleus. *Nature Neuroscience*, 13(7):889–895, 2010.

Asakawa, K. and Kawakami, K. Targeted gene expression by the Gal4-UAS system in zebrafish. *Development Growth and Differentiation*, 50(6):391–399, 2008.

Azeredo da Silveira, R. and Roska, B. Cell types, circuits, computation. *Current Opinion in Neurobiology*, 21(5):664–671, 2011.

Baier, H. Synaptic laminae in the visual system: molecular mechanisms forming layers of perception. *Annual Review of Cell and Developmental Biology*, 29:385–416, 2013.

Baier, H. and Scott, E. K. Genetic and optical targeting of neural circuits and behavior - zebrafish in the spotlight. *Current Opinion in Neurobiology*, 19(5):553–560, 2009.

Ball, W. and Tronick, E. Infant responses to impending collision: optical and real. *Science*, 171(3973):818–820, 1971.

Barth, K. A. , Miklosi, A. , Watkins, J. , Bianco, I. H. , Wilson, S. W. , and Andrew, R. J. fsi zebrafish show concordant reversal of laterality of viscera, neuroanatomy, and a subset of behavioral responses. *Current Biology*, 15(9):844–850, 2005.

Ben Fredj, N. , Hammond, S. , Otsuna, H. , Chien, C. B. , Burrone, J. , and Meyer, M. P. Synaptic activity and activity-dependent competition regulates axon arbor maturation, growth arrest, and territory in the retinotectal projection. *The Journal of Neuroscience*, 30(32):10939–10951, 2010.

Berlin, S. , Carroll, E. C. , Newman, Z. L. , Okada, H. O. , Quinn, C. M. , Kallman, B. , Rockwell, N. C. , Martin, S. S. , Lagarias, J. C. , and Isacoff, E. Y. Photoactivatable genetically encoded calcium indicators for targeted neuronal imaging. *Nature Methods*, 12(9):852–858, 2015.

Berson, D. M. Retinal ganglion cell types and their central projections. In *The Senses: A Comprehensive Reference. Vol. 1. Vision I.*, pages 491–520. Academic Press, San Diego, 2008.

Bianco, I. H. and Engert, F. Visuomotor transformations underlying hunting behavior in zebrafish. *Current Biology*, 25(7):831–846, 2015.

Bianco, I. H. , Kampff, A. R. , and Engert, F. Prey capture behavior evoked by simple visual stimuli in larval zebrafish. *Frontiers in Systems Neuroscience*, 5:101, 2011.

Biehlmaier, O. , Neuhauss, S. C. F. , and Kohler, K. Synaptic plasticity and functionality at the cone terminal of the developing zebrafish retina. *Journal of Neurobiology*, 56(3): 222–236, 2003.

Bilotta, J. , Saszik, S. , and Sutherland, S. E. Rod contributions to the electroretinogram of the dark-adapted developing zebrafish. *Developmental Dynamics*, 222(4):564–570, 2001.

Boniface, E. J. , Lu, J. , Victoroff, T. , Zhu, M. , and Chen, W. FlEx-based transgenic reporter lines for visualization of Cre and Flp activity in live zebrafish. *Genesis*, 47(7):484–491, 2009.

Borla, M. A. , Palecek, B. , Budick, S. , and O'Malley, D. M. Prey capture by larval zebrafish: evidence for fine axial motor control. *Brain, Behavior and Evolution*, 60(4):207–229, 2002.

Brand, A. H. and Perrimon, N. Targeted gene expression as a means of altering cell fates and generating dominant phenotypes. *Development*, 118(2):401–415, 1993.

Brockerhoff, S. E. , Hurley, J. B. , Janssen-Bienhold, U. , Neuhauss, S. C. , Driever, W. , and Dowling, J. E. A behavioral screen for isolating zebrafish mutants with visual system defects. *Proceedings of the National Academy of Sciences*, 92(23):10545–10549, 1995.

Budick, S. A. and O'Malley, D. M. Locomotor repertoire of the larval zebrafish: swimming, turning and prey capture. *The Journal of Experimental Biology*, 203:2565–2579, 2000.

Bulina, M. E. , Lukyanov, K. A. , Britanova, O. V. , Onichtchouk, D. , Lukyanov, S. , and Chudakov, D. M. Chromophore-assisted light inactivation (CALI) using the phototoxic fluorescent protein KillerRed. *Nature Protocols*, 1(2):947–953, 2006.

Burgess, H. A. and Granato, M. Modulation of locomotor activity in larval zebrafish during light adaptation. *The Journal of Experimental Biology*, 210:2526–2539, 2007.

Burgess, H. A. , Schoch, H. , and Granato, M. Distinct retinal pathways drive spatial orientation behaviors in zebrafish navigation. *Current Biology*, 20(4):381–386, 2010.

Burrill, J. D. and Easter, S. S. Development of the retinofugal projections in the embryonic and larval zebrafish (Brachydanio rerio). *The Journal of Comparative Neurology*, 346(4): 583–600, 1994.

Cajal, S. R. y. *The structure of the retina.* Thomas, Springfield, 1972.

Cameron, D. A. Mapping absorbance spectra, cone fractions, and neuronal mechanisms to photopic spectral sensitivity in the zebrafish. *Visual Neuroscience*, 19(3):365–372, 2002.

Canfield, J. G. Temporal constraints on visually directed C-start responses: behavioral and physiological correlates. *Brain, Behavior and Evolution*, 61(3):148–158, 2003.

Cederlund, M. L. , Morrissey, M. E. , Baden, T. , Scholz, D. , Vendrell, V. , Lagnado, L. , Connaughton, V. P. , and Kennedy, B. N. Zebrafish Tg(7.2mab21l2:EGFP)ucd2 transgenics reveal a unique population of retinal Amacrine cells. *Investigative Ophthalmology and Visual Science*, 52(3):1613–1621, 2011.

Chen, T.-W. , Wardill, T. J. , Sun, Y. , Pulver, S. R. , Renninger, S. L. , Baohan, A. , Schreiter, E. R. , Kerr, R. A. , Orger, M. B. , Jayaraman, V. , Looger, L. L. , Svoboda, K. , and Kim, D. S. Ultrasensitive fluorescent proteins for imaging neuronal activity. *Nature*, 499 (7458):295–300, 2013.

Chen, X. and Engert, F. Navigational strategies underlying phototaxis in larval zebrafish. *Frontiers in Systems Neuroscience*, 8:39, 2014.

Clark, K. J. , Urban, M. D. , Skuster, K. J. , and Ekker, S. C. Transgenic zebrafish using transposable elements. *Methods in Cell Biology*, 104:137–149, 2011.

Colwill, R. M. and Creton, R. Imaging escape and avoidance behavior in zebrafish larvae. *Reviews in the Neurosciences*, 22(1):63–73, 2011.

Connaughton, V. P. , Graham, D. , and Nelson, R. Identification and morphological classification of horizontal, bipolar, and amacrine cells within the zebrafish retina. *Journal of Comparative Neurology*, 477(4):371–385, 2004.

Connaughton, V. P. and Nelson, R. Spectral responses in zebrafish horizontal cells include a tetraphasic response and a novel UV-dominated triphasic response. *Journal of Neurophysiology*, 104(5):2407–2422, 2010.

Curado, S. , Stainier, D. Y. R. , and Anderson, R. M. Nitroreductase-mediated cell/tissue ablation in zebrafish: a spatially and temporally controlled ablation method with applications in developmental and regeneration studies. *Nature Protocols*, 3(6):948–954, 2008.

Currie, S. and Carlsen, R. Cranial components of startle behavior in larval and adult lampreys. *Neuroscience*, 24(2):709–718, 1988.

Dal Maschio, M. , Difato, F. , Beltramo, R. , Blau, A. , Benfenati, F. , and Fellin, T. Simultaneous two-photon imaging and photo-stimulation with structured light illumination. *Optics Express*, 18(18):18720–18731, 2010.

Davison, J. M. , Akitake, C. M. , Goll, M. G. , Rhee, J. M. , Gosse, N. , Baier, H. , Halpern, M. E. , Leach, S. D. , and Parsons, M. J. Transactivation from Gal4-VP16 transgenic insertions for tissue-specific cell labeling and ablation in zebrafish. *Developmental Biology*, 304 (2):811–824, 2007.

de Vries, S. E. J. and Clandinin, T. R. Loom-sensitive neurons link computation to action in the Drosophila visual system. *Current Biology*, 22(5):353–362, 2012.

Dean, P. , Redgrave, P. , and Westby, G. W. Event or emergency? Two response systems in the mammalian superior colliculus. *Trends in Neurosciences*, 12(4):137–147, 1989.

Del Bene, F. , Wyart, C. , Robles, E. , Tran, A. , Looger, L. , Scott, E. K. , Isacoff, E. Y. , and Baier, H. Filtering of visual information in the tectum by an identified neural circuit. *Science*, 330(6004):669–673, 2010.

Denk, W. , Strickler, J. H. , and Webb, W. W. Two-photon laser scanning fluorescence microscopy. *Science*, 248(4951):73–76, 1990.

DesJardin, J. T. , Holmes, A. L. , Forcelli, P. a. , Cole, C. E. , Gale, J. T. , Wellman, L. L. , Gale, K. , and Malkova, L. Defense-like behaviors evoked by pharmacological disinhibition of the superior colliculus in the primate. *Journal of Neuroscience*, 33(1):150–155, 2013.

Detrich, H. , Westerfield, M. , and Zon, L. *The Zebrafish: Cellular and Developmental Biology* Elsevier, 2nd edition, 2004.

Dhande, O. S. and Huberman, A. D. Retinal ganglion cell maps in the brain: Implications for visual processing. *Current Opinion in Neurobiology*, 24(1):133–142, 2014.

Dhande, O. S. , Estevez, M. E. , Quattrochi, L. E. , El-Danaf, R. N. , Nguyen, P. L. , Berson, D. M. , and Huberman, A. D. Genetic dissection of retinal inputs to brainstem nuclei controlling image stabilization. *The Journal of Neuroscience*, 33(45):17797–17813, 2013.

Dill, L. M. The Escape Response of the Zebra Danio (Brachydanio Rerio) I. the Stimulus for Escape *Animal Behaviour*, 22(3):711–722, 1974a.

Dill, L. M. The escape response of the zebra danio (Brachydanio rerio) II. The effect of experience *Animal Behaviour*, 22(3):723–730, 1974b.

Doubell, T. P. , Skaliora, I. , Baron, J. , and King, A. J. Functional connectivity between the superficial and deeper layers of the superior colliculus: an anatomical substrate for sensorimotor integration. *The Journal of Neuroscience*, 23(16):6596–6607, 2003.

Dreosti, E. , Odermatt, B. , Dorostkar, M. M. , and Lagnado, L. A genetically encoded reporter of synaptic activity in vivo. *Nature Methods*, 6(12):883–889, 2009.

Dreosti, E. , Esposti, F. , Baden, T. , and Lagnado, L. In vivo evidence that retinal bipolar cells generate spikes modulated by light. *Nature Neuroscience*, 14(8):951–952, 2011.

Dunn, T. W. , Gebhardt, C. , Naumann, E. A. , Riegler, C. , Ahrens, M. B. , Engert, F. , and Del Bene, F. Neural circuits underlying visually evoked escapes in larval zebrafish. *Neuron*, 89(3):613–628, 2016.

Dyer, M. A. and Cepko, C. L. Control of Müller glial cell proliferation and activation following retinal injury. *Nature Neuroscience*, 3(9):873–880, 2000.

Easter, S. S. and Nicola, G. N. The development of vision in the zebrafish (Danio rerio). *Developmental Biology*, 180(2):646–663, 1996.

Easter, S. S. and Nicola, G. N. The development of eye movements in the zebrafish (Danio rerio). *Developmental Psychobiology*, 31(4):267–276, 1997.

Emelyanov, A. and Parinov, S. Mifepristone-inducible LexPR system to drive and control gene expression in transgenic zebrafish. *Developmental Biology*, 320(1):113–121, 2008.

Emran, F. , Rihel, J. , Adolph, A. R. , Wong, K. Y. , Kraves, S. , and Dowling, J. E. OFF ganglion cells cannot drive the optokinetic reflex in zebrafish. *Proceedings of the National Academy of Sciences*, 104(48):19126–19131, 2007.

Engeszer, R. E. , Patterson, L. B. , Rao, A. A. , and Parichy, D. M. Zebrafish in the wild: a review of natural history and new notes from the field. *Zebrafish*, 4(1):21–40, 2007.

Ewert, J. P. , Buxbaum-Conradi, H. , Dreisvogt, F. , Glagow, M. , Merkel-Harff, C. , Röttgen, A. , Schürg-Pfeiffer, E. , and Schwippert, W. W. Neural modulation of visuomotor functions underlying prey-catching behaviour in anurans: perception, attention, motor performance, learning. *Comparative Biochemistry and Physiology*, 128(3):417–461, 2001.

Facchin, L. , Burgess, H. A. , Siddiqi, M. , Granato, M. , and Halpern, M. E. Determining the function of zebrafish epithalamic asymmetry. *Philosophical transactions of the Royal Society of London. Series B, Biological sciences*, 364(1519):1021–1032, 2009.

Fajardo, O. , Zhu, P. , and Friedrich, R. W. Control of a specific motor program by a small brain area in zebrafish. *Frontiers in Neural Circuits*, 7:67, 2013.

Fenno, L. , Yizhar, O. , and Deisseroth, K. The development and application of optogenetics. *Annual Review of Neuroscience*, 34:389–412, 2011.

Fernandes, A. M. , Fero, K. , Arrenberg, A. B. , Bergeron, S. A. , Driever, W. , and Burgess, H. A. Deep brain photoreceptors control light-seeking behavior in zebrafish larvae. *Current Biology*, 22(21):2042–2047, 2012.

Fero, K. , Yokogawa, T. , and Burgess, H. A. The behavioral repertoire of larval zebrafish. *Neuromethods*, 52:249–291, 2011.

Fleisch, V. C. and Neuhauss, S. C. F. Visual behavior in zebrafish. *Zebrafish*, 3(2):191–201, 2006.

Fosque, B. F. , Sun, Y. , Dana, H. , Yang, C. T. , Ohyama, T. , Tadross, M. R. , Patel, R. , Zlatic, M. , Kim, D. S. , Ahrens, M. B. , Jayaraman, V. , Looger, L. L. , and Schreiter, E. R. Labeling of active neural circuits in vivo with designed calcium integrators. *Science*, 347(6223): 755–760, 2015.

Fotowat, H. and Gabbiani, F. Relationship between the phases of sensory and motor activity during a looming-evoked multistage escape behavior. *The Journal of Neuroscience*, 27(37):10047–10059, 2007.

Fotowat, H. , Fayyazuddin, A. , Bellen, H. J. , and Gabbiani, F. A novel neuronal pathway for visually guided escape in Drosophila melanogaster. *Journal of Neurophysiology*, 102 (2):875–885, 2009.

Franconeri, S. L. and Simons, D. J. Moving and looming stimuli capture attention. *Perception & Psychophysics*, 65(7):999–1010, 2003.

Gabbiani, F. , Krapp, H. G. , and Laurent, G. Computation of object approach by a wide-field, motion-sensitive neuron. *The Journal of Neuroscience*, 19(3):1122–1141, 1999.

Gabbiani, F. , Mo, C. , and Laurent, G. Invariance of angular threshold computation in a wide-field looming-sensitive neuron. *The Journal of Neuroscience*, 21(1):314–329, 2001.

Gabriel, J. P. , Trivedi, C. A. , Maurer, C. M. , Ryu, S. , and Bollmann, J. H. Layer-specific targeting of direction-selective neurons in the zebrafish optic tectum. *Neuron*, 76(6): 1147–1160, 2012.

Gahtan, E. and Baier, H. Of lasers, mutants, and see-through brains: functional neuroanatomy in zebrafish. *Journal of Neurobiology*, 59(1):147–161, 2004.

Gahtan, E. , Tanger, P. , and Baier, H. Visual prey capture in larval zebrafish is controlled by identified reticulospinal neurons downstream of the tectum. *The Journal of Neuroscience*, 25(40):9294–9303, 2005.

Galbraith, J. A. and Terasaki, M. Controlled damage in thick specimens by multiphoton excitation. *Molecular Biology of the Cell*, 14(5):1808–1817, 2003.

Gallagher, S. P. and Northmore, D. P. M. Responses of the teleostean nucleus isthmi to looming objects and other moving stimuli. *Visual Neuroscience*, 23(2):209–219, 2006.

Goll, M. G. , Anderson, R. , Stainier, D. Y. R. , Spradling, A. C. , and Halpern, M. E. Transcriptional silencing and reactivation in transgenic zebrafish. *Genetics*, 182(3):747–755, 2009.

Gollisch, T. and Meister, M. Eye smarter than scientists believed: neural computations in circuits of the retina. *Neuron*, 65(2):150–164, 2010.

Grienberger, C. and Konnerth, A. Imaging calcium in neurons. *Neuron*, 73(5):862–885, 2012.

Güler, A. D. , Ecker, J. L. , Lall, G. S. , Haq, S. , Altimus, C. M. , Liao, H. W. , Barnard, A. R. , Cahill, H. , Badea, T. C. , Zhao, H. , Hankins, M. W. , Berson, D. M. , Lucas, R. J. , Yau, K. W. , and Hattar, S. Melanopsin cells are the principal conduits for rod-cone input to non-image-forming vision. *Nature*, 453(7191):102–105, 2008.

Hatsopoulos, N. , Gabbiani, F. , and Laurent, G. Elementary computation of object approach by a wide-field visual neuron. *Science*, 270(5238):1000–1003, 1995.

Hattar, S. , Kumar, M. , Park, A. , Tong, P. , Tung, J. , Yau, K. W. , and Berson, D. M. Central projections of melanopsin-expressing retinal ganglion cells in the mouse. *The Journal of Comparative Neurology*, 497(3):326–349, 2006.

Helmstaedter, M. , Briggman, K. L. , and Denk, W. 3D structural imaging of the brain with photons and electrons. *Current Opinion in Neurobiology*, 18(6):633–641, 2008.

Herrero, L. , Rodríguez, F. , Salas, C. , and Torres, B. Tail and eye movements evoked by electrical microstimulation of the optic tectum in goldfish. *Experimental Brain Research*, 120(3):291–305, 1998.

Higashijima, S. , Masino, M. A. , Mandel, G. , and Fetcho, J. R. Imaging neuronal activity during zebrafish behavior with a genetically encoded calcium indicator. *Journal of Neurophysiology*, 90(6):3986–3997, 2003.

Hisano, Y. , Sakuma, T. , Nakade, S. , Ohga, R. , Ota, S. , Okamoto, H. , Yamamoto, T. , and Kawahara, A. Precise in-frame integration of exogenous DNA mediated by CRISPR/Cas9 system in zebrafish. *Scientific Reports*, 5:8841, 2015.

Hochbaum, D. R. , Zhao, Y. , Farhi, S. L. , Klapoetke, N. , Werley, C. A. , Kapoor, V. , Zou, P. , Kralj, J. M. , Maclaurin, D. , Smedemark-Margulies, N. , Saulnier, J. L. , Boulting, G. L. , Straub, C. , Cho, Y. K. , Melkonian, M. , Wong, G. K. S. , Harrison, D. J. , Murthy, V. N. , Sabatini, B. L. , Boyden, E. S. , Campbell, R. E. , and Cohen, A. E. All-optical electrophysiology in mammalian neurons using engineered microbial rhodopsins. *Nature Methods*, 11(8):825–833, 2014.

Holmqvist, M. H. A visually elicited escape response in the fly that does not use the giant fiber pathway. *Visual Neuroscience*, 11(6):1149–1161, 1994.

Huang, K. H. , Ahrens, M. B. , Dunn, T. W. , and Engert, F. Spinal projection neurons control turning behaviors in zebrafish. *Current Biology*, 23(16):1566–1573, 2013.

Huberman, A. D. , Wei, W. , Elstrott, J. , Stafford, B. K. , Feller, M. B. , and Barres, B. A. Genetic identification of an On-Off direction-selective retinal ganglion cell subtype reveals a layer-specific subcortical map of posterior motion. *Neuron*, 62(3):327–334, 2009.

Huberman, A. D. , Clandinin, T. R. , and Baier, H. Molecular and cellular mechanisms of lamina-specific axon targeting. *Cold Spring Harbor Perspectives in Biology*, 2(3), 2010.

Hunter, P. R. , Lowe, A. S. , Thompson, I. D. , and Meyer, M. P. Emergent properties of the optic tectum revealed by population analysis of direction and orientation selectivity. *The Journal of Neuroscience*, 33(35):13940–13945, 2013.

Ishikane, H. , Gangi, M. , Honda, S. , and Tachibana, M. Synchronized retinal oscillations encode essential information for escape behavior in frogs. *Nature Neuroscience*, 8(8): 1087–1095, 2005.

Jusuf, P. R. and Harris, W. A. Ptf1a is expressed transiently in all types of amacrine cells in the embryonic zebrafish retina. *Neural Development*, 4:34, 2009.

Kaifosh, P. , Zaremba, J. D. , Danielson, N. B. , and Losonczy, A. SIMA: Python software for analysis of dynamic fluorescence imaging data. *Frontiers in Neuroinformatics*, 8:80, 2014.

Kalueff, A. V. , Gebhardt, M. , Stewart, A. M. , Cachat, J. M. , Brimmer, M. , Chawla, J. S. , Craddock, C. , Kyzar, E. J. , Roth, A. , Landsman, S. , Gaikwad, S. , Robinson, K. , Baatrup, E. , Tierney, K. , Shamchuk, A. , Norton, W. , Miller, N. , Nicolson, T. , Braubach, O. , Gilman, C. P. , Pittman, J. , Rosemberg, D. B. , Gerlai, R. , Echevarria, D. , Lamb, E. , Neuhauss, S. C. F. , Weng, W. , Bally-Cuif, L. , and Schneider, H. Towards a comprehensive catalog of zebrafish behavior 1.0 and beyond. *Zebrafish*, 10(1):70–86, 2013.

Kawakami, K. , Takeda, H. , Kawakami, N. , Kobayashi, M. , Matsuda, N. , and Mishina, M. A transposon-mediated gene trap approach identifies developmentally regulated genes in zebrafish. *Developmental Cell*, 7(1):133–144, 2004.

Kawakami, K. , Abe, G. , Asada, T. , Asakawa, K. , Fukuda, R. , Ito, A. , Lal, P. , Mouri, N. , Muto, A. , Suster, M. L. , Takakubo, H. , Urasaki, A. , Wada, H. , and Yoshida, M. zTrap: zebrafish gene trap and enhancer trap database. *BMC Developmental Biology*, 10(1): 105, 2010.

Kay, J. N. , Roeser, T. , Mumm, J. S. , Godinho, L. , Mrejeru, A. , Wong, R. O. , and Baier, H. Transient requirement for ganglion cells during assembly of retinal synaptic layers. *Development*, 131(6):1331–1342, 2004.

Kay, J. N. , Finger-Baier, K. C. , Roeser, T. , Staub, W. , and Baier, H. Retinal ganglion cell genesis requires lakritz, a zebrafish atonal homolog. *Neuron*, 30(3):725–736, 2001.

Kay, J. N. , De la Huerta, I. , Kim, I. J. , Zhang, Y. , Yamagata, M. , Chu, M. W. , Meister, M. , and Sanes, J. R. Retinal ganglion cells with distinct directional preferences differ in molecular identity, structure, and central projections. *The Journal of Neuroscience*, 31 (21):7753–7762, 2011.

Kay, J. N. , Chu, M. W. , and Sanes, J. R. MEGF10 and MEGF11 mediate homotypic interactions required for mosaic spacing of retinal neurons. *Nature*, 483(7390):465–469, 2012.

Kerr, J. N. D. and Denk, W. Imaging in vivo: watching the brain in action. *Nature reviews. Neuroscience*, 9(3):195–205, 2008.

Khakhalin, A. S. , Koren, D. , Gu, J. , Xu, H. , and Aizenman, C. D. Excitation and inhibition in recurrent networks mediate collision avoidance in Xenopus tadpoles. *The European Journal of Neuroscience*, 40(6):2948–2962, 2014.

Kicliter, E. Flux, wavelength and movement discrimination in frogs: forebrain and midbrain contributions. *Brain, Behavior and Evolution*, 8(5):340–365, 1973.

Kim, I. J. , Zhang, Y. , Yamagata, M. , Meister, M. , and Sanes, J. R. Molecular identification of a retinal cell type that responds to upward motion. *Nature*, 452(7186):478–482, 2008.

Kimmel, C. B. , Patterson, J. , and Kimmel, R. O. The development and behavioral characteristics of the startle response in the zebrafish. *Developmental Psychobiology*, 7(1): 47–60, 1974.

Kimmel, C. B. , Ballard, W. W. , Kimmel, S. R. , Ullmann, B. , and Schilling, T. F. Stages of embryonic development of the zebrafish. *Developmental Dynamics*, 203(3):253–310, 1995.

King, J. G. , Lettvin, J. Y. , and Gruberg, E. D. Selective, unilateral, reversible loss of behavioral responses to looming stimuli after injection of tetrodotoxin of cadmium chloride into the frog optic nerve. *Brain Research*, 841(1-2):20–26, 1999.

Kohashi, T. , Nakata, N. , and Oda, Y. Effective sensory modality activating an escape triggering neuron switches during early development in zebrafish. *Journal of Neuroscience*, 32(17):5810–5820, 2012.

Kohashi, T. and Oda, Y. Initiation of Mauthner- or non-Mauthner-mediated fast escape evoked by different modes of sensory input. *The Journal of Neuroscience*, 28(42):10641–10653, 2008.

Koide, T. , Miyasaka, N. , Morimoto, K. , Asakawa, K. , Urasaki, A. , Kawakami, K. , and Yoshihara, Y. Olfactory neural circuitry for attraction to amino acids revealed by transposon-mediated gene trap approach in zebrafish. *Proceedings of the National Academy of Sciences of the United States of America*, 106(24):9884–9889, 2009.

Kubo, F. , Hablitzel, B. , DalMaschio, M. , Driever, W. , Baier, H. , and Arrenberg, A. B. Functional architecture of an optic flow-responsive area that drives horizontal eye movements in zebrafish. *Neuron*, 81(6):1344–1359, 2014.

Kuffler, S. W. S. W. Discharge patterns and functional organization of mammalian retina. *Journal of Neurophysiology*, 16(1):37–68, 1953.

Lacoste, A. M. B. , Schoppik, D. , Robson, D. N. , Haesemeyer, M. , Portugues, R. , Li, J. M. , Randlett, O. , Wee, C. L. , Engert, F. , and Schier, A. F. A convergent and essential interneuron pathway for mauthner-cell-mediated escapes. *Current Biology*, 25(11):1526–1534, 2015.

Lettvin, J. Y. , Maturana, H. R. , Mcculloch, W. S. , and Pitts, W. H. What the frog's eye tells the frog's brain. *Proceedings of The Institute of Radio Engineers*, 47:1940–1951, 1959.

Levick, W. R. Receptive fields and trigger features of ganglion cells in the visual streak of the rabbits retina. *The Journal of Physiology*, 188(3):285–307, 1967.

Li, L. and Dowling, J. E. A dominant form of inherited retinal degeneration caused by a non-photoreceptor cell-specific mutation. *Proceedings of the National Academy of Sciences*, 94(21):11645–11650, 1997.

Li, Y. N. , Matsui, J. I. , and Dowling, J. E. Specificity of the horizontal cell-photoreceptor connections in the zebrafish (Danio rerio) retina. *Journal of Comparative Neurology*, 516(5):442–453, 2009.

Liu, K. S. and Fetcho, J. R. Laser ablations reveal functional relationships of segmental hindbrain neurons in zebrafish. *Neuron*, 23(2):325–335, 1999.

Liu, Y. C. and Hale, M. E. Alternative forms of axial startle behaviors in fishes. *Zoology*, 117 (1):36–47, 2014.

Liu, Y. C. , Bailey, I. , and Hale, M. E. Alternative startle motor patterns and behaviors in the larval zebrafish (Danio rerio). *Journal of Comparative Physiology*, 198(1):11–24, 2012.

Liu, Y. J. , Wang, Q. , and Li, B. Neuronal responses to looming objects in the superior colliculus of the cat. *Brain, Behavior and Evolution*, 77(3):193–205, 2011.

Livet, J. , Weissman, T. A. , Kang, H. , Draft, R. W. , Lu, J. , Bennis, R. A. , Sanes, J. R. , and Lichtman, J. W. Transgenic strategies for combinatorial expression of fluorescent proteins in the nervous system. *Nature*, 450(7166):56–62, 2007.

Looger, L. L. and Griesbeck, O. Genetically encoded neural activity indicators. *Current Opinion in Neurobiology*, 22(1):18–23, 2012.

Lowe, A. S. , Nikolaou, N. , Hunter, P. R. , Thompson, I. D. , and Meyer, M. P. A systems-based dissection of retinal inputs to the zebrafish tectum reveals different rules for different functional classes during development. *The Journal of Neuroscience*, 33(35): 13946–13956, 2013.

Luo, L. , Callaway, E. M. , and Svoboda, K. Genetic dissection of neural circuits. *Neuron*, 57(5):634–660, 2008.

Lutz, C. , Otis, T. S. , DeSars, V. , Charpak, S. , DiGregorio, D. A. , and Emiliani, V. Holographic photolysis of caged neurotransmitters. *Nature Methods*, 5(9):821–827, 2008.

Marc, R. E. and Cameron, D. A molecular phenotype atlas of the zebrafish retina. *Journal of Neurocytology*, 30(7):593–654, 2001.

Masland, R. H. The fundamental plan of the retina. *Nature Neuroscience*, 4(9):877–886, 2001.

Maurer, C. M. , Schönthaler, H. B. , Mueller, K. P. , and Neuhauss, S. C. F. Distinct retinal deficits in a zebrafish pyruvate dehydrogenase-deficient mutant. *The Journal of Neuroscience*, 30(36):11962–11972, 2010.

Maximino, C. , da Silva, A. W. B. , Gouveia, A. , and Herculano, A. M. Pharmacological analysis of zebrafish (Danio rerio) scototaxis. *Progress in Neuro-psychopharmacology & Biological Psychiatry*, 35(2):624–631, 2011.

Miklósi, A. and Andrew, R. J. The zebrafish as a model for behavioral studies. *Zebrafish*, 3 (2):227–234, 2006.

Miklósi, A. , Andrew, R. J. , and Gasparini, S. Role of right hemifield in visual control of approach to target in zebrafish. *Behavioural Brain Research*, 122(1):57–65, 2001.

Miyawaki, A. , Llopis, J. , Heim, R. , McCaffery, J. M. , Adams, J. A. , Ikura, M. , and Tsien, R. Y. Fluorescent indicators for Ca2+ based on green fluorescent proteins and calmodulin. *Nature*, 388(6645):882–887, 1997.

Morin, L. P. and Studholme, K. M. Retinofugal projections in the mouse. *Journal of Comparative Neurology*, 522(16):3733–3753, 2014.

Mu, Y. , Li, X. Q. , Zhang, B. , and Du, J. L. Visual input modulates audiomotor function via hypothalamic dopaminergic neurons through a cooperative mechanism. *Neuron*, 75(4):688–699, 2012.

Münch, T. A. , da Silveira, R. A. , Siegert, S. , Viney, T. J. , Awatramani, G. B. , and Roska, B. Approach sensitivity in the retina processed by a multifunctional neural circuit. *Nature Neuroscience*, 12(10):1308–1316, 2009.

Muto, A. , Orger, M. B. , Wehman, A. M. , Smear, M. C. , Kay, J. N. , Page-McCaw, P. S. , Gahtan, E. , Xiao, T. , Nevin, L. M. , Gosse, N. J. , Staub, W. , Finger-Baier, K. , and Baier, H. Forward genetic analysis of visual behavior in zebrafish. *PLoS Genetics*, 1(5):e66, 2005.

Muto, A. , Ohkura, M. , Kotani, T. , Higashijima, S. , Nakai, J. , and Kawakami, K. Genetic visualization with an improved GCaMP calcium indicator reveals spatiotemporal activation of the spinal motor neurons in zebrafish. *Proceedings of the National Academy of Sciences*, 108(13):5425–5430, 2011.

Muto, A. , Ohkura, M. , Abe, G. , Nakai, J. , and Kawakami, K. Real-time visualization of neuronal activity during perception. *Current Biology*, 23(4):307–311, 2013.

Nakagawa, H. and Hongjian, K. Collision-sensitive neurons in the optic tectum of the bullfrog, Rana catesbeiana. *Journal of Neurophysiology*, 104(5):2487–99, 2010.

Nakai, J. , Ohkura, M. , and Imoto, K. A high signal-to-noise Ca(2+) probe composed of a single green fluorescent protein. *Nature Biotechnology*, 19(2):137–141, 2001.

Naumann, E. A. , Kampff, A. R. , Prober, D. A. , Schier, A. F. , and Engert, F. Monitoring neural activity with bioluminescence during natural behavior. *Nature Neuroscience*, 13 (4):513–520, 2010.

Neuhauss, S. C. , Biehlmaier, O. , Seeliger, M. W. , Das, T. , Kohler, K. , Harris, W. A. , and Baier, H. Genetic disorders of vision revealed by a behavioral screen of 400 essential loci in zebrafish. *The Journal of Neuroscience*, 19(19):8603–8615, 1999.

Neuhauss, S. C. F. Behavioral genetic approaches to visual system development and function in zebrafish. *Journal of Neurobiology*, 54(1):148–160, 2003.

Nevin, L. M. , Robles, E. , Baier, H. , and Scott, E. K. Focusing on optic tectum circuitry through the lens of genetics. *BMC Biology*, 8:126, 2010.

Niell, C. M. and Smith, S. J. Functional imaging reveals rapid development of visual response properties in the zebrafish tectum. *Neuron*, 45(6):941–951, 2005.

Nikolaou, N. , Lowe, A. S. , Walker, A. S. , Abbas, F. , Hunter, P. R. , Thompson, I. D. , and Meyer, M. P. Parametric functional maps of visual inputs to the tectum. *Neuron*, 76(2): 317–324, 2012.

Nikolenko, V. , Peterka, D. S. , Araya, R. , Woodruff, A. , and Yuste, R. Spatial light modulator microscopy. *Cold Spring Harbor Protocols*, 2013(12):1132–1141, 2013.

Nüsslein-Volhard, C. and Dahm, R. *Zebrafish : a practical approach - NLM Catalog - NCBI* 2002.

Odermatt, B. , Nikolaev, A. , and Lagnado, L. Encoding of luminance and contrast by linear and nonlinear synapses in the retina. *Neuron*, 73(4):758–773, 2012.

O'Malley, D. M. , Kao, Y. H. , and Fetcho, J. R. Imaging the functional organization of zebrafish hindbrain segments during escape behaviors. *Neuron*, 17(6):1145–1155, 1996.

Orger, M. B. and Baier, H. Channeling of red and green cone inputs to the zebrafish optomotor response. *Visual Neuroscience*, 22(3):275–281, 2005.

Orger, M. B. , Kampff, A. R. , Severi, K. E. , Bollmann, J. H. , and Engert, F. Control of visually guided behavior by distinct populations of spinal projection neurons. *Nature Neuroscience*, 11(3):327–333, 2008.

Ott, M. , Walz, B. C. , Paulsen, U. J. , Mack, A. F. , and Wagner, H. J. Retinotectal ganglion cells in the zebrafish, Danio rerio. *The Journal of Comparative Neurology*, 501(4):647–658, 2007.

Packer, A. M. , Roska, B. , and Häusser, M. Targeting neurons and photons for optogenetics. *Nature Neuroscience*, 16(7):805–815, 2013.

Pang, J. J. , Gao, F. , and Wu, S. M. Light-evoked excitatory and inhibitory synaptic inputs to ON and OFF alpha ganglion cells in the mouse retina. *The Journal of Neuroscience*, 23(14):6063–6073, 2003.

Papagiakoumou, E. , Anselmi, F. , Bègue, A. , de Sars, V. , Glückstad, J. , Isacoff, E. Y. , and Emiliani, V. Scanless two-photon excitation of channelrhodopsin-2. *Nature Methods*, 7 (10):848–854, 2010.

Park, H. C. , Kim, C. H. , Bae, Y. K. , Yeo, S. Y. , Kim, S. H. , Hong, S. K. , Shin, J. , Yoo, K. W. , Hibi, M. , Hirano, T. , Miki, N. , Chitnis, A. B. , and Huh, T. L. Analysis of upstream elements in the HuC promoter leads to the establishment of transgenic zebrafish with fluorescent neurons. *Developmental Biology*, 227(2):279–293, 2000.

Patterson, B. W. , Abraham, A. O. , MacIver, M. A. , and McLean, D. L. Visually guided gradation of prey capture movements in larval zebrafish. *The Journal of Experimental Biology*, 216:3071–3083, 2013.

Pologruto, T. A. , Sabatini, B. L. , and Svoboda, K. ScanImage: flexible software for operating laser scanning microscopes. *Biomedical Engineering Online*, 2:13, 2003.

Portugues, R. and Engert, F. The neural basis of visual behaviors in the larval zebrafish. *Current Opinion in Neurobiology*, 19(6):644–647, 2009.

Portugues, R. , Feierstein, C. E. , Engert, F. , and Orger, M. B. Whole-brain activity maps reveal stereotyped, distributed networks for visuomotor behavior. *Neuron*, 81(6):1328–1343, 2014.

Preuss, S. J. , Trivedi, C. A. , vom Berg-Maurer, C. M. , Ryu, S. , and Bollmann, J. H. Classification of object size in retinotectal microcircuits. *Current Biology*, 24(20):2376–2385, 2014.

Preuss, T. , Osei-Bonsu, P. E. , Weiss, S. A. , Wang, C. , and Faber, D. S. Neural representation of object approach in a decision-making motor circuit. *The Journal of Neuroscience*, 26 (13):3454–3464, 2006.

Quirin, S. , Jackson, J. , Peterka, D. S. , and Yuste, R. Simultaneous imaging of neural activity in three dimensions. *Frontiers in Neural Circuits*, 8:29, 2014.

Ramdya, P. and Engert, F. Emergence of binocular functional properties in a monocular neural circuit. *Nature Neuroscience*, 11(9):1083–1090, 2008.

Ramdya, P. , Reiter, B. , and Engert, F. Reverse correlation of rapid calcium signals in the zebrafish optic tectum in vivo. *Journal of Neuroscience Methods*, 157(2):230–237, 2006.

Ratnapriya, R. and Swaroop, A. Genetic architecture of retinal and macular degenerative diseases: the promise and challenges of next-generation sequencing. *Genome Medicine*, 5(9):84, 2013.

Reese, B. E. Mosaics, tiling, and coverage by retinal neurons. In *The Senses: A Comprehensive Reference*, volume 1, pages 439–456. 2010.

Renninger, S. L. and Orger, M. B. Two-photon imaging of neural population activity in zebrafish. *Methods*, 62(3):255–267, 2013.

Rick, J. M. , Horschke, I. , and Neuhauss, S. C. F. Optokinetic behavior is reversed in achiasmatic mutant zebrafish larvae. *Current Biology*, 10(10):595–598, 2000.

Rind, F. C. and Simmons, P. J. Orthopteran DCMD neuron: a re-evaluation of responses to moving objects. I. Selective responses to approaching objects. *Journal of neurophysiology*, 68(5):1654–1666, 1992.

Robel, S. , Berninger, B. , and Götz, M. The stem cell potential of glia: lessons from reactive gliosis. *Nature reviews. Neuroscience*, 12(2):88–104, 2011.

Roberts, A. Pineal eye and behaviour in Xenopus tadpoles. *Nature*, 273(5665):774–775, 1978.

Robles, E. , Filosa, A. , and Baier, H. Precise lamination of retinal axons generates multiple parallel input pathways in the tectum. *The Journal of Neuroscience*, 33(11):5027–5039, 2013.

Robles, E. , Laurell, E. , and Baier, H. The Retinal Projectome Reveals Brain-Area-Specific Visual Representations Generated by Ganglion Cell Diversity. *Current Biology*, 24(18): 2085–2096, 2014.

Roeser, T. and Baier, H. Visuomotor behaviors in larval zebrafish after GFP-guided laser ablation of the optic tectum. *The Journal of Neuroscience*, 23(9):3726–3734, 2003.

Roska, B. and Werblin, F. Vertical interactions across ten parallel, stacked representations in the mammalian retina. *Nature*, 410(6828):583–587, 2001.

Roska, B. and Meister, M. The retina dissects the visual scene into distinct features. In *The New Visual Neurosciences*, pages 163–182. Cambridge, MA: MIT Press, 2014.

Roska, B. and Werblin, F. Rapid global shifts in natural scenes block spiking in specific ganglion cell types. *Nature Neuroscience*, 6(6):600–608, 2003.

Sahibzada, N. , Dean, P. , and Redgrave, P. Movements resembling orientation or avoidance elicited by electrical stimulation of the superior colliculus in rats. *The Journal of Neuroscience*, 6(3):723–733, 1986.

Sajovic, P. and Levinthal, C. Inhibitory mechanism in zebrafish optic tectum: visual response properties of tectal cells altered by picrotoxin and bicuculline. *Brain Research*, 271(2):227–240, 1983.

Sander, J. D. and Joung, J. K. CRISPR-Cas systems for editing, regulating and targeting genomes. *Nature Biotechnology*, 32(4):347–355, 2014.

Sanes, J. R. and Masland, R. H. The Types of Retinal Ganglion Cells: Current Status and Implications for Neuronal Classification. *Annual Review of Neuroscience*, 38:221–246, 2015.

Sanes, J. R. and Zipursky, S. L. Design principles of insect and vertebrate visual systems. *Neuron*, 66(1):15–36, 2010.

Schiff, W. , Caviness, J. A. , and Gibson, J. J. Persistent fear responses in rhesus monkeys to the optical stimulus of "looming". *Science*, 136(3520):982–983, 1962.

Schmitt, E. A. and Dowling, J. E. Early retinal development in the zebrafish, Danio rerio: light and electron microscopic analyses. *The Journal of Comparative Neurology*, 404(4): 515–536, 1999.

Schoonheim, P. J. , Arrenberg, A. B. , Del Bene, F. , and Baier, H. Optogenetic localization and genetic perturbation of saccade-generating neurons in zebrafish. *The Journal of Neuroscience*, 30(20):7111–7120, 2010.

Schweigart, G. , Mergner, T. , Evdokimidis, I. , Morand, S. , and Becker, W. Gaze stabilization by optokinetic reflex (OKR) and vestibule-ocular reflex (VOR) during active head rotation in man. *Vision Research*, 37(12):1643–1652, 1997.

Scott, E. K. and Baier, H. The cellular architecture of the larval zebrafish tectum, as revealed by gal4 enhancer trap lines. *Frontiers in Neural Circuits*, 3:13, 2009.

Scott, E. K. , Mason, L. , Arrenberg, A. B. , Ziv, L. , Gosse, N. J. , Xiao, T. , Chi, N. C. , Asakawa, K. , Kawakami, K. , and Baier, H. Targeting neural circuitry in zebrafish using GAL4 enhancer trapping. *Nature Methods*, 4(4):323–326, 2007.

Semmelhack, J. L. , Donovan, J. C. , Thiele, T. R. , Kuehn, E. , Laurell, E. , and Baier, H. A dedicated visual pathway for prey detection in larval zebrafish. *eLife*, 3, 2014.

Severi, K. E. , Portugues, R. , Marques, J. a. C. , O'Malley, D. M. , Orger, M. B. , and Engert, F. Neural control and modulation of swimming speed in the larval zebrafish. *Neuron*, 83 (3):692–707, 2014.

Shang, C. , Liu, Z. , Chen, Z. , Shi, Y. , Wang, Q. , Liu, S. , Li, D. , and Cao, P. A parvalbumin-positive excitatory visual pathway to trigger fear responses in mice. *Science*, 348(6242): 1472–1477, 2015.

Simmons, P. J. and Rind, F. C. Orthopteran DCMD neuron: a reevaluation of responses to moving objects. II. Critical cues for detecting approaching objects. *Journal of neurophysiology*, 68(5):1667–1682, 1992.

Simmons, P. J. and Rind, F. C. Responses to object approach by a wide field visual neurone, the LGMD2 of the locust: Characterization and image cues. *Journal of Comparative Physiology*, 180(3):203–214, 1997.

Simmons, P. J. , Sztarker, J. , and Rind, F. C. Looming detection by identified visual interneurons during larval development of the locust Locusta migratoria. *The Journal of experimental biology*, 216(12):2266–2275, 2013.

Sparks, D. L. and Nelson, J. S. Sensory and motor maps in the mammalian superior colliculus. *Trends in Neurosciences*, 10(8):312–317, 1987.

Stepien, A. E. , Tripodi, M. , and Arber, S. Monosynaptic Rabies Virus Reveals Premotor Network Organization and Synaptic Specificity of Cholinergic Partition Cells. *Neuron*, 68(3):456–472, 2010.

Straw, A. D. Vision egg: an open-source library for realtime visual stimulus generation. *Frontiers in Neuroinformatics*, 2:4, 2008.

Streisinger, G. , Walker, C. , Dower, N. , Knauber, D. , and Singer, F. Production of clones of homozygous diploid zebra fish (Brachydanio rerio). *Nature*, 291(5813):293–296, 1981.

Sumbre, G. , Muto, A. , Baier, H. , and Poo, M. M. Entrained rhythmic activities of neuronal ensembles as perceptual memory of time interval. *Nature*, 456(7218):102–106, 2008.

Sümbül, U. , Song, S. , McCulloch, K. , Becker, M. , Lin, B. , Sanes, J. R. , Masland, R. H. , and Seung, H. S. A genetic and computational approach to structurally classify neuronal types. *Nature Communications*, 5:3512, 2014.

Sun, H. and Frost, B. J. Computation of different optical variables of looming objects in pigeon nucleus rotundus neurons. *Nature Neuroscience*, 1(4):296–303, 1998.

Suster, M. L. , Abe, G. , Schouw, A. , and Kawakami, K. Transposon-mediated BAC transgenesis in zebrafish. *Nature Protocols*, 6(12):1998–2021, 2011.

Temizer, I. , Donovan, J. C. , Baier, H. , and Semmelhack, J. L. A Visual Pathway for Looming-Evoked Escape in Larval Zebrafish. *Current Biology*, 25(14):1823–1834, 2015.

Thiele, T. R. , Donovan, J. C. , and Baier, H. Descending control of swim posture by a midbrain nucleus in zebrafish. *Neuron*, 83(3):679–691, 2014.

Trinh, L. A. and Fraser, S. E. Enhancer and gene traps for molecular imaging and genetic analysis in zebrafish. *Development, Growth & Differentiation*, 55(4):434–445, 2013.

Trivedi, C. A. and Bollmann, J. H. Visually driven chaining of elementary swim patterns into a goal-directed motor sequence: a virtual reality study of zebrafish prey capture. *Frontiers in Neural Circuits*, 7:86, 2013.

Tsien, R. Y. New calcium indicators and buffers with high selectivity against magnesium and protons: design, synthesis, and properties of prototype structures. *Biochemistry*, 19 (11):2396–2404, 1980.

Ullén, F. , Deliagina, T. G. , Orlovsky, G. N. , and Grillner, S. Visual pathways for postural control and negative phototaxis in lamprey. *Journal of Neurophysiology*, 78(2):960–976, 1997.

Vladimirov, N. , Mu, Y. , Kawashima, T. , Bennett, D. V. , Yang, C. T. , Looger, L. L. , Keller, P. J. , Freeman, J. , and Ahrens, M. B. Light-sheet functional imaging in fictively behaving zebrafish. *Nature Methods*, 11(9):883–884, 2014.

Vogel, A. , Noack, J. , Hüttman, G. , and Paltauf, G. Mechanisms of femtosecond laser nanosurgery of cells and tissues. *Applied Physics B: Lasers and Optics*, 81(8):1015–1047, 2005.

Vogel, A. and Venugopalan, V. Mechanisms of pulsed laser ablation of biological tissues. *Chemical Reviews*, 103(2):577–644, 2003.

von Reyn, C. R. , Breads, P. , Peek, M. Y. , Zheng, G. Z. , Williamson, W. R. , Yee, A. L. , Leonardo, A. , and Card, G. M. A spike-timing mechanism for action selection. *Nature Neuroscience*, 17(7):962–970, 2014.

Walker, A. S. , Burrone, J. , and Meyer, M. P. Functional imaging in the zebrafish retinotectal system using RGECO. *Frontiers in Neural Circuits*, 7:34, 2013.

Wässle, H. Parallel processing in the mammalian retina. *Nature reviews. Neuroscience*, 5 (10):747–757, 2004.

Wei, P. , Liu, N. , Zhang, Z. , Liu, X. , Tang, Y. , He, X. , Wu, B. , Zhou, Z. , Liu, Y. , Li, J. , Zhang, Y. , Zhou, X. , Xu, L. , Chen, L. , Bi, G. , Hu, X. , Xu, F. , and Wang, L. Processing of visually evoked innate fear by a non-canonical thalamic pathway. *Nature Communications*, 6: 6756, 2015.

Weng, S. , Sun, W. , and He, S. Identification of ON-OFF direction-selective ganglion cells in the mouse retina. *The Journal of physiology*, 562(3):915–923, March 2005.

Wietek, J. , Wiegert, J. S. , Adeishvili, N. , Schneider, F. , Watanabe, H. , Tsunoda, S. P. , Vogt, A. , Elstner, M. , Oertner, T. G. , and Hegemann, P. Conversion of channelrhodopsin into a light-gated chloride channel. *Science*, 344(6182):409–412, 2014.

Wu, L. Q. , Niu, Y. Q. , Yang, J. , and Wang, S. R. Tectal neurons signal impending collision of looming objects in the pigeon. *The European Journal of Neuroscience*, 22(9):2325–2331, 2005.

Wyart, C. , Del Bene, F. , Warp, E. , Scott, E. K. , Trauner, D. , Baier, H. , and Isacoff, E. Y. Optogenetic dissection of a behavioural module in the vertebrate spinal cord. *Nature*, 461(7262):407–410, 2009.

Xiao, T. and Baier, H. Lamina-specific axonal projections in the zebrafish tectum require the type IV collagen Dragnet. *Nature Neuroscience*, 10(12):1529–1537, 2007.

Yaksi, E. and Friedrich, R. W. Reconstruction of firing rate changes across neuronal populations by temporally deconvolved Ca2+ imaging. *Nature Methods*, 3(5):377–383, 2006.

Yamamoto, K. , Nakata, M. , and Nakagawa, H. Input and output characteristics of collision avoidance behavior in the frog Rana catesbeiana. *Brain, Behavior and Evolution*, 62(4): 201–211, 2003.

Yazulla, S. and Studholme, K. M. Neurochemical anatomy of the zebrafish retina as determined by immunocytochemistry. *Journal of Neurocytology*, 30(7):551–592, 2001.

Yilmaz, M. and Meister, M. Rapid innate defensive responses of mice to looming visual stimuli. *Current Biology*, 23(20):2011–2015, 2013.

Yuste, R. From the neuron doctrine to neural networks. *Nature Reviews Neuroscience*, 16 (8):487–497, 2015.

Zhang, Y. , Kim, I. J. , Sanes, J. R. , and Meister, M. The most numerous ganglion cell type of the mouse retina is a selective feature detector. *Proceedings of the National Academy of Sciences*, 109(36):2391–2398, 2012.

Zhu, P. , Narita, Y. , Bundschuh, S. T. , Fajardo, O. , Schärer, Y. P. Z. , Chattopadhyaya, B. , Bouldoires, E. A. , Stepien, A. E. , Deisseroth, K. , Arber, S. , Sprengel, R. , Rijli, F. M. , and Friedrich, R. W. Optogenetic dissection of neuronal circuits in zebrafish using viral gene transfer and the Tet system. *Frontiers in Neural Circuits*, 3:21, 2009.

Zottoli, S. J. Correlation of the startle reflex and Mauthner cell auditory responses in unrestrained goldfish. *The Journal of Experimental Biology*, 66(1):243–254, 1977.

Zottoli, S. J. , Hordes, A. R. , and Faber, D. S. Localization of optic tectal input to the ventral dendrite of the goldfish Mauthner cell. *Brain Research*, 401(1):113–121, 1987.